DSPACE

https://dspace.org/

Gold mineralisation in the Pietersburg Greenstone Belt, Eersteling Gold Mine

Chalale, Reitumetse

2022

https://hdl.handle.net/10539/33845

Downloaded from a DSpace repository. https://dspace.org/

Gold Mineralisation in the Pietersburg Greenstone Belt, Eersteling Gold Mine

MSc (CW & RR) Research Project



UNIVERSITY OF THE WITWATERSRAND, JOHANNESBURG

Reitumetse Chalale (1474227)

Supervised by: Prof Paul Nex

School of Geoscience

1 Jan Smuts Avenue, Braamfontein 2000 Johannesburg, South Africa, Private Bag 3, Wits 2050

05 January 2022

Declaration

I Reitumetse Chalale (Student number: 1474227) am a student registered for Master of Science (CW/RR) in the year 2021. I hereby declare the following:

- I am aware that plagiarism (the use of someone else's work without their permission and/or without acknowledging the original source) is wrong.
- I confirm that the work submitted for assessment for the above course is my own unaided work except where I have explicitly indicated otherwise.
- I have followed the required conventions in referencing the thoughts and ideas of others.
- I understand that the University of the Witwatersrand may take disciplinary action against me if there is a belief that this is not my own unaided work or that I have failed to acknowledge the source of the ideas or words in my writing.

Signature: ___  _____ Date: 05 January 2022

Abstract

The Eersterling Gold Mine was South Africa's first hard rock commercial gold mine, and it is situated in the Pietersburg Greenstone Belt (PGB). The gold mineralisation in this Archaean greenstone belt is sediment and shear zone hosted. Borehole samples were taken from multiple gold reefs; Pienaar, Girlie – Pienaar, Maltz and Zandrivier – Arsenopyrite. The material was described, documented, and analysed to determine the occurrences of gold mineralisation and associated sulphides. The results collected from the various methodologies illustrated that the different reefs experienced multiple phases of deformation and mineralisation which was associated with a hydrothermal system – that produced quartz and carbonate veins. The different sulphides found within these reefs include pyrite, chalcopyrite, galena, sphalerite, pyrrhotite, and arsenopyrite. These sulphides occur in massive, net textured and disseminated forms and indicate phases of remobilisation. Visible gold was noted using petrological techniques from Z01 samples taken from the Zandrivier Reef. Elemental maps from TESCAN Scanning Electron Microscope (SEM) mineralogical analysis of the Pienaar and Girlie – Pienaar Reefs indicate enrichment of invisible gold within pyrite, pyrrhotite and chalcopyrite. However, this may be an analytical artifact because the traces of gold are far too uniform to be real. This observation requires further analysis which is beyond the scope of this research project. In contrast, gold in the Zandrivier Reef mainly occurs as inclusions on the margins of these sulphides. The Zandrivier Reef also contains insignificant traces of native gold in arsenopyrite. The traces of gold from these reefs are also associated with high traces of bismuth, which is a common gold pathfinder element. From gold fire assay results provided by the SGS laboratory, the Pienaar and Zandrivier Reefs have the highest gold grades at an average of 4 to 7 ppm Au. However, the limited petrographic results collected in this research report do not necessarily support this result. Therefore, it is recommended that more research should be undertaken to determine the enrichment of gold within these sulphides.

Acknowledgements

I would like to thank Prof. Paul Nex, my supervisor, for his guidance throughout this entire process. Thank you for your constructive criticism, which assisted me in better understanding the theory and application of gold mineralisation in the geological industry.

I would also like to thank the Eersterling Gold Mine for providing the samples, borehole core logs, gold assay results and drilling site maps that allowed me to complete this research report despite the constraints of the 2020 Covid pandemic. Thank you to the Witwatersrand School of Geoscience for their assistance in preparing my polished thin sections and providing the necessary equipment for my TESCAN Integrated Mineral Analyzer (TIMA) analysis.

A special thanks to my friends and family for their unwavering support throughout this entire journey. Thank you for your constant words of encouragement and faith in me. Thank you for believing in my work ethic. I will always be grateful for your contribution to my success. Lastly but not least, I thank God for giving me the strength to see this into completion; especially on days, I felt like giving up.

Table of Contents

Declaration i
Abstract ii
Acknowledgements iii
List of Figures vii
List of Tables xii
1. INTRODUCTION 1
1.1 Aim 5
1.2 Hypothesis 5
1.3 Research Questions 5
1.4 Research Limitations 5
2. PREVIOUS WORK 5
2.1 Regional Geology 5
2.2 Igneous Intrusions 7
2.2.1 Bavlaanskloof Gneiss 7
2.2.2 Goudplaas Gneiss 8
2.2.3 Geysers Granite 9
2.2.4 Hout River Gneiss 10
2.2.5 Turfloop Batholith 10
2.2.6 Roodepoort Pluton 10
2.2.7 Lunsklip Pluton 11
2.2.8 Uitloop Pluton 11
2.3 Deformation Events 11
2.3.1 First Deformational Event 11
2.3.2 Second Deformational Event 12
2.3.3 Third - Fourth Deformational Events 13
2.4 Major Shear Zones 13
2.4.1 Snymansdrift Shear Zone 13
2.4.2 Hout River Shear Zone 14
2.4.3 Kuschke Shear Zone 15
2.4.4 Hollandsdrift Shear Zone 16
2.4.5 Willemse Shear Zone 16
2.5 Metamorphism 17
2.5.1 First Metamorphic Event 17
2.5.2 Second Metamorphic Event 17
2.5.3 Third Metamorphic Event 18

2.6 Goldfields 18
2.6.1 Eersteling Goldfield 18
2.6.2 Marabastad Goldfield 19
2.7 Gold reefs in the Eersteling Goldfield 19
2.7.1 Girlie Reef 20
2.7.2 Pienaar Reef 20
2.7.3 Doreen Reef 20
2.7.4 Maltz Reef 21
2.7.5 Dog and Unnamed Reef 21
2.8 Gold reefs in the Marabastad Goldfield 21
2.8.1 Zandrivier Deposit/ Reef 21
3. METHODOLOGY 23
3.1 Hand Sample Descriptions 23
3.2 Petrographic Analysis 23
3.3 TESCAN Integrated Mineral Analyser (TIMA) 23
3.5 Strater 5 Borehole Core Logging Software 24
4. RESULTS 24
4.1 Lithology and Mineralogy 24
4.2 Structural Features 31
4.3 TIMA - Primary Phase Maps 35
P11 – 1A 35
GP02 – 2B 36
Z01 – 1A 37
Z01 – 2B 37
Z01 – 2C 38
Z02 – 1C 40
4.4 TIMA – Elemental Maps 40
Z01 – 1A 40
Z01 – 2B 43
Z01 – 2C 44
Z02 – 1C 45
P11 – 1A 46
GP02 – 2B 46
5. DISCUSSION 48
5.1 Lithology and Mineralogy 48
5.2 Structural Features 49

5.3 TIMA – Primary Phase Maps 50
5.4 TIMA – Elemental Maps 51
6. CONCLUSIONS AND RECOMMENDATIONS 52
REFERENCES 53
APPENDIX 58
Borehole Samples Localities 58
Petrographic Analysis 59
Structural Features 59
TIME – Primary Phase and Elemental Maps 60
Borehole Core Logging 61
Pienaar Reef 62
Girlie – Pienaar Reef 64
Zandrivier Reef 65

List of Figures

Figure 1: Map showing the Pietersburg Greenstone Belts extension and location of the Eersterling Project area where samples were collected. The map is modified from Kalbskopf and Barton (2003).1

Figure 2: Image showing the assemblage of the sub – cratonic blocks that make up the Kaapvaal Craton. The blocks are subdivided by regional lineaments and the locality of the greenstone terranes is shown (Zeh and Gerdes, 2012).....2

Figure 3: A detailed tectono – stratigraphic map showing the locality of the Pietersburg Greenstone Belt in South Africa and the Eersteling and Marabastard - Mount Maré areas (de Wit et al., 1993). ...4

Figure 4: Localities of the different Archean Granite – Gneiss found within the Pietersburg Greenstone Belt. The figure shows the spatial relationship between the granite – gneiss complex and the greenstone successions in the Pietersburg Greenstone Belt (Barton et al., 1990). 8

Figure 5: Geological map highlighting the different granitoids that occur near the Pietersburg and Murchison Greenstone Belt (Robb et al., 2006). 9

Figure 6: Detailed geology of the Mount Maré area including (1) Locality of the Zandrivier Deposit, (2) Major regional shear zones that go through the area and (3) Surrounding granite-greenstone terrane (Anthony and Flanders, 1992).....14

Figure 7: Cross-sectional view showing the Hout River Shear Zone acting as a terrane boundary between the Kaapvaal Craton and Limpopo Belt South Marginal Zone. Northward and Southward thrusting that occurred in the Pietersburg Greenstone belt during the regions deformational events is also indicated, including the direction of lithologies (van Schalkwyk et al., 1993). 15

Figure 8: Map showing the different gold reefs within the Eersterling Goldfield and their locations. The also indicates the different lithologies with each reef (Hancox, pers comm., 2021). 20

Figure 9: Schematic cross-section of the Zandrivier Deposit showing the geological sequences and the two different workings that host gold mineralisation, upper quartz veins and basal tourmaline- gold-bearing contact between the chlorite schist and quartz-chlorite phyllonite (Kalbskopf, and Barton, 2003). 22

Figure 10: Photomicrographs of samples from the Maltz Reef (A) The mineral assemblage of metabasalts with image showing Qz - quartz groundmass being crosscut by Amp - amphibole veins (Borehole M03 at 75.60 – 75.91 m). (B) Disseminated anhedral sulphides in the Maltz Reef are predominantly Py - pyrite with minor Ccp - chalcopyrite.....25

Figure 11: Photomicrographs of samples from the Pienaar Reef (A) Mineral lens that occurs within metabasalts and comprises a Cb – Carbonate (calcite) that is enclosed by Srp - serpentine. The mineral lens is in contact with a large Qz - quartz vein that crosscuts the host rock. In (B) the quartz contains mineralisation of Sp - sphalerite which is concentrated on top of the carbonates in the quartz vein. (C) Carbonate exhibiting deformational lamellae and illustrating a cleavage normally seen in Gn – galena even though the ore mineral has not crystallised completely. (D) Ore mineral assemblage found in the Pienaar Reefs quartz veins which comprise Py - pyrite, Ccp - chalcopyrite and Sp – sphalerite (Borehole P11 at 130.87 – 131.07 m).....26

Figure 12: Photograph of the Pienaar Reef's hand sample with an observed sharp-sheared contact between the quartz veins and metabasalts, indicated by a rectangle. The area enriched in quartz also contains sulphide mineralisation (Borehole P11 at 130.84 – 131.07 m).....27

Figure 13: Photomicrographs of samples from the Pienaar Reef (A) Footwall mineralisation of the Pienaar Reef with disseminated Ccp - chalcopyrite and Py – pyrite that is hosted in quartz veins. (B) Anhedral Gn – galena crystal with perfect triangular cleavage, the galena only occurs in the carbonates (Borehole P11 at 130.87 – 131.07 m). 27

Figure 14: Photograph of the Pienaar Reefs footwalls hand sample that comprises coarse-grained breccia with angular fragments of quartz, carbonates, amphiboles and metabasalts. The hand sample also contains multiple fractures and cross-cutting quartz veins (Borehole P11 at 1302.34 – 132.43 m). 28

Figure 15: Photograph of hand samples that represent the Girlie - Pienaar Reefs hanging wall (A) and quartz reef (B). Metabaslats and recrystallised quartz make up the handing wall and coarse-grained quartz with pyrrhotite mineralisation make up the quartz reef (Borehole GP022: Hanging wall (A) at 62.60 – 62.80 m and Reef (B) at 73.65 – 73.82 m). 28

Figure 16: Photomicrographs of samples from the Girlie - Pienaar Reef (A) Full scan image of the Girlie – Pienaar's quartz reef that comprises highly fractured coarse-grained quartz. The fractures are filled with pyrrhotite, alteration material and carbonates. (B) Image showing the different sulphides that occur within the quartz reef. These include Po – Pyrrhotite, Py – Pyrite and Ccp – chalcopyrite (Borehole GP022 - Reef at 73.65 – 73.82 m). 29

Figure 17: Photograph that shows a hand sample from the Zandrivier Reef (Borehole Z02 at 123.07 – 123.24 m). The hand sample also demonstrates the different styles of Apy - arsenopyrite mineralisation which includes massive, layered, and disseminated grains..... 29

Figure 18: Photomicrographs of samples from the Zandrivier Reef (A) Occurrence of Apy - arsenopyrite mineralisation hosted in a vein that is undergoing serpentinization, Srp - serpentine (Borehole Z02 at 123.07 – 123.24 m). The arsenopyrite mainly occurs on top of carbonates that enclose it. (B) Euhedral – subhedral fractured arsenopyrites that are spatially associated with Iim - ilmenite (Borehole Z01 at 132.88 – 133.09 m). C and D illustrate massive arsenopyrite crystals that are fractured and deformed with micro inclusions of Au – gold (Borehole Z01 at 184.78 – 185.10 m). 30

Figure 19: (A) Photograph that represents the Z11 hand sample. The sulphides morphologies are shown under thin section in B and C. These images indicate a poly – sulphide mineral assemblage from the Z11 borehole core log. The sulphides comprise of Py – pyrite, Po – pyrrhotite and Ccp – chalcopyrite with inclusions of Hem – hematite or Mag – magnetite (Borehole Z11 at 235.41 – 235.81 m). 31

Figure 20: Full scan image of multiple veins with different orientations. The veins comprise quartz, berthierine and calcite. Some of the veins are mineralised and contain sphalerite, chalcopyrite, and galena. These ore minerals are highlighted with purple in the image and hosted in a quartz vein, which is highlighted in red (Borehole P11 at 130.87 – 131.07 m). 32

Figure 21: Full scan image showing two different deformations regimes with different sulphide occurrences. The left-hand side represents the ductile regime and contains anhedral pyrrhotite mineralisation. The right-hand side represents the brittle regime and contains net textured, fractured, and massive arsenopyrite mineralisation. The brittle regime also contains pyrrhotite and chalcopyrite poly - sulphides (Borehole Z01 at 184.78 – 185.10 m). 33

Figure 22: Image showing different structural features associated with quartz veins (1) Boudin structures and (2) Curving quartz veins (Borehole P11 at 130.84 – 131.07 m). 33

Figure 23: Full scan image that represents the brittle regime with different sulphide mineralisation occurrences. The dominant sulphide is arsenopyrite and occurs as (1) massive, fractured, and anhedral

crystals and (2) disseminated - euhedral arsenopyrites which were deposited by a hydrothermal fluid that intersected the country rock (highlighted in blue). The arsenopyrite is later crosscut by quartz veins (highlighted in yellow) which contain small inclusions of arsenopyrite (Borehole Z01 at 132.88 – 133.09 m). 34

Figure 24: Primary Phase Map of P11 – 1A illustrating a mineral assemblage that comprises chalcopyrite, sphalerite, and pyrite with minor pyrrhotite and galena. The ore minerals only occur within the calcite (Borehole P11 at 130.87 – 131.07 m). 35

Figure 25: Primary Phase Map of P11 – 1A representing the host rocks composition which is undergoing aluminosilicate alteration. These areas of alteration are also associated with the development of albite, orthoclase and anorthite (Borehole P11 at 130.87 – 131.07 m). 36

Figure 26: Primary Phase Map of GP02 – 2B indicating that the Girlie – Pienaar Quartz Reef comprises pyrrhotite with minor pyrite, hematite/ magnetite, rutile and titanite. The minerals are also concentrated in areas that have alteration forming (Borehole GP02 at 62.60 – 62.80 m). 36

Figure 27: Primary Phase map of Z01 – 1A that contains euhedral – subhedral arsenopyrite grains that occur as layers with associated ilmenite. The map also indicates the host rocks composition which comprises muscovite, albite, actinolite, schorl, and ankerite (Borehole Z01 at 132.88 – 133.09 m). . 37

Figure 28: Primary Phase Map for Z01 – 2B which contains massive, anhedral, and fractured arsenopyrite that has a sharp contact with pyrrhotite. The pyrrhotite also contains inclusions of chalcopyrite, pyrite, and hematite/magnetite. The pyrite only occurs as chalcopyrite inclusions and the hematite/magnetite grains are associated with berthierine inclusions (Borehole Z01 at 184.78 – 185.10 m). 38

Figure 29: Primary Phase Map of Z01 – 2C representing massive arsenopyrite that is in equilibrium with pyrrhotite and a groundmass of hematite/magnetite that contains berthierine inclusions. The berthierine also surrounds the arsenopyrite and occurs as inclusions within the arsenopyrite (Borehole Z01 at 184.78 – 185.10 m). 39

Figure 30: Primary Phase Map of Z01 – 2C showing massive and disseminated pyrrhotite that contains inclusions of chalcopyrite, ilmenite, berthierine, and rutile. The dominant ore mineral in the image is hematite/magnetite and contains inclusions of berthierine, which also occurs along the pyrrhotite grain boundaries (Borehole Z01 at 184.78 – 185.10 m). 39

Figure 31: Primary Phase Map of Z02 – 1C with massive arsenopyrite being crosscut by a carbonate (calcite and ankerite) and quartz vein. The vein contains pyrite mineralisation and minor inclusions of rutile, sphalerite and pyrrhotite (Borehole Z02 123.07 – 123.24 m)..... 40

Figure 32: Element Maps showing a field view of 13.5 mm for Z01 – 1A. In A and B, the host rocks composition contains traces of aluminium and calcium which can be associated with muscovite, schorl, and ankerite (Borehole Z01 at 132.88 – 133.09 m). 41

Figure 33: Element Maps (A – C) for Z01 – 1A showing a field view of 13.5 mm. Element Maps indicate arsenopyrite having high traces of arsenic (bright grey) and B associates these areas with bismuth. However, the pyrite and pyrrhotite have a higher bismuth composition in comparison to the arsenopyrite. C focuses on the occurrence of gold with traces of gold being identified as micro inclusions in arsenopyrite and some covering the whole pyrite grains surface area. The different morphologies for gold are shown in C1 and C2. (Borehole Z01 at 132.88 – 133.09 m). 42

Figure 34: Element Maps for the Z01 – 2B Primary Phase Map showing a field view of 6 mm. In A the poly sulphide mineral assemblage contains predominantly pyrrhotite with inclusions of chalcopyrite

and pyrite. The image indicates that the sulphides have a high sulphur composition (bright white – grey). The sulphides also have a high iron composition which is shown in B, however, the amount of the traces of iron detected depends on the mineral. The hematite/magnetite has the highest trace of iron and pyrrhotite and arsenopyrite have the lowest, respectively. In C the arsenopyrite is the only mineral with traces of arsenic. The traces of gold detected in the mineral assemblage is shown in D. The gold occurs as micro inclusions within arsenopyrite (red circles) and as inclusions that cover the whole surface area for the other sulphides – pyrrhotite (Borehole Z01 at 184.78 – 185.10 m). 43

Figure 35: Element Maps for the Z01 – 2C Primary Phase Map showing a field view of 6 mm. In A the pyrrhotite and arsenopyrite represent a poly – sulphide and pyrrhotite has a higher trace of sulphur (bright white). However, the arsenopyrite has a higher trace of arsenic which is shown in C. The element map in B indicates a very high background of iron composition which is associated with hematite, magnetite, berthierine and pyrrhotite. The arsenopyrite on the other hand does not contain significant iron that could be detected by the TIMA analysis. In D the iron serpentine – berthierine indicates an aluminium composition. The gold traces detected are shown in E and E1. The gold occurs as micro inclusion within the arsenopyrite and inclusions that cover the pyrrhotite surface area (red circles). In E1 there is a larger gold inclusion detected (bright white) which can be seen under the microscope. This gold inclusion has a bigger grain size in comparison to the other gold inclusions detected (Borehole Z01 at 184.78 – 185.10 m). 44

Figure 36: Element Maps for the Z02 – 1C Primary Phase Map showing a field view of 4.50 mm. In A the areas that indicate high traces of sulphur which are associated with pyrite and pyrrhotite mineralisation. These sulphides occur only in the quartz, calcite and ankerite vein that crosscuts the massive arsenopyrite. In B traces of arsenic are shown in arsenopyrite. In C traces of bismuth are shown in arsenopyrite, pyrite and pyrrhotite. The gold traces in D only occur as inclusions that cover the pyrite and pyrrhotite surface areas. The areas of gold traces can be associated with traces of bismuth (Borehole Z02 123.07 – 123.24 m). 45

Figure 37: Element Maps for the P11 – 1A Primary Phase Map showing a field view of 1.50 mm. In A the pyrite has the highest sulphide composition (bright white), and the composition decreases from chalcopyrite to sphalerite, respectively. In B the sphalerite has less to no iron, but the other sulphides including an iron serpentine – berthierine reflect a bright grey colour. The element map shown in C indicates an insignificant arsenic composition associated with the sulphides. In D the image shows areas with a high zinc composition, and these are associated with sphalerite. The element maps E and F represent lead and gold composition, respectively. The gold in F is invisible and covers the whole surface area of the sulphides. The highest gold-bearing sulphide is pyrite (bright white) and is followed by chalcopyrite and sphalerite – grey (Borehole P11 at 130.87 – 131.07 m). 46

Figure 38: Element Maps showing a field view of 6 mm for the Girlie – Pienaar Quartz Reef, sample GP02 – 2B. In A the sulphur composition for pyrite is higher (bright white) and pyrrhotite is relatively low (grey). These sulphides contain iron (B) and the samples areas of alteration are associated with aluminium and magnesium (C and D). The occurrence of gold is indicated in E and is situated all over the pyrrhotite and pyrite grains surface area (grey). In F gold mineralisation is associated with bismuth (Borehole GP02 at 62.60 – 62.80 m). 47

Figure 39: Map showing the localities of the boreholes: GP022; P06c; M03; and P11 from the Eerterling 17KS farm. The map also indicates the different reefs orientations and permit boundary surrounding the project area (Eersterling Gold Mine, 2020). 58

Figure 40: Map showing the localities of the boreholes: Z01; Z02; and Z11 from the Zandrivier 742LS farm (Eersterling Gold Mine, 2020). 58

Figure 41: Photomicrograph of a sample from the Girlie – Pienaar Reef. Occurrence of berithierine (Srp) in massive quartz veins fractures (Borehole GP022: Reef at 73.65 – 73.82 m). 59

Figure 42: Photomicrograph of a sample from the Zandrivier Reef illustrating a more ductile regime with anhedral elongated pyrrhotite (Po) and serpentine (Srp). The arsenopyrite (Apy) has a different morphology even though both ore minerals are sourced from the same sample (Borehole Z01 at 184.78 – 185.10 m). 59

Figure 43: Photomicrograph of a sample from the Zandrivier Reef illustrating a more brittle regime with anhedral elongated pyrrhotite (Po) and serpentine (Srp). The arsenopyrite (Apy) still has its euhedral crystal shape and occurs as net textured, fractured, and massive grains. The serpentine in the brittle regime is concentrated along the sulphide's edges and encloses. 60

Figure 44: Primary Phase Map of P11 – 1A illustrating a mineral assemblage that comprises chalcopyrite, sphalerite, and pyrite. The ore minerals only occur within the calcite and the host rock is rich in anorthite and berthierine - a serpentine alteration mineral (Borehole P11 at 130.87 – 131.07 m). 60

Figure 45: Element Maps for the P11– 1A Primary Phase Map showing a field view of 2mm. The elemental maps illustrate a correlation between bismuth and gold. In addition, areas that reflect high bismuth concentrations are closely associated with gold mineralisation. Both elements are structurally hosted in pyrite (Borehole P11 at 130.87 – 131.07 m). 61

Figure 46: Stratigraphic view of the Pienaar Reefs borehole core log (P06c) which indicated the different lithologies that make up the reef. The dominant rock type is metabasalt which is crosscut by thin layers of chlorite, quartz, and granite as you move down the stratigraphic column. Sample P06c was extracted from a depth of 91.70 – 92.0 m and the quartz and metabasalt along this depth exhibited a gradational contact at 70 – 75°. In comparison to the host rock, the quartz is coarser and has no foliation. 62

Figure 47: Stratigraphic view of the Pienaar Reefs borehole core log (P11) that comprises of different lithologies. The dominant rock type is metabasalt which is crosscut by thin layers of chlorite, quartz and breccias as you move down the stratigraphic column. The reef also experienced some shearing at 61 – 62m which is associated with disseminated sulphides. Sample P11 was extracted from a depth of 129 – 133 m and exhibited a shear contact with the neighbouring lithology. 63

Figure 48: Stratigraphic view of the Girlie - Pienaar Reefs borehole core log (GP0) that comprises different lithologies. The dominant rock type is metabasalt that covered by chlorite overburden and crosscut by quartz veins at a depth range of 60 – 76 m. The quartz veins represent the reef where most sulphide mineralisation occurs. The average contact angle between the different lithologies is between 5 and 20° and exhibits a sharp and sheared contact. 64

Figure 49: Stratigraphic view of the Zandrivier Reefs borehole core log (Z01) that comprises metabasalts and interbedded carbonates within the metasediments - as you go down stratigraphy. The overburden is mainly broken rock that cannot be identified. The average contact angle between the metabasalts and carbonaceous units is 85° and this region is associated with massive arsenopyrite mineralisation with sulphides preserving their cubic crystal shape. 65

Figure 50: Stratigraphic view of the Zandrivier Reefs borehole core log (Z02) that comprises metabasalts, mixed zone (transition zone), carbonates and metasediments - as you go down stratigraphy. The overburden is mainly broken rock that cannot be identified. 66

Figure 51: Stratigraphic view of the Zandrivier Reefs borehole core log (Z11) that comprises metabasalts, mixed zone (transition zone), carbonates and metasediments - as you go down

stratigraphy. The stratigraphy is crosscut by a dyke (at 140 - 160m) which exhibits a sharp contact with the surrounding rocks. The contact angle between the lithologies is gentle at depths of 60 – 140m (40 - 50°) and transitions into a steeper angle at 150 – 220m (70 - 80°)..... 67

List of Tables

Table 1: Detailed Lithostratigraphic subdivision of the Pietersburg Group, with detailed descriptions of the rock sequences found in all the different formations: Mothiba, Ysterberg, Eersteling, Zandrivierspoort, Vrischawaaryd and Uitkyk (Zeh and Gerdes, 2012). 6

Table 2: Approximation of Gold produced in the Pietersburg Greenstone Belt indicating that the Eersteling farm produced the highest amount of gold. Farms listed in descending order of gold ounces recovered. This table recordings were compiled by Willemse, 1938 (Saager and Muff, 1986)..... 19

1. INTRODUCTION

The Eersterling Gold Mine hosts South Africa's first hard rock gold mine and mining was initiated in 1874 until the late 1980s when the mine was shut down (Eersterling Gold Mining, 2007). In 1987, the Eersterling Gold Mining Company acquired prospecting rights over the project area but in 2004 the Caledonia Mining Company bought shares and now has full ownership of the gold mine (Eersterling Gold Mining, 2007). Exploration ceased in 1997 because there were inconsistencies in gold production and gold prices were low (Eersterling Gold Mining, 2007). Three years (1994 – 1997) before closing, the old Eersterling and newer Zandrivier operational sections contributed to the mine's gold production. Since 1997 the mine has been undergoing care and maintenance, however, discoveries and renewed interest has resulted in recent exploration.

The geological area of the project is situated in the Pietersburg Greenstone Belt (PGB) a narrow East-Northeast– trending geological structure that covers an estimated strike length of 125 km, a width of 25 km and a depth extent of 4-7 km (Stettler and du Plessis, 1988; Kröner et al., 2000; Zeh and Gerdes, 2012). The PGB is located between Mokopane and Polokwane (Figure 1) and comprises the volcanic (Basal Simatic Unit) and sedimentary (Cover Unit) rock sequences of the Pietersburg Group, which have undergone deformation and metamorphism (de Wit, 1991; de Wit et al., 1992; Zeh and Gerdes, 2012). Tonalite-trondhjemite-granodiorites (TTG's) and granitoids surround and intrude the PGB, respectively, and regional scale East-Northeast and East-Southeast trending shear zones crosscut it (Stettler and du Plessis, 1988; Byron and Barton, 1990; Barton et al., 1990; de Wit, 1991).

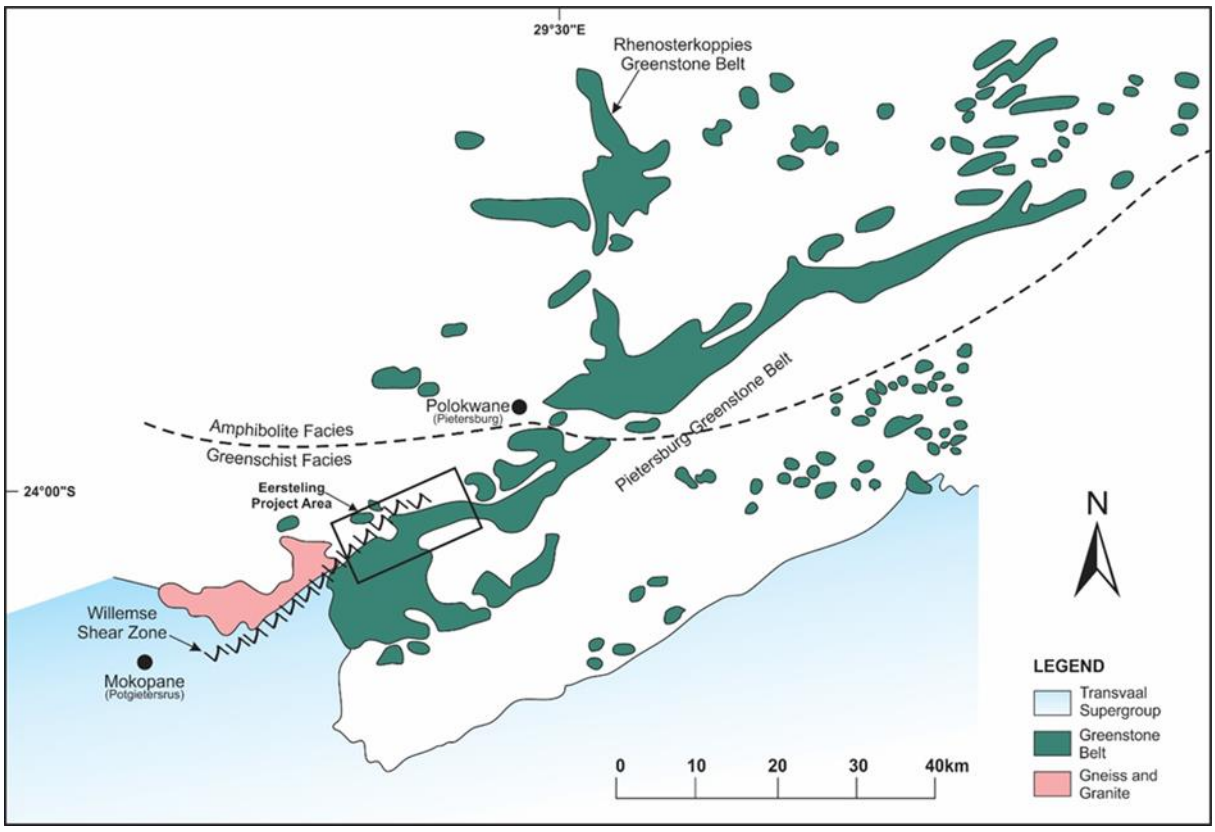


Figure 1: Map showing the Pietersburg Greenstone Belts extension and location of the Eersterling Project area where samples were collected. The map is modified from Kalbskopf and Barton (2003).

The PGB is a low to medium grade metamorphic greenstone belt that is preserved in the Northern – Northeastern area of the Kaapvaal Craton (KC) (Foster and Piper, 1993; Zeh and Gerdes, 2012).

According to Kramers et al., (2014) the greenstone belts that surround the KC can be interpreted as suture zones that formed during terrane accretion when the KC was assembled. This spatial association between the different blocks to the PGB is shown in Figure 2 below.

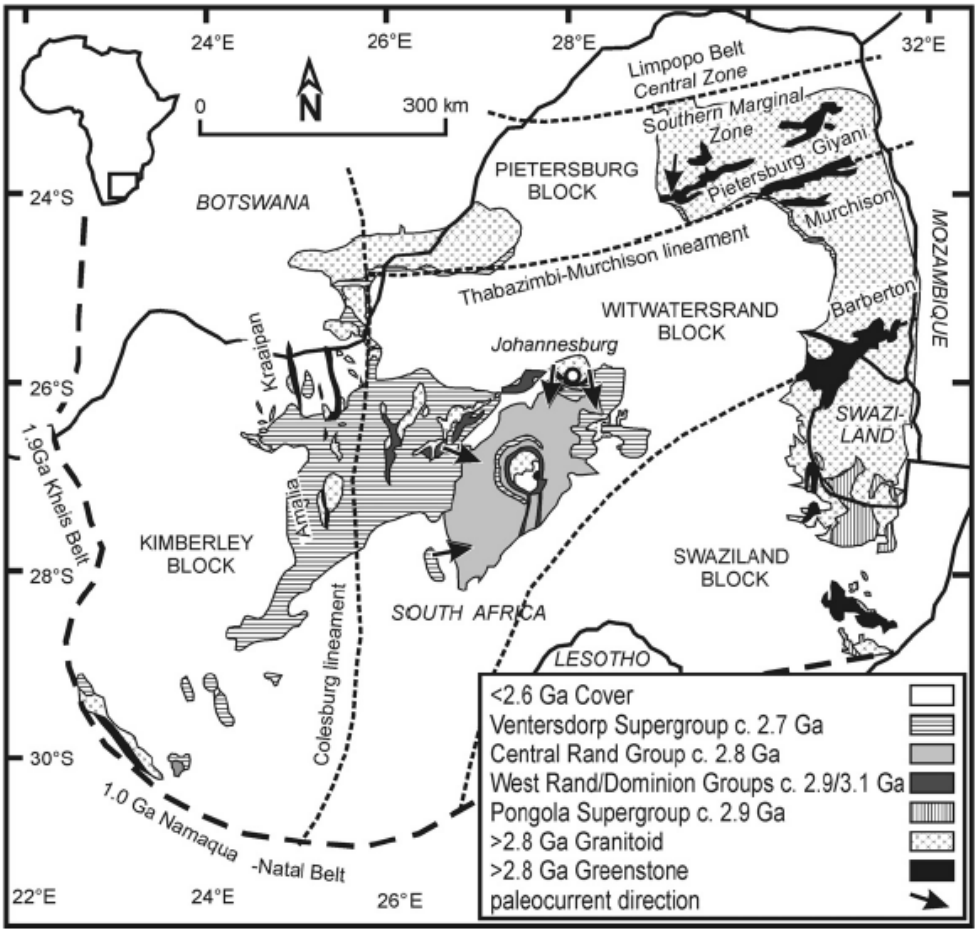


Figure 2: Image showing the assemblage of the sub – cratonic blocks that make up the Kaapvaal Craton. The blocks are subdivided by regional lineaments and the locality of the greenstone terranes is shown (Zeh and Gerdes, 2012).

After the discovery of the Eersterling Goldfield in 1871, the PGB only received attention in geological literature at a later stage (ca. 1970). The research papers published at the time covered regional geology, geochemistry, age, and structure of the PGB - using geophysical methods. According to de Wit et al., (1992), the PGB is a significant gold producer in South Africa and contains similar features to Archean greenstone belts worldwide. Most of the previous work related to gold production rates within the PGB's goldfields was dependent on Willemse (1983). This is because there has been a lack of research on gold production in the area over the last 3 decades and data being either inaccessible or unreliable at the time (Saager and Muff, 1986; Byron and Barton, 1990). Work done by Franey (1987) focuses on the general occurrence of gold mineralisation within the PGB and suggested that gold mineralisation is associated with primary and secondary systems. The gold mineralisation in these systems occurs as: (1) Fine disseminated grains in quartz veins or shear zones; (2) Impregnated gold-bearing schists; and (3) Secondary supergene enrichment grains hosted in banded iron formation (BIF) (Saager and Muff, 1986; Foster and Piper, 1993).

Even though certain scientific aspects of the PGB have been researched. There has been less work done on the sulphide mineral assemblages and gold occurrences of each goldfield in detail. Hence,

this research project is important because the information obtained from the petrographic, and TESCAN Integrated Mineral Analyser (TIMA) can help determine the potential and occurrence of gold mineralisation and associated sulphides from the gold reefs in the Eersterling and Marabastad (Mount Maré) goldfields (Figure 3). The petrographic data collected, and interpretations presented by (Willemse, 1983) suggests that mineralisation in the PGB is structurally controlled. In addition, this research project adds more information regarding the PGB's gold occurrences, the structural control on mineralisation and the sulphide mineral assemblages found in the various gold reefs.

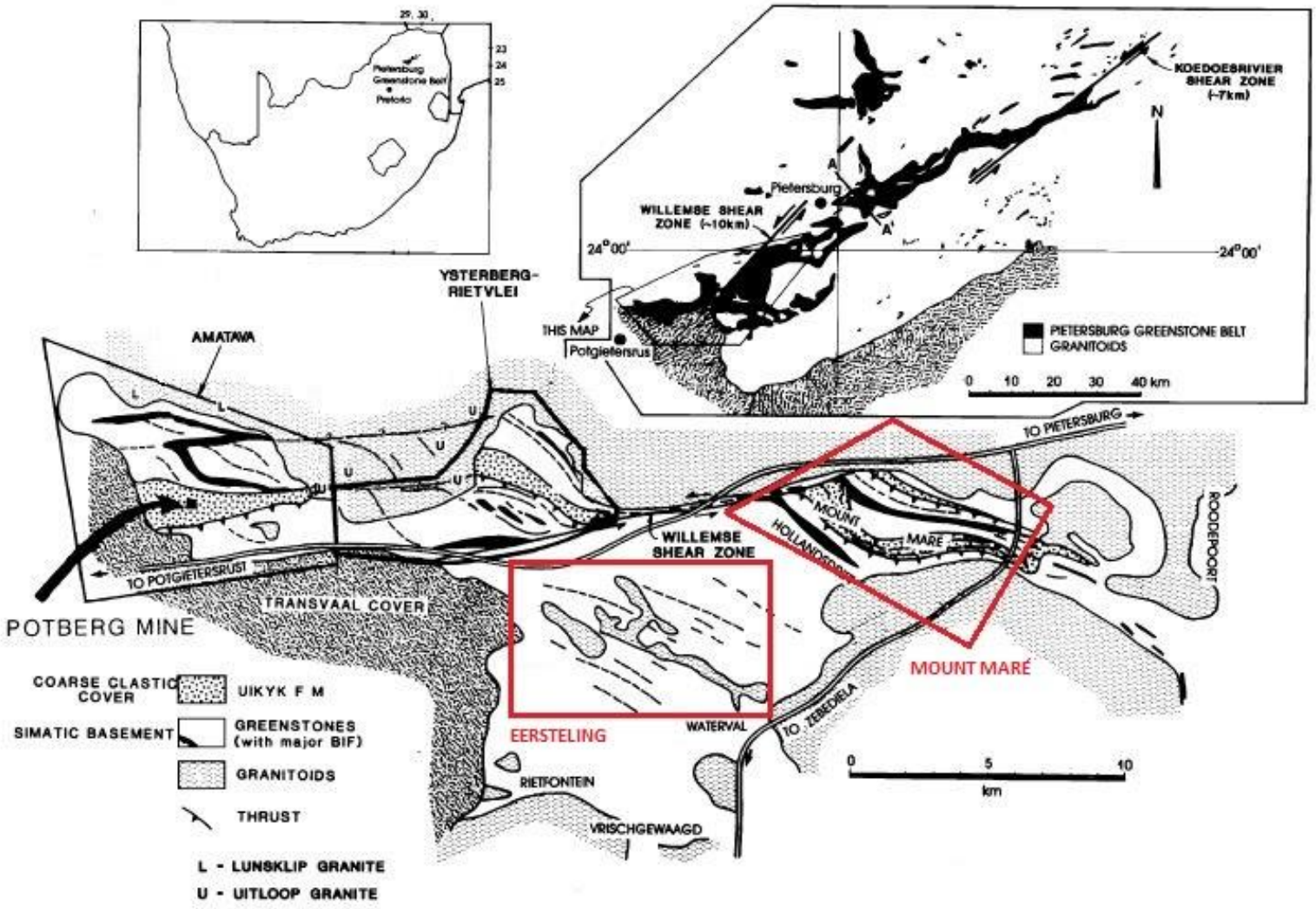


Figure 3: A detailed tectono – stratigraphic map showing the locality of the Pietersburg Greenstone Belt in South Africa and the Eersteling and Marabastard - Mount Maré areas (de Wit et al., 1993).

1.1 Aim

To determine and describe the sulphide assemblages and occurrence of gold mineralisation in the various reefs of the Eersteling Gold Mine by using seven non – oriented borehole cores from the farms: Eersteling 17 KS and Zandrivier 742 LS. The borehole samples available for this research project intersect the Pienaar, Girlie – Pienaar, Maltz and Zandrivier – Arsenopyrite reefs.

1.2 Hypothesis

The occurrence of gold mineralisation and its sulphide assemblages are different in the Eersteling and Zandrivier farms, but mineralisation from both areas is structurally controlled and remobilised by multiple cross-cutting quartz veins.

1.3 Research Questions

- What is the distribution of gold in the different lithologyies?
- What is the morphology of the microstructures associated with sulphide and gold mineralisation?
- What are the structural controls on gold mineralisation?
- Are there any quartz veins that are associated with gold mineralisation since the PGB is mainly defined as a shear-hosted hydrothermal system?
- What are the comparable characteristics observed between the intersected gold reefs?
- Are there any indications for sulphide remobilisation?
- Did the wall rock alteration and metamorphic grade affect the quantity and quality of gold mineralisation?
- What is the relationship between the gold grade, sulphide assemblages and structures (if any)?

1.4 Research Limitations

The geology and mineralisation represented in the research project are dependent on the information and observations gathered from previous literature and the drilled core. Therefore, the concluding remarks may not apply to the whole PGB but are rather focused on a local scale. In addition, Covid 19 restrictions in 2020 ruled out the possibility of any fieldwork, such as going to the mine site and personally logging the core.

2. PREVIOUS WORK

2.1 Regional Geology

The PGB comprises two major stratigraphic sequences from the Pietersburg Group, these are the Simatic and Cover Units (Franey, 1987; Zeh and Gerdes, 2012). The stratigraphic sequences can be further subdivided into five formations (Table 1). The Simatic Unit is the oldest and contains volcanic rocks (greenstones) from the Mothiba, Ysterberg, Eersteling and Vrischawaaryd formations (Stettler and du Plessis, 1988; de Wit et al., 1992; Zeh and Gerdes, 2012). The Simatic Units rocks have a tholeiitic affinity that is represented by dunite, peridotite and pyroxene (de Wit, 1991; Kröner et al., 2000). This rock sequence is overlain by the Cover Unit that comprises coarse-grained sedimentary rocks of the Uitkyk Formation (Kramers et al., 2014).

Table 1: Detailed Lithostratigraphic subdivision of the Pietersburg Group, with detailed descriptions of the rock sequences found in all the different formations: Mothiba, Ysterberg, Eersteling, Zandrivierspoort, Vrischawaaryd and Uitkyk (Zeh and Gerdes, 2012).

Formation	**Stratigraphic Sequence**	**Lithology (Pietersberg Group)**	**Lithology (Mount Maré)**
Uitkyk	Cover	Quarzites, conglomerates, shales, quartz – mica schists	Conglometrates, shales, no BIF maximum thickness: 1km
Vrischgewaagd		Chloritic and quartzitic shales	Various schist zones
Unconformity			
Zandrivierspoort	Simatic	Mafic metalava with interlayered magnetic quartzite	Metaperidodites, metagabbros (massive and layered), and pillowed massive metatholeiites Amphibole spinifex texture
Eersteling		Mafic metalava with subordinate ultramafics, quartz – feldspar porphyry and salic lava	
Ysterberg		Felsic lavas and tuffs, shale, interbedded quartzite schist, banded chert/ironstone quartzite	Hollandrift and Kuschke BIF and shales
Mothiba		Ultramafics with minor amphibole, quartzitic schist, quartz – feldspar porphyry, BIF	

The Mothiba Formation is situated underneath the Marabastad Goldfield and is made up of coarse-grained ultramafic lavas which are rich in serpentine and interbedded with alternating layers of chert and banded iron formation (Saager and Muff, 1986; Franey, 1987; Stettler and du Plessis, 1988; de Wit et al., 1992) (Table 1). In comparison to the Mothiba Formation, the lavas of the overlying Ysterberg Formation are more aluminium-rich and interbedded with bands of volcanic material (Stettler and du Plessis, 1988). As you move towards the Northern area of the Ysterberg Formation the lithology changes into the Zandrivierspoort Formation, its stratigraphic equivalent (Stettler and du Plessis, 1988). However, the Zandrivierspoort Formation contains amphiboles that are interbedded with magnetite rich quartzites (Stettler and du Plessis, 1988). There is a similarity between the Eersteling and Zandrivierspoort formation, but the amphiboles from the Eersteling Formation are massive to fine-grained and have a schistose texture (Stettler and du Plessis, 1988).

The Eersteling Formation forms the dominant lithology of the Eersteling Goldfield and is also associated with minor iron formations, large-scale volcanic remnants and metabasalts (Saager and Muff, 1986; Foster and Piper, 1993). The greenstones from the Eersteling Formation have an East-West strike and dip towards the South with a mineral assemblage of chloritoid, carbonate, chlorite, quartz, and serpentine (Franey, 1987; Saager and Muff, 1986; Byron and Barton, 1990). The

stratigraphic units from the Eersteling Formation are also crosscut by dolerite dykes that have a North to South strike (Byron and Barton, 1990).

In Table 1, an unconformity is illustrated between the Vrischawaaryd and Zandrivierspoort Formation. The Vrischawaaryd Formation mainly comprises coarse-grained quartz-carbonate rocks which are crosscut by numerous quartz veins. It isolates the underlying ultramafic - mafic rock lenses from the underlying formations and exhibits a gradational contact with the mafic sequences (Saager and Muff, 1986; Franey, 1987; de Wit et al., 1992). The ultramafic rocks of the Simatic Units are highly resistant and contain preserved pillow structures. The rock composition of these units gradually changes from albite-actinolite-chlorite mafic rocks to albite-hornblende-chlorite amphiboles from the outer to the inner areas of the PGB (Byron and Barton, 1990; de Wit et al., 1993).

The Uitkyk Formation of the Cover Unit comprises gritstones, conglomerates, breccias, siltstones and sandstones (de Wit et al., 1992; Zeh and Gerdes, 2012). The sandstones are immature and contain sedimentary structures including trough cross-beds, forests, and planar cross-beds (Franey, 1987; de Wit 1991). The lower Uitkyk Formations contact boundary is erosional and hosts greenstone remnants from the basement rocks of the Simatic Units (Stettler and du Plessis, 1988; Zeh and Gerdes, 2012). This relationship is also observed between the upper Cover Unit and intruding granitoids, as granitoid clasts and fragments are found in the conglomerates and breccias of the Cover Units (de Wit et al., 1992; Zeh and Gerdes, 2012). It has been suggested that these conglomerates can be correlated with the Witwatersrand Basins Central Rand Group (de Wit et al., 1992; McCourt, 1995).

The difference in lithology between the Simatic and Cover Units highlights a distinctive unconformity (Table 1), and the units have an upward coarsening relationship (Franey, 1987; de Wit, 1991; Kramers et al., 2014; Vezinet et al., 2018.). This subdivision is also illustrated by tectonically induced thrusts that formed during the second deformation event (de Wit et al., 1992; Zeh and Gerdes, 2012; Kramers et al., 2014). According to van Schalkwyk et al., (1993), deposition of the Uitkyk Formation occurred right after the Simatic Units underwent metamorphism with the Simatic and Cover Units having an approximated age of 3450Ma and 2900-2700Ma respectively (Sieber, 1991; de Wit et al., 1992; van Schalkwyk et al., 1993; Zeh and Gerdes, 2012).

2.2 Igneous Intrusions

The PGB is surrounded by tonalite-trondhjemite-granodiorites (TTG's) on its Northern flank (Bavlaanskloof and Goudplaas gneiss) and intruded by granitoids on its Southern margin (Geysers Granite, Turfloop Batholith, Hout River Gneiss and Roodepoort, Lunsklip and Uitloop Plutons) (Stettler and du Plessis, 1988; Byron and Barton, 1990; Barton et al., 1990; de Wit, 1991). More detail on each granitoid and gneiss is given further below.

2.2.1 Bavlaanskloof Gneiss

The Bavlaanskloof Gneiss (Figure 4) comprises the oldest unit of rocks that surround the Pietersburg Granite - Greenstone Terrane (Byron and Barton, 1990; Barton et al., 1990; Sieber, 1991; Beattie and Barton, 1992). These rocks are grey tonalite-trondhjemite-granodiorites (TTG's) that have a dismembered contact with the greenstone rocks of the PGB (Kröner et al., 2000). The contact was obscured by pegmatitic granite intrusions that were emplaced around 2650 Ma (Byron and Barton, 1990; Anhaeusser, 1992; Kröner et al., 2000; Zeh and Gerdes, 2012). The lithological units that have a trondhjemite and tonalite affinity are concentrated along the Southern margin and Northern flank of the PGB (Kröner et al., 2000; Zeh and Gerdes, 2012; Rajesh et al., 2020). The contact between the

TTG's and the PGB's greenstones also illustrates a lit – par- lit relationship and contains migmatite or mylonitic foliation zones (Beattie and Barton, 1992; van Reenen et al., 1992; Kröner et al., 2000). The Bavlaanskloof Gneiss is considered a result of a Mesoarchean magmatic event that was emplaced between 3000 – 2900 Ma (Barton et al., 1990, Zeh and Gerdes, 2012; Rajesh et al., 2020).

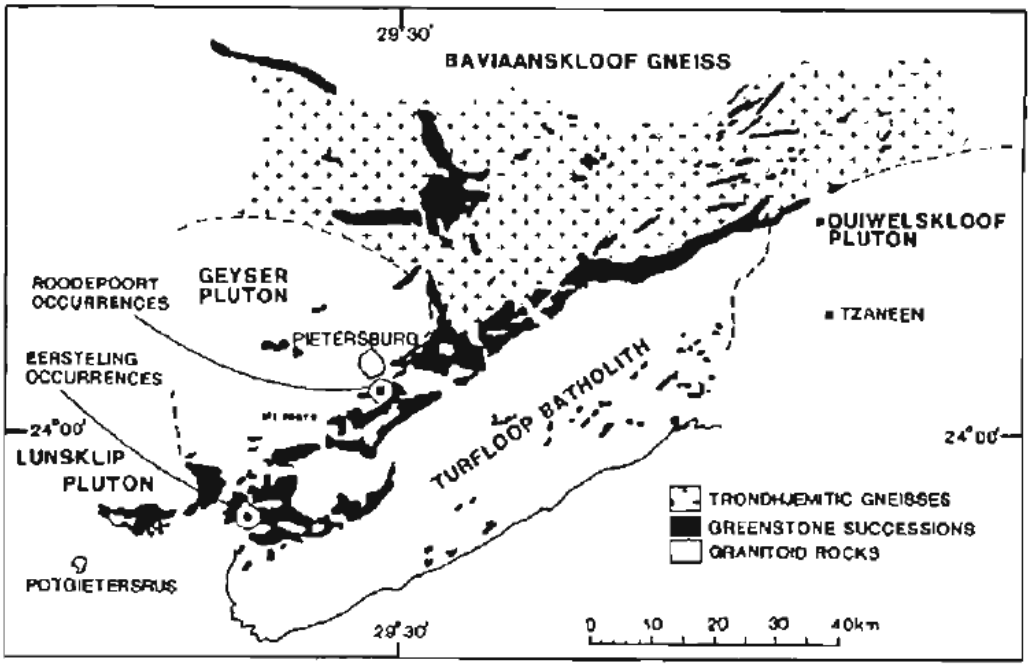


Figure 4: Localities of the different Archean Granite – Gneiss found within the Pietersburg Greenstone Belt. The figure shows the spatial relationship between the granite – gneiss complex and the greenstone successions in the Pietersburg Greenstone Belt (Barton et al., 1990).

According to Rajesh et al., (2020), the Bavlaanskloof Gneiss represents a region of low to high-pressure TTG's and is spatially associated with the Hout River Shear Zone (HRSZ). The gneiss is more highly deformed closer to the HRSZ. The Bavlaanskloof Gneisses consists of predominantly plagioclase, biotite and quartz with minor potassium feldspar that has undergone exsolution. The mafic minerals are hornblende, magnetite, and pyroxene (van Reenen et al., 1992; Rajesh et al., 2020). Roering et al., (1992) suggest the Bavlaanskloof Gneiss texture to be derived from high-grade metamorphism and intense tectonism.

2.2.2 Goudplaas Gneiss

The Goudplaas Gneiss is suggested to form the basement of the PGB which comprises magmatic and banded gneisses of a trondhjemite and tonalite affinity (Anthony and Flanders, 1992). This gneiss is located beneath the South Marginal Zone of the Limpopo Belt and is spatially associated with the Bavlaanskloof Gneiss and HRSZ, Figure 7 (Robb et al., 2006; Rajesh et al., 2020). The Goudplaas Gneiss is found in the low-grade cratonic domain of the HRSZ (Rajesh et al., 2020). It is a highly peraluminous syenogranite that comprises plagioclase, quartz, and minor alkali feldspar (Robb et al., 2006). It also exhibits leucocratic, melanocratic, and pegmatitic alternating layers which occur as flat dipping, sub-horizontal and foliated pegmatitic sheets that have a temporal relationship with the leucocratic gneisses (Anhaeusser, 1992; Robb et al., 2006; Laurent et al., 2013). The leucocratic composition is believed to have been generated during anatexis with the gneissic texture indicating an early-post tectonic lineation with a 050° azimuth and 45° ENE plunge (Anhaeusser, 1992).

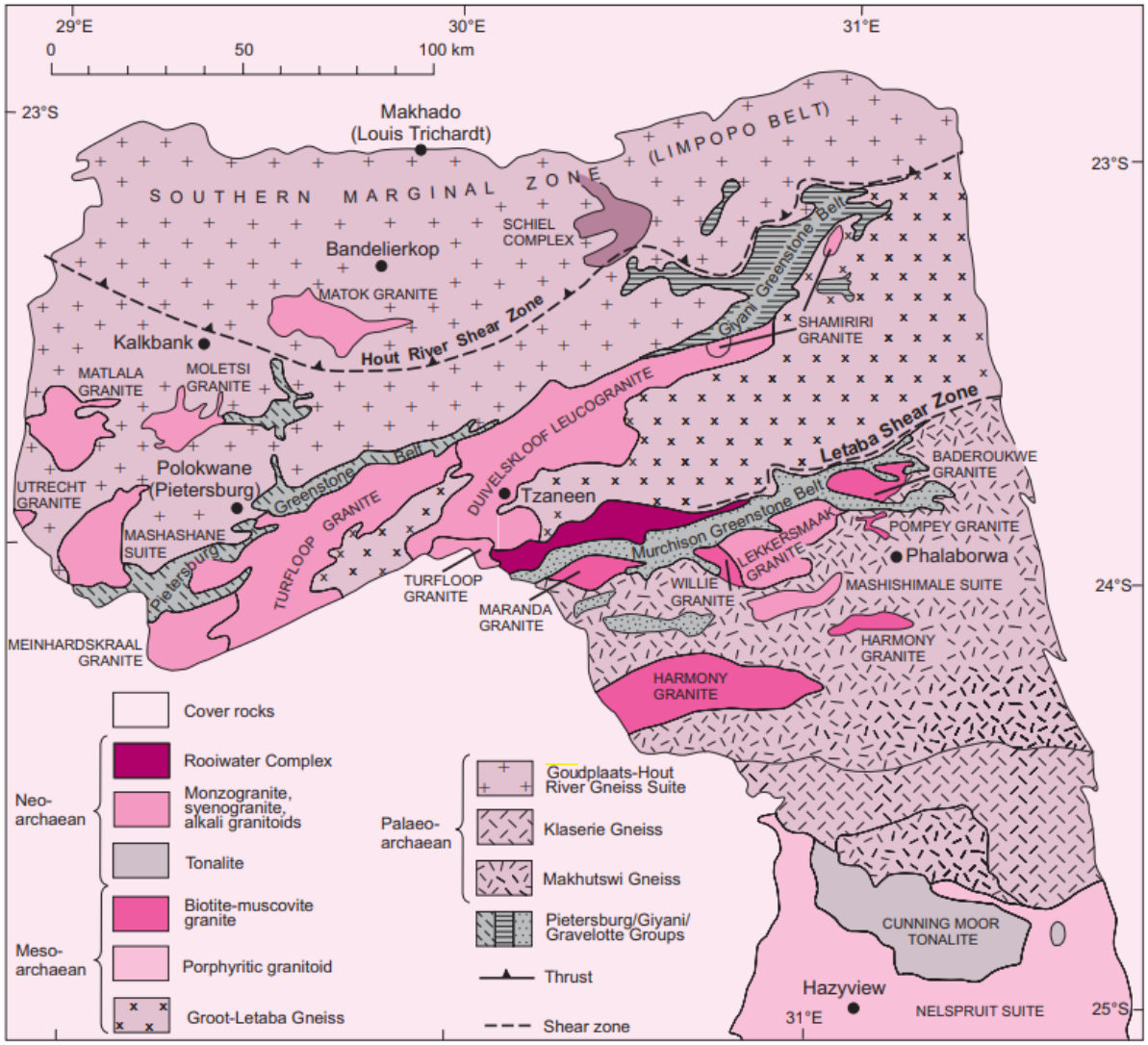


Figure 5*:* Geological map highlighting the different granitoids that occur near the Pietersburg and Murchison Greenstone Belt (Robb et al., 2006).

The Goudplaas Gneiss illustrates two generational phases, an early phase of deformational structures which intersects the light grey gneisses and an older phase of darker amphibolite gneisses (Robb et al., 2006). According to Robb et al., (2006), the Goudplaas Gneiss is considered a Paleoarchean intrusion that was emplaced between 3300 – 2900Ma. The gneiss also contains debris fragments of the PGB's greenstones that are sheared, dismembered, and shredded (Anhaeusser, 1992).

2.2.3 Geysers Granite

The Geysers Granite comprises a biotite granite gneiss that hosts large tourmaline veins and was emplaced between 2900 – 2800 Ma (Franey, 1987; Anthony and Flanders, 1992; Byron and Barton, 1990). It is located along the Eastern margin of the Mount Maré area (Marabastad Goldfield) and contains shear-hosted gold deposits (Franey, 1987). According to Barton et al., (1990) the emplacement of the Geysers Granite is related to the tectonic event related to the deposition of the Witwatersrand Supergroup sediments.

2.2.4 Hout River Gneiss

The Hout River Gneiss is located on the Northern flank of the PGB and was emplaced around 2800 Ma (Byron and Barton, 1990; Anthony and Flanders, 1992). It is similar in composition to the Goudplaas Gneiss (Figure 5) and contains a range of granodioritic, pegmatitic and tonalitic rocks with minor leucocratic biotite gneisses (Stettler and du Plessis, 1988; Anthony and Flanders, 1992). The granites associated with the Hout River Gneiss comprise a hornblende and biotite mineralogy which form a planar fabric whose orientation is parallel to the S2 fabrics of the PGB (Anthony and Flanders, 1992; de Wit et al., 1993).

2.2.5 Turfloop Batholith

The Turfloop Batholith is located on the Southern margin of the PGB (Figure 4) and is spatially associated with the Ysterberg Fault on the PGB's Northern boundary (Barton et al., 1990; Henderson et al., 2000). On the Eersteling Farm, the batholith exhibits an intrusive relationship to the greenstone lithologies of the PGB. Direct offshoots of multiple granite dykes from the batholith crosscut the greenstones (Franey, 1987; Stettler and du Plessis, 1988; Byron and Barton, 1990). The granite dykes have a felsic composition and exhibit sericitization and chloritization (Byron and Barton, 1990; Henderson et al., 2000). These dykes are not sheared and easily weathered, forming a flat surface outcrop that surrounds the PGB (Franey, 1987; Byron and Barton, 1990). The Turfloop Batholith is a Neoarchean intrusion (2700 – 2650 Ma) that forms a North-East trending elongated structure that is similar in age to the Limpopo Orogeny (Byron and Barton, 1990; Barton et al., 1990; Robb et al., 2006). Previous work indicates that the Turfloop Batholith comprises multiple phases of intruding plutons that formed concurrently from a similar magmatic source (Beattie and Barton, 1992; Henderson et al., 2000; Robb et al., 2006).

During the Turfloop Batholith's intrusion, the PGB experienced prograde contact metamorphism from greenschist to amphibolite facies. The batholith was emplaced after the PGB's low-grade metamorphism, Northward thrusting, and regional deformation (Henderson et al., 2000). It has a metaluminous affinity of monzogranite and granodiorite (Anthony and Flanders, 1992; Kröner et al., 2000; Robb et al., 2006). The granitoids that make up the Turfloop Batholiths are medium to coarse-grained and have a grey-green, light pink and grey appearance (Henderson et al., 2000). There is also an increase in gold mineralisation at the contact between the Turfloop Batholiths and the PGB's granites and greenstones. The gold mineralisation was caused by hydrothermal shearing and alteration (Byron and Barton, 1990; Anthony and Flanders, 1992). The various gold deposits that are spatially associated with the Turfloop Batholith are of Archaean age (Henderson et al., 2000). Some of these deposits are hosted in the batholiths shear zones, namely the Palmietfontein and Wildebeesfontein deposits, while the Waterval deposit occurs along the contact of the Turfloop Batholiths with the greenstones (Anthony and Flanders, 1992).

2.2.6 Roodepoort Pluton

The Roodepoort Pluton is located 300 m to the South of the Turfloop Batholith (Beattie and Barton, 1992). According to Franey (1987), the pluton is a product of the evolution of the Turfloop Batholiths magma. The Roodepoort Pluton is a massive, tabular, sheet-like and albitised granitoid that extends over a strike length of 1 km (Barton et al., 1990; Beattie and Barton, 1992). The rock types hosted within the pluton have a leucocratic composition and can be structurally subdivided into two phases (Barton et al., 1990). The Roodepoort Pluton has a sheared contact with the PGB's greenstone and the mineral lineations plunge steeply towards the North (Barton et al., 1990). The pluton is not deformed,

but rather exhibits intense alteration with the quartz-bearing sericite schist it is in contact with (Beattie and Barton, 1992). These areas of alteration are associated with gold mineralisation.

According to Barton et al., (1990), the outcrop appearance of the Roodepoort Pluton follows a folded pattern of the Knights-Pietersburg line. The lineament contains three different gold occurrences: (1) Within the Roodepoort Pluton, (2) Between chlorite – magnesite talc schists and Roodepoort albite contact and (3) Within the dolomite rocks in massive chrome-bearing micas that are associated with chlorite, quartz, and magnesite (Beattie and Barton, 1992). The Roodepoort Pluton intruded a North (N70°) trending shear zone that hosts pyrite with gold inclusions that predate the pyrite growth (Barton et al., 1990; Foster and Piper, 1993). The shear zone also contains quartz filled extensional fractures with the same orientation (Barton et al., 1990). Other minerals found within the pluton include tourmaline, carbonates, and chromium-rich muscovite (Barton et al., 1990).

2.2.7 Lunsklip Pluton

The Lunsklip Pluton is located on the Western and Southern margins of the PGB (Figure 4) and comprises granites with a calc-alkaline affinity (Stettler et al., 1990; Beattie and Barton, 1992). These granitoids are medium to coarse-grained, have a grey to pink-grey appearance, metaluminous composition and a porphyritic texture (Stettler et al., 1990; Anthony and Flanders, 1992; Robb et al., 2006). According to Stettler et al., (1990), the Lunsklip Pluton intruded into the TTG's and the Turfloop Batholith around 2600 Ma. It can also be recognised in the field because of the presence of blue opaline quartz (Robb et al., 2006).

2.2.8 Uitloop Pluton

The Uitloop Pluton is a medium to coarse-grained biotite-bearing granite with a porphyritic texture (Franey, 1987; Anthony and Flanders, 1992). It has a reddish to pink colour appearance, a peraluminous alkali granite composition and was emplaced around 2545±55 - 2687±2 Ma (Robb et al., 2006). The Uitloop pluton can also be found as quartz-feldspar-bearing dykes intruding into older TTG's that surround the PGB (Robb et al., 2006). The pluton exhibits two magma phases that have a distinct transitional contact between them (Franey, 1987). The occurrence of the Uitloop Plutons could be associated with the Bushveld Complex, however, there is no substantial evidence to prove this (Byron and Barton, 1990).

2.3 Deformation Events

The PGB has experienced four deformation events, with the second deformation (D2) event having the greatest impact. The third and fourth deformation (D3 and D4) events can be combined into a single event that only affected the Cover Unit (Anthony and Flanders, 1992). The regional and local structures that represent these deformational events are further detailed below.

2.3.1 First Deformational Event

The first deformational (D1) event occurred before the deposition of the sediments of the Uitkyk Formation and the Cover Unit was not affected by D1 (Franey, 1987; de Wit et al., 1992). The controlling mechanisms that initiated D1 are unknown. However, its existence is supported by: (1) Deformed chlorite and magnetite planar fabrics hosted in the serpentinites of the Simatic Unit; (2) Folded clasts that comprise banded iron formations from the basement of the Simatic Unit; and (3) A well preserved angular unconformity between the Simatic and Cover Units, which indicates that the Simatic Unit was displaced before the deposition of the Cover Units (Franey, 1987; van Schalkwyk et al., 1993; Kramers et al., 2014). The fabrics and East-West trending inclined folds associated with D1

are located along the Western area of the Kuschke Shear Zone and South-Western area of the PGB (Franey, 1987; van Schalkwyk et al., 1993). These inclined folds also produced open anticlinal and synclinal structures in the Southwestern area of the PGB. The same structures occur in the North-Eastern area of the PGB and exhibit a pervasive North – East trending foliation along their axial plane (Kröner et al., 2000).

The first deformational event (D1) is observed on a local scale within the PGB greenstones and only affected specific localities (Anthony and Flanders, 1992). According to Sieber (1991), D1 can be temporally related to the formation of the Limpopo Belts fabric due to crustal thickening, which occurred before the first major peak in metamorphic events associated with the PGB (Sieber, 1991; Beattie and Barton, 1992; Laurent et al., 2013). D1 is also spatially associated with low dipping shear zones, Northward thrusting (2700 – 2760Ma) within the PGB and D2's steeply plunging fold axes (Franey, 1987; Laurent et al., 2013; Kramers et al., 2014).

2.3.2 Second Deformational Event

The second deformational (D2) event is the most dominant of the four deformational events, affecting both the Simatic and Cover Units rock (Franey, 1987; de Wit et al., 1992, Kramers et al., 2014). The D2 event is observed on a regional scale and the PGB's North-Eastern area contains a well-defined stretching mineral lineation (L2) and schistosity (S2) (Franey, 1987; Anthony and Flanders, 1992; de Wit et al., 1992; van Schalkwyk et al., 1993). During D2, numerous Southward dipping, Northwest – Southeast (N 110°) trending shear zones developed which host a pervasive lineation with a 90°plunge (Franey, 1987; Anthony and Flanders, 1992; van Schalkwyk et al., 1993). The shear zones are also the host of high-grade gold mineralisation that occurs within PGB veins (de Wit et al., 1992). According to Franey (1987), there are major folds associated with D2 and the schistosity (S2) preserved within the folds forms their axial planar cleavage. This foliation has a Northeast – Southwest trend that is subparallel to the PGB's major shear zones (Franey, 1987).

High strain zones are more prevalent close to the D2 shear zones and L2 structures are preserved in these areas (Franey, 1987). This observation helps explain why the D2 event is thought to be a period of progressive compressional deformation (de Wit, 1991; Anthony and Flanders, 1992). In deep crustal areas, the D2 shear zones were intruded by granitoids that were emplaced during active tectonism, whereas syntectonic sedimentation occurred in higher crustal regions (de Wit, 1991; Anthony and Flanders, 1992). The D2 event is also accompanied by emplacement of the TTG's between 2867±3 - 2882±3 Ma (van Schalkwyk et al., 1993). It can be assumed that the age of the TTGs' corresponds with D2, which is suggested to have occurred before the South Marginal Zone of the Limpopo Belt thrust Southwards over the Northern margin of the Kaapvaal Craton (van Schalkwyk et al., 1993). The D2 Northward thrusting also produced an extensive Northwest verging foreland which resulted in the formation of a decollement layer along the PGB's basement (Zeh and Gerdes, 2012). The layer comprises an imbricate fan thrust complex and the rocks of the Simatic Units are displaced over the Cover Units (Anthony and Flanders, 1992; Zeh and Gerdes, 2012). According to Beattie and Barton (1992), the D2 event can be linked to a series of events that occurred in the PGB during the Limpopo Orogeny; (1) Gold deposits that formed concurrently with post-peak metamorphism, (2) Carbonate alteration and (3) Granitoid intrusions.

2.3.3 Third - Fourth Deformational Events

The third deformational (D3) reactivated the structural features formed during D2, resulting in D3 isoclinal folds refolding D2 structures within the PGB (Franey, 1987; Sieber, 1991). The third and fourth deformational events (D3 – D4) are both associated with sub-vertical to vertically orientated shear zones (Anthony and Flanders, 1992; de Wit et al., 1992; van Schalkwyk et al., 1993). During D3 and D4 pre-existing D2 shear zones were horizontally and vertically displaced over 8-10km and 3-10km, respectively (Anthony and Flanders, 1992; de Wit et al., 1992). The folds that developed during D2 and D3 have a common axis, however, the axial plane for D3 folds has an offset orientation of 10-20° when compared to the D2 folds (Franey, 1987).

According to Beattie and Barton (1992), the D3 and D4 events occurred before the carbonatization of the PGB. However, during D3 – D4 the PGB granite and greenstone terrane was disrupted (de Wit et al., 1992). Only the cover rocks were affected during D3 – D4. This is observed on a regional scale and considered to have a syn – post deformational age of 2687±2 Ma (van Schalkwyk et al., 1993). The D3 event is also associated with ductile deformation and formation of numerous North (N70°) trending strike-slip shear zones that are separated at 20 km (Sieber, 1991; Kröner et al., 2000). These shear zones also indicate a left lateral displacement of 045° which displaced the Transvaal rock sequence (Anthony and Flanders, 1992; Kröner et al., 2000). Franey (1987), suggested that the D3-D4 events accompanied the intrusion of granitoid plutons as a structural chain reaction.

2.4 Major Shear Zones

The PGB is crosscut by regional East-Northeast and East-Southeast trending shear zones. Some of these structures might have acted as structural control conduits for hydrothermal mineralizing fluids and are namely the Snymansdrift, Hout River, Kuschke, Hollandsdrift and Willemse Shear Zones, Figures 5 and 6 (Franey, 1987; Barton et al., 1990).

2.4.1 Snymansdrift Shear Zone

The Snymansdrift Shear Zone (SSZ) is a D2 event shear zone that forms the brecciated lower contact to the Cover Unit and crosscuts the basal greenstones, Figure 6 (Franey, 1987; Kalbskopf and Barton, 2003). It is observed on a regional scale and extends along the strike of the PGB with a measured length of 5 km and 100 m thickness (Franey, 1987; Kalbskopf and Barton, 2003). The breccia rocks associated with the SSZ indicate a conformable transition zone into the overlying sediments (Franey, 1987). The Snymansdrift Shear Zone comprises metabasic schists that have exhibited an intense foliation, with its tectonic – sedimentary mélange zone containing chaotic breccia clasts (Franey, 1987). These clasts are situated at a higher angle than the shear zones general fabric and indicate no internal deformation. According to de Wit (1991), this mélange zone can be related to an earlier period of bulk shortening and simple shear within the PGB. The supporting evidence includes pervasive D2 thrusts and S2 structures being distributed over the mélange zone area (Jones, 1990; de Wit, 1991).

The Snymansdrift Shear Zone has a NE-SW trend and dips to the SE with a 50-80° dip angle and a down dip plunging orientation (Jones, 1990; de Wit, 1991). It is better exposed in the South marginal boundary of the central Mount Maré area and is considered a high strain zone that forms the allochthonous unit of the Simatic rock sequences (Jones, 1990). The Zandrivier Deposit acts as the central point for the deformation associated with the SSZ and the intensity of the deformations decreases away from the deposit toward the SW and NE (Jones, 1990).

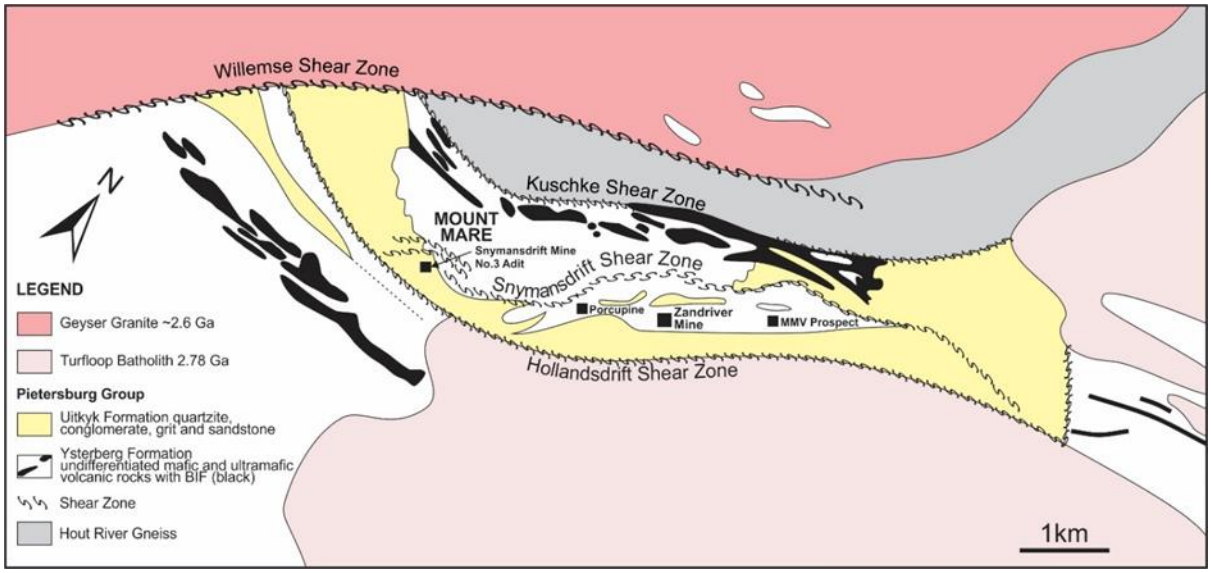


Figure 6: Detailed geology of the Mount Maré area including (1) Locality of the Zandrivier Deposit, (2) Major regional shear zones that go through the area and (3) Surrounding granite-greenstone terrane (Anthony and Flanders, 1992).

Within the Zandrivier Deposit, the Snymansdrift Shear – Mélange Zone can be spatially related to a D2 imbricate fan thrust complex. The relationship between the two structures can either be strained, gradational or conformable across its strike length (Jones, 1990; Kalbskopf and Barton, 2003). The lithologies associated with the shear zone in the deposit comprises (1) Tourmaline and chert-bearing white quartz – mica schists, (2) Chlorite – quartz phyllonites and (3) Quartz augen schists which exhibit a sharp contact with the overlying SSZ (Jones, 1990; Kalbskopf and Barton, 2003). The Snymansdrift Shear Zone contains gold mineralisation with some of the gold hosted in the breccia and conglomerates of the Portberg Mine's (de Wit, 1991). This gold occurs as buckshot inclusions in pyrite grains. Kalbskopf and Barton, (2003) suggest that the Zandrivier Deposit was a resultant of strike-slip movement in the SSZ which created episodes of metasomatism and hydraulic fracturing. These processes later produced a mineral assembly of chrome-bearing micas, carbonates, and quartz within the mélange zone (Kalbskopf and Barton, 2003). The gold mineralisation discovered in the Zandrivier Deposit is structurally controlled and related to tourmalisation or quartz veins (Jones, 1990).

2.4.2 Hout River Shear Zone

The Hout River Shear Zone (HRSZ) is defined on a regional scale as the boundary between the low-grade granite-greenstone terranes of the Kaapvaal Craton and high-grade Limpopo Belt granulite terranes, Figure 5 (Roering et al., 1992; Kramers et al., 2014). It has a steeply dipping orientation to the North, but it tends to flatten further North (Roering et al., 1992; Ruygrok, 1992). The HRSZ has a W-E strike length of 200 -250 km along the Southern Margin of the Limpopo Belt and an estimated width of 4 km (Anhaeusser, 1992; Smit et al., 1992). However, its orientation changes in the central area of the Limpopo Belts South Margins with the development of lateral and frontal ramps. These structures are respectively oblique and subparallel – parallel to the regional foliation of the shear zone (Smit et al., 1992). The Hout River Shear Zone is spatially associated with the D2 NE – SW thrust complex (Figure 7) and it is suggested to have been superimposed over the thrust complex (Anhaeusser, 1992; Roering et al., 1992). According to Roering et al., (1992) the HRSZ was structurally responsible for the emplacement of hot granulite magma by acting as a conduit for H_2O and CO_2 rich fluids.

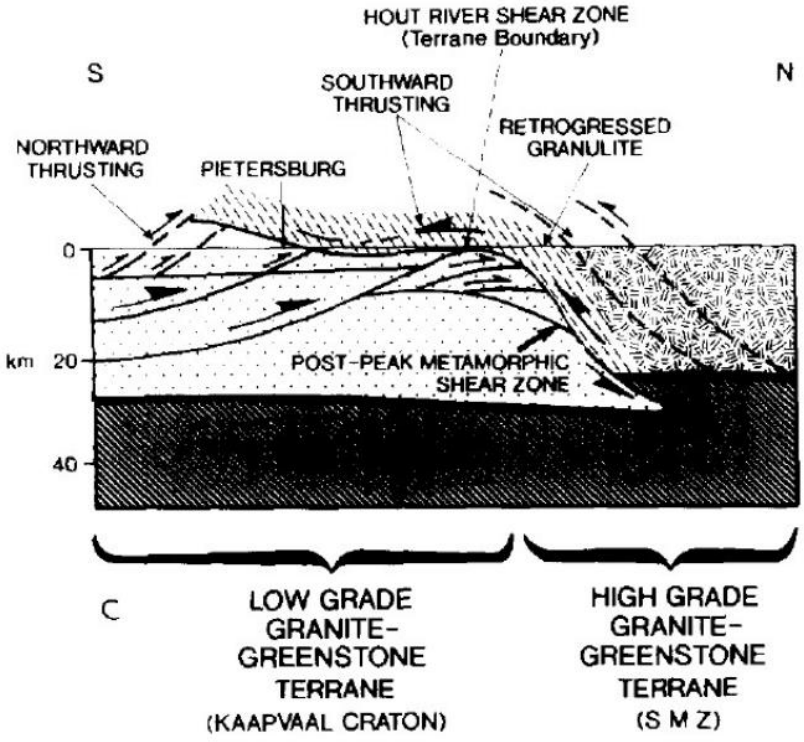


Figure 7: Cross-sectional view showing the Hout River Shear Zone acting as a terrane boundary between the Kaapvaal Craton and Limpopo Belt South Marginal Zone. Northward and Southward thrusting that occurred in the Pietersburg Greenstone belt during the regions deformational events is also indicated, including the direction of lithologies (van Schalkwyk et al., 1993).

The Hout River Shear Zone can also be temporally related to D2 because of decompression and upliftment which indicate ductile movements (Sieber, 1991; Smit et al., 1992). It reactivated earlier formed D1 NE – SW shear zones and resulted in changes in the regions metamorphic grade and mylonitic fabrics (Smit et al., 1992). During 2.96 – 2.69 Ga the Northern area of the HRSZ experienced SW thrusting and the host rocks were transposed over the Pietersburg Block (Zeh and Gerdes, 2012). According to Smit et al., (1992), the HRSZ is better exposed along the Hout River and various lithologies occur along the HRSZ at different localities. These include (1) Greenstone xenoliths with an amphibolite grade, (2) Granitoids with strong planar fabrics that developed during intense deformation and (3) West-Northwest to East-Southeast trending granulites that have undergone retrogression. The HRSZ's Northern boundary also comprises a large-scale fault zone - the Hout River Shear Plane that exhibits D1 folds with variable orientation and forming boudin-rod structures and sheath folds (Smit et al., 1992).

2.4.3 Kuschke Shear Zone

The Kuschke Shear Zone (KSZ) is a high strain shear zone that also developed during D2 (Jones, 1990). It comprises phyllonite which experienced chemical and mechanical weathering, these features are also evident in the Hollandsdrift Shear Zone (Jones, 1990). The KSZ is orientated parallel to the Snymansdrift Shear Zone (Figure 6) and dips steeply towards the SE (Jones, 1990). The rock sequences associated with this shear zone are predominantly volcanic and intrusive with minor banded iron formation (BIF) xenoliths (Franey, 1987). The upper boundary of the shear zone is well defined and located abruptly below the BIF xenoliths. The lower boundary, on the other hand, is less apparent but

can be identified by an increase in the shear zones strain gradient measurements which are indicated by elongated and flattened pillow lavas that form a foliation (Jones, 1990). The greenstone sequences of the Simatic Unit can also be found as shear lenses which are isoclinal folds within the KSZ (Franey, 1987). Certain rocks were faulted during the formation of the KSZ, including (1) Chlorite – quartz ankerite, (2) Talc and chlorite-bearing carbonate phyllonite cherts and (3) Fuchsite - carbonate quartz gneisses (Franey, 1987; Jones, 1990). The Kuschke Shear Zone also contains internal D2 fabrics and crenulation structures that form a horizontal lineation (Jones, 1990). This crenulation foliation formed during the D3 event and is concentrated along the hinge zone of the KSZ (Franey, 1987).

2.4.4 Hollandsdrift Shear Zone

In comparison to the KSZ, the Hollandsdrift Shear Zone (HSZ) is a moderate to high angle D2 shear zone. It has a West-Northwest to East-Southeast strike and dips towards the South-Southwest with a moderate to steep angle, Figure 6 (Jones, 1990). Within the Mount Maré area, the HSZ forms the tectonic transition zone between the greenstone rocks and cover sequence from the Snymansdrift No. 3 Hill (Franey, 1987). The HSZ also deformed the rock sequences of the Uitkyk Formation in the central West area of Mount Maré, making it hard to determine the true thickness of the formation in the region (Jones, 1990). The shear zone comprised of undeformed greenstones and Uitkyk sediments that hosted pillow structures and cross beddings, respectively (Franey, 1987; Jones, 1990). These lithologies represented a piggyback basin after deformation. The HSZ's basal unit comprises chlorite and quartz-bearing phyllonites and gneissic fuchsite quartz-carbonate tectonics from the Southeast to the Northwest region of the shear zone (Franey, 1987; Jones, 1990). The shear zone is also associated with a sinistral sense of rotation that is suggested to form a lateral ramp structure for the adjacent SSZ and KSZ structures in the Mount Maré area (Franey, 1987; Jones, 1990).

2.4.5 Willemse Shear Zone

The Willemse Shear Zone (WSZ) forms part of D3 – D4 events and is also known as the Ysterberg Shear Zone, Figure 6 (Byron and Barton, 1990). During the WSZ 's development, the shear zone truncated the D2 thrusts in the Mount Maré area and can be associated with an extensive crustal tectonic break in the region (Jones, 1990; de Wit, 1991; de Wit et al. 1992). The Willemse Shear Zone illustrates vertical and horizontal displacement as a product of extensional and compressional processes (de Wit, 1991; de Wit et al. 1992). Within this shear zone, crenulation structures with various orientations occur on a much smaller and local scale. The structures that formed during D2 were refolded on a 1-10 m scale when the WSZ developed (de Wit et al. 1992). According to Byron and Barton (1990), the shear zone hosts minor to no gold mineralisation. The time of formation for the WSZ is inconclusive with respect to the Transvaal Supergroup rock sequences. In certain regions, the Willemse Shear Zone indicates movements that may have developed after the deposition of the Transvaal rock sequences, destroying the Uitkyk sediments (Franey, 1987; Good and de Wit, 1997). However, in other areas, the WSZ is found beneath the Transvaal rock sequences.

The Willemse Shear Zone displaces the PGB in a sinistral sense and contains a general strike-slip displacement of 10 km (Jones, 1990). The D3 events earlier movement altered the D2 imbricated thrust fan complex and later reactivated the WSZ (Zeh and Gerdes, 2012). The WSZ can also be identified as a schist zone that is weakly exposed at the surface over a width of 1 km. The granites hosted within this schist zone created a chain reaction of faulting which postdates the granite intrusions (Jones, 1990). The WSZ is an East-Northeast trending regional scale shear zone with a steep dip angle towards the South and is situated along the Thabazimbi – Murchison Lineaments Eastern

extremity (Beattie, 1991; Good and de Wit, 1997). Along the PGB's Northern margin the WSZ truncates the Turfloop Batholith and separates it from the PGB's supracrustal rocks in the SE area (Beattie, 1991). The WSZ also separates the Hout River Gneiss from the Turfloop Batholith in the Northwest region. The WSZ deformation is hosted in the greenstone lithologies as anatomising shear structures, with some of these rock sequences experiencing intense carbonatization (Beattie, 1991; Good and de Wit, 1997). The Willemse Shear Zone also exhibits a flower structure, this is quite evident in high crustal regions where it outcrops (de Wit, 1991; Good and de Wit, 1997).

2.5 Metamorphism

There are four metamorphic peaks observed in the PGB and every period is temporarily correlated with the individual deformation events. According to de Wit (1991), the intensity of metamorphism decreases as one moves across the PGB from North to South.

2.5.1 First Metamorphic Event

The first metamorphic event (M1) affected the Simatic greenstone rocks and occurred before the development of the unconformity between the Simatic and Cover Units (Jones, 1990; de Wit et al., 1992; Ruygrok, 1992). It can be described as an open system event that is related to metasomatic processes (Franey, 1987; de Wit et al., 1992). M1 is synchronous with D1, and tectonically induced fabrics are absent in association with M1 (de Wit et al., 1992; Ruygrok, 1992). This excludes places that contain D1 shear zones. According to Franey, (1987), the evidence that the Cover Unit was not affected by M1 includes greenstone clasts hosted in the conglomerates of the Uitkyk Formation. These greenstones underwent metamorphism but there is no other change related to M1. During M1 the Simatic rock sequences experienced a change from greenschist to amphibolite facies (Franey, 1987; de Wit et al., 1992; Ruygrok, 1992). These rocks were also altered by carbonation and hydration, which occurred simultaneously with large scale movements of elements hosted in these rock sequences, including gold (de Wit et al., 1992; Ruygrok, 1992). These fluid and rock interaction phases are indicated by the presence of pillow lavas (Anthony and Flanders, 1992).

During M1 a modern mid-ocean ridge environment prevailed, with periods of mafic-ultramafic igneous activity and granitic plutons related to hydrothermal and contact metamorphism respectively (Franey, 1987; Anthony and Flanders, 1992). M1 also affected the Limpopo Belts Southern Margin and is associated with prograde metamorphism due to progressive crustal thickening (Laurent et al., 2013). This phase of metamorphism is temporarily related to D1 and can be regarded as a period where metamorphism reached its peak of granulite facies at ca. 2691Ma were P-T conditions were 800 – 850°C and 8.5kbar (Smit et al., 1992; Laurent et al., 2013).

2.5.2 Second Metamorphic Event

The second metamorphic event (M2) is a dynamothermal metamorphic event that is expressed within the D2 shear zones (Anthony and Flanders, 1992; de Wit et al., 1992; Ruygrok, 1992). The metamorphic event was caused by lower to upper greenschist facies that formed after the PGB region underwent greenschist static metamorphism (de Wit et al., 1992; Ruygrok, 1992). According to Smit et al., (1992), M2 was a period of isothermal decompression that resulted after the Southern Margin of the Limpopo Belt rapidly overrode the Kaapvaal Craton along the Hout River Shear Zone. However, M2 and D2 peaks are also suggested to have been resultants of heat expelled during the emplacement of syntectonic granite sheets that deformed and crosscut the D2 shear zones (Anthony and Flanders, 1992; de Wit et al., 1992).

The M2 affected the whole PGB and exhibits the following mineral assemblage: tremolite, actinolite, mica (biotite and muscovite), hornblende and chlorite (Franey, 1987; Anthony and Flanders, 1992). These minerals are associated with the S2 foliation that formed during D2 and subsequently destroyed the M1 texture that had developed at certain localities in the PGB (Franey, 1987).

2.5.3 Third Metamorphic Event

The third metamorphic event (M3) is a late-stage metamorphic peak that is related to the thermal activity created by the Bushveld Complex intrusion, which is located on PGB's Western area (de Wit et al., 1992; Ruygrok, 1992). M3 is sometimes considered to comprise two separate peaks that are related to shearing during D3 - D4 and when the gold during M4 was mobilised into associated shear zones (Anthony and Flanders, 1992; Laurent et al., 2013). Along the Northern margin of the Hout River Shear Zone retrograde isograd processes are observed and isobaric cooling produced a fluid phase (Smit et al., 1992). The P-T conditions related to M3 are 600-620°C and 6 kbar (Smit et al., 1992). According to Ruygrok (1992), M3 can be regarded as a period of static greenschist facies metamorphism. The mineral assemblage associated with M3 comprises D2 brittle mica like ephesite or margarite that occurs as porphyroblasts (Franey, 1987).

2.6 Goldfields

Gold mineralisation in the PGB can be sediment or shear-zone hosted and is situated in the Southwestern region of Pietersburg (Franey, 1987). The gold mineralisation is associated with primary and secondary systems and mainly produced by the Eersteling, Roodepoort and Marabastad Goldfields (Franey, 1987).

2.6.1 Eersteling Goldfield

The Eersteling Goldfield is located along the SW margin of the PGB and underlain by the greenstones of the Eersteling Formation (Byron and Barton, 1990; Sieber, 1991, Foster and Piper, 1993). These rock sequences are intruded by East-West trending, - elongated granitoids whose orientation is parallel to the regional S2 foliation within the goldfield (Franey, 1987). The lithologies in the goldfield can be grouped into: (1) Northern and Southern extremities that comprise albite – actinolite – chlorite schists and (2) Central massive plagioclase-bearing amphiboles (Byron and Barton, 1990). The schists are later crosscut by calcite and quartz veins and the amphiboles indicate less deformation than the schists. These greenstones contain gold mineralisation that is structurally controlled and confined to the: (1) Regional N70° Northwest trending Shear Zones and (2) Local South-dipping Pienaar and Doreen East to West Shear Zones (Byron and Barton, 1990; Foster and Piper, 1993). The local shear zones are products of shearing and deformation that occurred at the contact between the central amphibole and outer mafic rocks from either side. Other local shear zones that developed in the Eersteling Goldfield are the Dog and Maltz Shear Zones, which crosscut the central amphiboles at an oblique angle and later extend into the Pienaar and Doreen Shear Zones (Byron and Barton, 1990).

The Eersteling Goldfield is also spatially related to the regional Nuwe Smitsdorp and Willemse Shear zones (Byron and Barton, 1990). As a result of the Eersteling Goldfields structural complexity, the gold deposits that occur in the goldfield are greenstone shear-zone hosted. These deposits are in the Pienaar, Doreen, Girlie, Maltz, Dog and Unnamed reefs (Franey, 1987; Byron and Barton, 1990). The gold occurs in (1) Brecciated or boudin schists, (2) Sheared quartz veins, (3) Sulphur-bearing BIF (4) Pay shoots and (5) Alluvial deposits (Saager and Muff, 1986; Foster and Piper, 1993). The quartz veins and deformed schists are surrounded by volcanic country rocks that have an actinolite, albite and

epidote mineral assemblage due to regional metamorphism (Saager and Muff, 1986; Sieber, 1991). The sulphur-bearing BIF deposits in the Eersterling Goldfield are stratiform and gold mineralisation was caused by supergene enrichment during weathering (Saager and Muff, 1986). The gold mineralisation is also associated with stages of potassic metasomatism, which was suggested to have produced carbonate veins and pyrrhotite – chalcopyrite mineralisation (Sieber, 1991).

The horizons associated with gold mineralisation and greenstones sequences in the Eersteling Goldfield are displaced by Northeast trending faults which contain 10m thick metamorphosed gabbroic dykes (Byron and Barton, 1990). The areas where gabbroic dykes crosscut the goldfields pay shoots are also associated with high grade - gold mineralisation (Byron and Barton, 1990). These gabbroic dykes experienced metamorphism when the Turfloop Batholith was emplaced (Saager and Muff, 1986; Beattie, 1991). Other structures found in the goldfield are right lateral North to South trending faults which are intruded by dolerite dykes (Byron and Barton, 1990). In comparison to other goldfields in the PGB, the Eersteling Goldfield has produced the largest amount of gold and covers a much bigger surface area, Table 2 (Franey, 1987).

Table 2: Approximation of Gold produced in the Pietersburg Greenstone Belt indicating that the Eersteling farm produced the highest amount of gold. Farms listed in descending order of gold ounces recovered. This table recordings were compiled by Willemse, 1938 (Saager and Muff, 1986).

Farm	**Period**	**Tons of Ore Crushed**	**Fine ounces recovered**
Eersterling 17KS	1906 – 1937	54024	10302*
Snymansdrift 738 LS	1907 – 1910	24071	8948
Roodepoort 744 LS	1905 – 1937	28415	4935
Palmietfontein 24 KS	1907 – 1936	11097	2293
Zandrivier 742 LS	1907 – 1937	5055	1809
Vrischgewaagd 33 KS	1905 – 1937	4712	544
Waterval 18 KS	1913 – 1935	1887	140

2.6.2 Marabastad Goldfield

The Marabastad Goldfield is located along the Mount Maré Range's Southern hills and is clearly shown along the Kuschke Shear Zone (Franey, 1987). The goldfield comprises the Zandrivier Deposit that is situated in the PGB Cover Unit, Figure 6 (Franey, 1987). The deposits in the Marabastad Goldfield exhibit a conformable and cross-cutting relationship with the surrounding chloritoid – ephesite-bearing schists (Kalbskopf and Barton, 2003). The goldfield is a sediment-hosted shear zone deposit (Franey, 1987) and strike-slip East-Northeast trending brittle-ductile shear zones host the gold and sulphide mineralisation (Foster and Piper, 1993). These shear zones also illustrate a reverse dip-slip displacement movement.

2.7 Gold reefs in the Eersteling Goldfield

Gold mineralisation in the Eersteling Goldfield is found in 6 gold-bearing reefs, Figure 8 illustrates 5 of these. These are situated in the Eastern region of the Eersteling Gold Mine - Eersterling Farm and include the Girlie, Pienaar, Doreen, Maltz, Dog and Unnamed Reef (Saager and Muff, 1986; Byron and Barton, 1990).

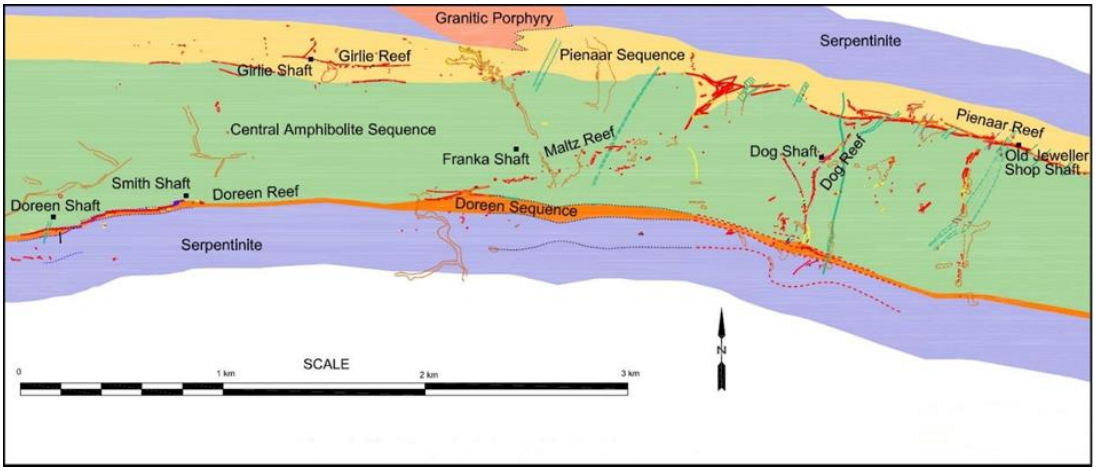


Figure 8: Map showing the different gold reefs within the Eersterling Goldfield and their locations. The also indicates the different lithologies with each reef (Hancox, pers comm., 2021).

2.7.1 Girlie Reef

The Girlie Reef occurs in the Eersteling Goldfields Western area (Figure 8) and has a strike length of 3km, an average width of 0.6m and a mean dip of 60° towards the South, (Figure 8) (Saager and Muff, 1986; Byron and Barton, 1990). The reef is an East to West trending shear zone that comprises iron-rich quartz, carbonates and sericite-bearing schists (Byron and Barton, 1990). As you move Eastwards from the Girlie Reef, the reef encounters the Pienaar Reef and ultimately terminates (Saager and Muff, 1986). The shear zone also contains quartz and tourmaline infill structures which are associated with arsenopyrite and gold mineralisation (Byron and Barton, 1990). Subsequently, the schists in the shear zone only host pyrrhotite and pyrite mineralisation. The gold mineralisation in the Girlie Reef mainly occurs in the reefs pay shoots, which cover a strike length of 640 m (Franey, 1987; Byron and Barton, 1990). The wall rock in the Girlie Reef also exhibits alteration that was associated with metasomatism which later resulted in a change in mineralogy from plagioclase and hornblende to quartz, tremolite, actinolite, and clay (Franey, 1987).

2.7.2 Pienaar Reef

The Pienaar Reef extends over a 6 km East-West strike length, with a width of 0.8 m and an average dip angle of 60° in the South, Figure 8 (Saager and Muff, 1986; Byron and Barton, 1990). These are the orientation and measurements observed for the Doreen Reef because both reefs emerge from the Pienaar and Doreen Complex. The gold mineralisation in the Pienaar Reef is in the Pienaar Shear Zone and hosted in quartz veins which exhibit boudin structures, brecciation and quartz-carbonate alteration (Byron and Barton, 1990). The boudin structures are related to pay shoots which occur along the reef at intervals of 100 - 300 m (Byron and Barton, 1990). These pay shoots are steeply dipping toward the East and contain mineralisation of arsenopyrite, pyrite and chalcopyrite (Byron and Barton, 1990). According to Saager and Muff (1986), the Pienaar Reef illustrates complete oxidation and comprises fragmented greenschists that have no mineralisation.

2.7.3 Doreen Reef

The Doreen Reef displays a parallel orientation to the ultramafic sills that are found on the Eersteling Goldfields Southern area, (Figure 8) (Saager and Muff, 1986). The reef iron-rich schists contain chalcopyrite, pyrrhotite, minor pyrite and no gold mineralisation (Byron and Barton, 1990). There are also 120 m thick down-plunging pay shoots in the reef that contain arsenopyrite, gold and minor pyrite grains which occur in fragmented quartz and chert clasts (Byron and Barton, 1990).

2.7.4 Maltz Reef

The Maltz Reef is an East-Northeast trending reef that extends over a strike length of 1.6km and has a dip angle of 55° towards the Northwest, (Figure 8) (Byron and Barton, 1990; Sieber, 1991). The reef is in the local Maltz Shear Zone that comprises altered amphibole rock sequences and a preserved schistosity that is formed by actinolite and chlorite (Sieber, 1991). The Maltz Reef represents a hydrothermal quartz-carbonate vein system that contains gold mineralisation with an average width of 1.3 m (Byron and Barton, 1990; Sieber, 1991). Gold mineralisation in the reef is concentrated in the pay shoots which are distributed over its length at intervals of approximately 100 m (Byron and Barton, 1990). These pay shoots illustrate a pay shoot within pay shoot relationship with increasing gold grade. The pay shoot comprises (1) Brecciated fragments that are enclosed by calcite; (2) Reef contacts that indicate external fractures that are filled with coarse-grained calcite; and (3) Chalcopyrite and Pyrite mineralisation (Byron and Barton, 1990). There are also 3 cm long tourmaline crystals that are found in the Maltz Reef. The gold grains in the reef occurs as free gold or gold inclusions within pyrrhotite and quartz (Byron and Barton, 1990). The gold is suggested to have developed before the Maltz Shear Zone experienced any shearing or brecciation.

2.7.5 Dog and Unnamed Reef

The Dog Reef is located on the Eersteling Goldfields Eastern area (Figure 8), along with the Unnamed Reef – 700 m away from the goldfield (Byron and Barton, 1990). The Dog Reef extends over an average width of 0.7 m and has a 60° dip angle towards the NW direction (Byron and Barton, 1990). This reef is located within the local Dog Shear Zone that exhibits an S-C structural relationship with the Pienaar and Doreen Shear Zone (Saager and Muff, 1986; Byron and Barton, 1990). The Dog Shear Zone is only associated with gold mineralisation when they occur as inclusion within quartz fragments and boudin structures (Byron and Barton, 1990). The Unnamed Reef is not fully explored but it intersects the Pienaar Reef. It is orientated parallel to the Dog Reef and contains gold mineralisation in quartz boudin structures as well (Byron and Barton, 1990).

2.8 Gold reefs in the Marabastad Goldfield

Gold mineralisation in the Marabastard Goldfield – Mount Maré area is hosted in the Zandrivier Reef. Depending on the host rocks and mineral assemblages, the Zandrivier Reef can be subdivided into the Arsenopyrite and Quartz Vein Reefs (Franey, 1987; Kalbskopf and Barton, 2003).

2.8.1 Zandrivier Deposit/ Reef

The Zandrivier Deposit is situated in the central portion of the Snymansdrift Shear Zone (SSZ) along a zone of low strain, Figure 6 (Franey, 1987; Jones, 1990). The host rock lithologies do not exhibit any intense wall rock alteration and comprise brecciated metasedimentary rocks, chert bars or bands, mudstones, sandstones, quartz-chlorite schists, and quartz-mica schists (Jones, 1990, Kalbskopf and Barton, 2003) (Figure 9). The predominant mineralogy assemblage in the deposit is quartz, carbonates, tourmaline, arsenopyrite, chlorite, gold and minor pyrite and chalcopyrite (Franey, 1987; Jones, 1990, Kalbskopf and Barton, 2003). The gold and arsenopyrite mineralisation in the deposit is suggested to have formed during periods of brittle and ductile deformation, which can be temporally related to D2 tectonism along the SSZ when the shear zones strain intensity decreased (Kalbskopf and Barton, 2003). There are also pay shoots that occur in the deposits central section, which are like the ones that developed in the Maltz Reef. These pay shoots have an E-SE strike trend, plunge towards the S-SSW with a dip angle of 45° and form part of the brittle-ductile regime (Kalbskopf and Barton, 2003). The

Zandrivier Deposit can be subdivided into two gold reefs namely: (1) Deep crustal layered Arsenopyrite Reef and (2) Surface Quartz – Vein Reef (Franey, 1987; Jones, 1990).

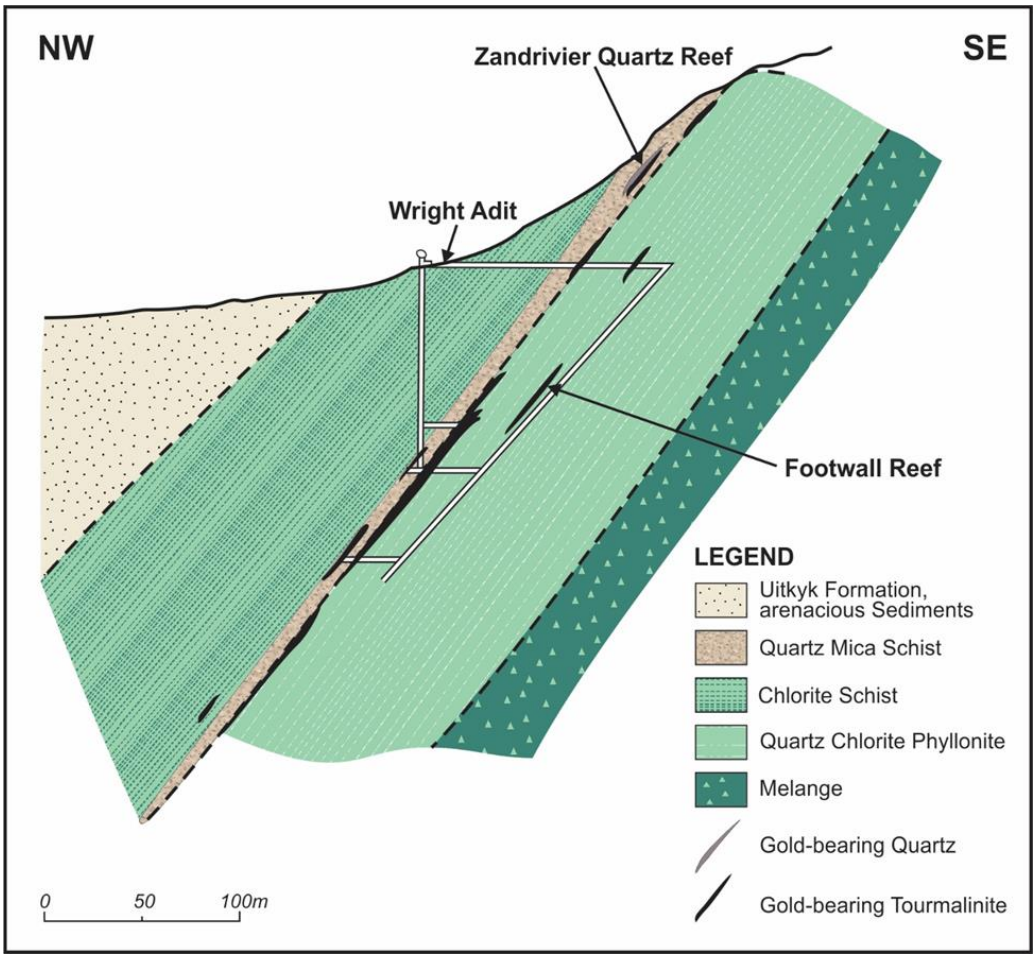


Figure 9: Schematic cross-section of the Zandrivier Deposit showing the geological sequences and the two different workings that host gold mineralisation, upper quartz veins and basal tourmaline- gold-bearing contact between the chlorite schist and quartz-chlorite phyllonite (Kalbskopf, and Barton, 2003).

2.8.1.1 Arsenopyrite Reef

The Arsenopyrite Reef can be identified by a network of concordant quartz-carbonate stockworks and tourmaline-rich quartz-mica schist, with high amounts of arsenopyrite (Franey, 1987; Jones, 1990). In most cases, the quartz and carbonate (dolomite) occur as: (1) Intergrowths or granoblastic layers that are enclosed by chlorite; or (2) Veins that crosscut the country rocks and create fluid conduits for arsenopyrite and tourmaline mineralisation (Franey, 1987). The morphology of the arsenopyrites in the reef is either disseminated grains, undeformed euhedral crystals or fine-grained stringers or inclusions hosted in silicate veins that tend to cut across the larger fractured crystals (Jones, 1990; Kalbskopf and Barton, 2003). In some cases, the undeformed arsenopyrite grains contain inclusions of pyrite, iron-rich sphalerite, pyrrhotite and gold (Franey, 1987; Jones, 1990). The gold grade in the Arsenopyrite Reef illustrates an inverse proportionality to the strain intensity. A gradational contact is observed in the wall rock between areas enriched with tourmaline and the original quartz-sericite phyllonite country rock (Jones, 1990). This contact can be defined by surrounding wall rocks brown colour due to its tourmaline composition of approximately 90-100%.

2.8.1.2 Quartz Vein Reef

The country rocks to the Quartz Vein Reef are metasedimentary rocks from the Uitkyk Formation, with some preserving soft sedimentary deformation structures (Jones, 1990; Kalbskopf and Barton, 2003). Other rock sequences found in this reef are chert bar lenses and brecciated rock fragments that have undergone intense ductile processes (Jones, 1990) Evidence for this includes (1) A shear contact zone between green-brown and knotted grey schists and (2) A regional foliation formed by brecciated clasts in a fault zone (Franey, 1987; Jones, 1990). The foliation has a similar orientation to the one observed in the SSZ but has a lower dip angle between 30-40° (Jones, 1990). The sulphide mineralisation found along and within the sheared contact comprises pyrite and chalcopyrite (Franey, 1987). These sulphides are hosted in smoky-grey quartz veins or between the schists and quartz veins contacts (Kalbskopf and Barton, 2003). The quartz veins are highly fractured and comprise late-stage gold mineralisation and minor tourmaline grains (Jones, 1990).

3. METHODOLOGY

The methods used to satisfy the aim, and research questions of this research reports include hand sample descriptions, petrographic analysis, use of a TESCAN Integrated Mineral Analyser (TIMA) and Strater 5 Borehole Core Logging Software.

3.1 Hand Sample Descriptions

A total of 18 samples were collected from seven different boreholes (Z01, Z02, Z11, GP022, P11, P06c and M03). Z01, Z02 and Z11 were collared on the farm Zandrivier 742 LS and GP022, P06c, P11 and M03 on the farm Eersteling 17 KS. Each sample was described based on its physical characteristics with the intent to provide the rock name, mineral assemblages and general features seen with the naked eye.

3.2 Petrographic Analysis

Specific areas of interest on the 18 hand samples were then marked and cut to make polished thin sections for further petrographic analysis. These thin sections were used to identify the mineral assemblages – ore minerals, textural variations and microstructures associated with the different rock types on a microscopic scale. The analysis was completed using an Olympus B×41 microscope from the University of Witwatersrand's School of Geosciences and included both transmitted and reflected light analysis. There were also photomicroscope images and full section scans of the polished thin sections taken using the Olympus Stream Basic and Olympus Stream Essential software applications, respectively.

3.3 TESCAN Integrated Mineral Analyser (TIMA)

TIMA helps in understanding and quantifying the textural relationship between minerals by mapping the distribution of minerals and mineral inclusions or their occurrence with one another. For this project, the focus was on the occurrence of gold with different sulphide mineral assemblages (Hrstka et al., 2018). The methods that were used to determine the elemental composition of the specific sections in the polished thin section, and to illustrate any gold grains found in association with arsenopyrite or poly - sulphide assemblages at a micro-scale, are Primary Phase and Element Mapping. The samples chosen either had (1) Gold grain inclusions hosted in sulphides which could be seen using a microscope or (2) No gold grains observed when using a microscope even though Au fire assays done by the SGS laboratory in Randfontein indicated high gold grades in that specific sample. The gold fire assays were performed with an Atomic Absorption Spectroscopy (AAS) finish.

The analysis was conducted at the University of the Witwatersrand's School of Geoscience (WAMLAB) and the instrument used was a VEGA3 Scanning Electron Microscope (SEM). The mineral phase and element maps are quantified by energy-dispersive X-ray spectroscopy (EDS). SEM is a method that was used to define the chemical composition and microstructure morphology of the polished thin section or samples surfaces (Zhou et al., 2006). The images taken during this method were used to determine the distribution of grains and second phase particles (Suryanarayana, 2017). The microscope uses the VEGA3 X64 TESCAN TIMA 1.7.0 software application. The beam condition specifications employed for quantitative analysis were (1) Accelerating voltage of 25kV ;(2) Working distance of 21.33mm; (3) Emission current of 43µ; (4) Absorption current less than 1pA; (5) Spot size of 590.00 nm and (6) A specimen beam current of 17.68nA. The filament live time duration was set at 431 hours and the scanning was on resolution mode. The heat and pressure settings were 47% for heat, 1.6×10^{-3} Pa (gun pressure) and $5.5\times^{-3}$ Pa (column pressure).

3.5 Strater 5 Borehole Core Logging Software

This is a geological interpretation method that is used to portray the stratigraphic column of the different borehole logs from the different gold reefs. The data to construct the different borehole logs was provided by the Eersteling Gold Mine and included the lithology, specifications – dimensions, lithological contacts, mineralisation, contact angles and alterations. The successions were then correlated were applicable and used to check if there are any geological or petrological similarities between the reefs, considering the depth of the succession.

4. RESULTS

The results collected from the various methodologies provided information on the lithology, mineralogy, and structural features of the different reefs and samples. In addition, the mineralogy was also analysed using primary phase and elemental maps.

4.1 Lithology and Mineralogy

The host rocks of the Maltz Reef are fine-grained chlorite rich metabasalts that have undergone alteration and metamorphism (Sample M03 - A, B). The mineral assemblage of the metabasalts comprises calcite, quartz, biotite, and cross-cutting amphibole veins, (Figure 10A). The rocks are foliated with chlorite and quartz alternating veins exhibiting a mylonitic texture. The quartz in these metabasalts occurs in two morphologies: (1) Veins and veinlets that crosscut one another and (2) Medium to coarse-grained granoblastic – polygonal grains that are fractured and recrystallised. Chlorite is the dominant groundmass mineral and encloses around biotite crystal boundaries. However, some of the biotite occurs as stringers and chlorite inclusions. Sericitization is indicated on the hand samples with fine-grained white mica forming. The metabasalts are mineralised, and the sulphides are concentrated in chlorite rich areas, specifically as interstitial material or along the chlorite's foliation. The sulphides are shown in Figure 10B and occur as anhedral disseminated pyrite grains with minor chalcopyrite.

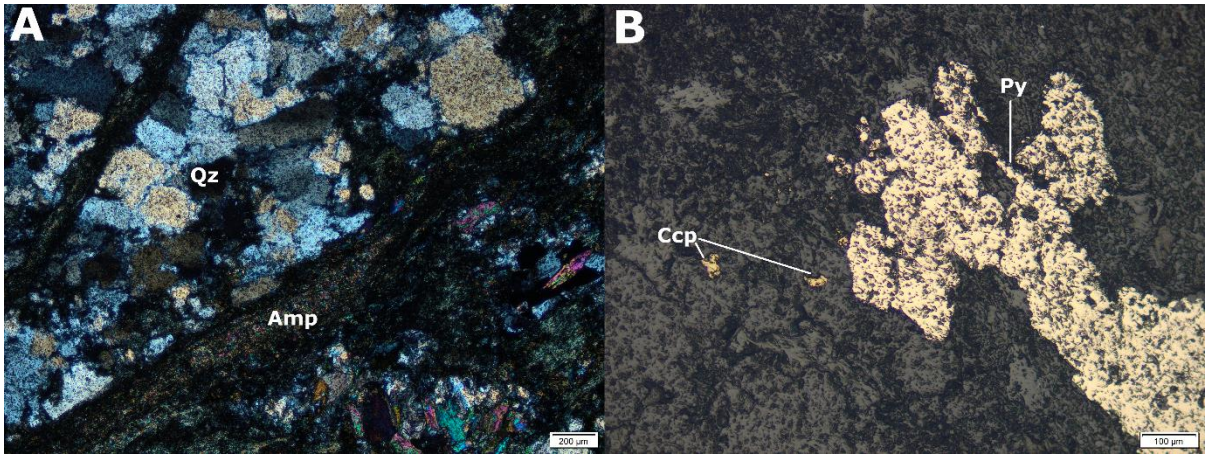


Figure 10: Photomicrographs of samples from the Maltz Reef (A) The mineral assemblage of metabasalts with image showing Qz - quartz groundmass being crosscut by Amp - amphibole veins (Borehole M03 at 75.60 – 75.91 m). (B) Disseminated anhedral sulphides in the Maltz Reef are predominantly Py - pyrite with minor Ccp - chalcopyrite.

The footwall (FW) to the Pienaar Reef is highly metamorphosed, and its host rocks are fine-grained metabasalts with a serpentine, quartz, and carbonates mineral assemblage (Samples P11 – 1A, 1B, 2A, 2B). The metabasalts are crosscut by a network of highly fractured fine to coarse-grained quartz veins that contain thin stringer inclusions of serpentine undergoing serpentinization. In thin section, the serpentine stringers indicate a spatial relationship with the carbonates as shown in Figure 11A. The serpentine encloses carbonate lenses. The quartz vein hosts patches of carbonates that are mineralised with sporadic - disseminated galena, chalcopyrite, pyrite, and sphalerite (Figure 11 B, C and D). In some areas the galena cleavage is observed on the carbonate surface, (Figure 11 C). Parallel deformation lamellae in the carbonates suggest that the metabasalts have also experienced deformation.

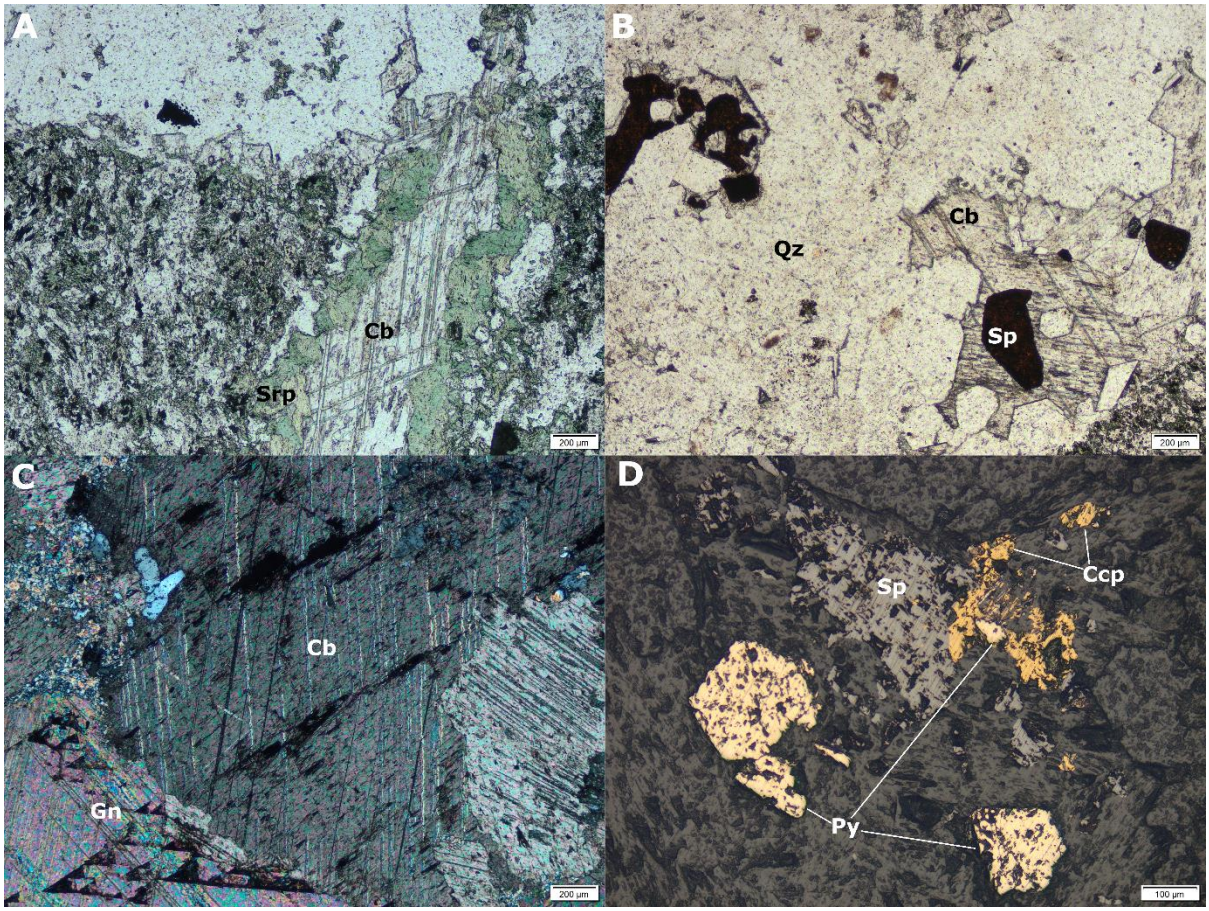


Figure 11: Photomicrographs of samples from the Pienaar Reef (A) Mineral lens that occurs within metabasalts and comprises a Cb – Carbonate (calcite) that is enclosed by Srp - serpentine. The mineral lens is in contact with a large Qz - quartz vein that crosscuts the host rock. In (B) the quartz contains mineralisation of Sp - sphalerite which is concentrated on top of the carbonates in the quartz vein. (C) Carbonate exhibiting deformational lamellae and illustrating a cleavage normally seen in Gn – galena even though the ore mineral has not crystallised completely. (D) Ore mineral assemblage found in the Pienaar Reefs quartz veins which comprise Py - pyrite, Ccp - chalcopyrite and Sp – sphalerite (Borehole P11 at 130.87 – 131.07 m).

There is a sharp and sheared contact between the quartz veins and metabasalts, (Figure 12). In thin section, the contact area is seen as quartz veins that contain medium-grained fragments of the country-rock (metabasalts) closer to the contact between the two lithologies. The quartz veins have also undergone sericitization shown by fine-grained white mica, this is clearly shown in the hand samples. The quartz from the Pienaar Reef samples occur as: (1) Interstitial granoblastic material that surrounds the carbonates; (2) Multiple cross-cutting networks of veins; and (3) Thin veins with micro faulting and successive displacement in a boudin manner.

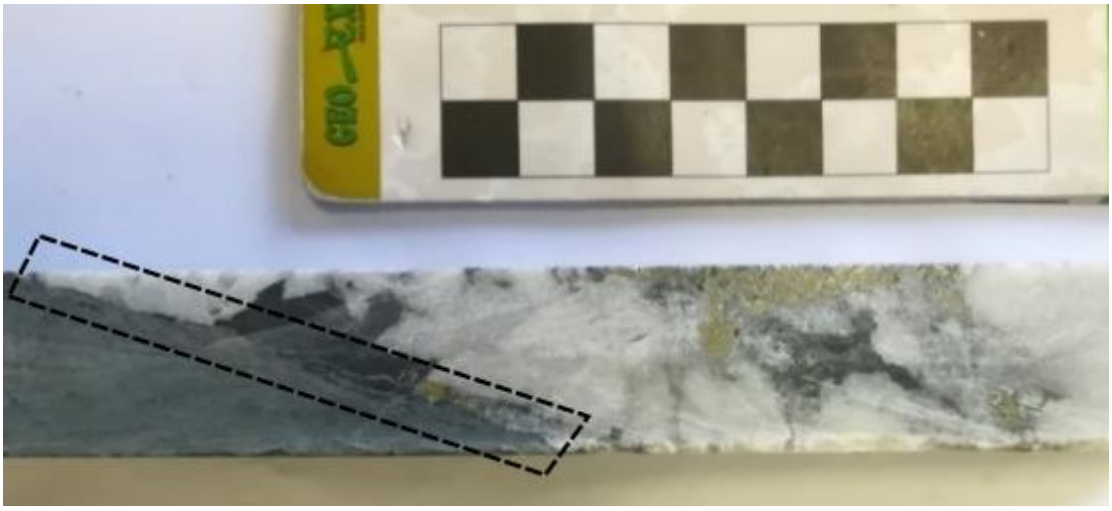


Figure 12: Photograph of the Pienaar Reef's hand sample with an observed sharp-sheared contact between the quartz veins and metabasalts, indicated by a rectangle. The area enriched in quartz also contains sulphide mineralisation (Borehole P11 at 130.84 – 131.07 m).

Footwall (FW) mineralisation to the Pienaar Reef comprises fine to medium-grained disseminated sulphides (pyrite and chalcopyrite) that are concentrated within the quartz veins (Figure 13A). The pyrites have a euhedral to subhedral crystal shape and form aggregates with the same orientation as the serpentine stringer inclusions within the quartz vein. In some areas, the chalcopyrite crystals are anhedral and enclosed by pyrite. The galena is anhedral exhibits perfect triangular cleavage (Figure 13B). In the hand sample, it is also observed that some of the areas where mineralisation occurs created a brown – rust discolouration on the quartz veins. The petrographic and TIMA analysis for this sample clearly showed that these discolouration areas are associated with anhedral sphalerite crystals which contain minor inclusions of chalcopyrite and pyrite.

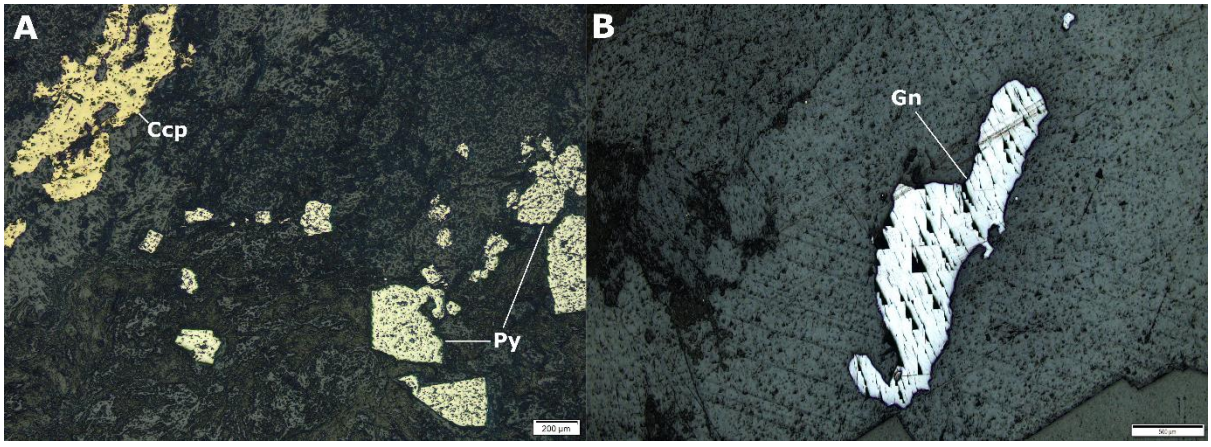


Figure 13: Photomicrographs of samples from the Pienaar Reef (A) Footwall mineralisation of the Pienaar Reef with disseminated Ccp - chalcopyrite and Py – pyrite that is hosted in quartz veins. (B) Anhedral Gn – galena crystal with perfect triangular cleavage, the galena only occurs in the carbonates (Borehole P11 at 130.87 – 131.07 m).

At greater depths in the borehole core, the FW changes into a coarse-grained breccia (Figure 14). The breccia contains angular fragments of quartz, carbonates, metabasalts (FW), fine-grained - tabular shaped amphibole aggregates and a banded rock that contains alternating layers of metabasalts and smoky quartz (Sample P11 – 3). The quartz in this area is fractured and crosscut by late-stage carbonate veins which contain disseminated and interstitial sulphides (pyrite and chalcopyrite).



Figure 14: Photograph of the Pienaar Reefs footwalls hand sample that comprises coarse-grained breccia with angular fragments of quartz, carbonates, amphiboles and metabasalts. The hand sample also contains multiple fractures and cross-cutting quartz veins (Borehole P11 at 1302.34 – 132.43 m).

Hand Samples from the Girlie – Pienaar Reef represent both the hanging wall (HW – Figure 15A) and reef (Figure 15B). The HW comprises fine to medium-grained metabasalts, and the reef comprises a medium to coarse-grained quartz with recrystallised smoky-grey quartz, sulphide mineralisation and areas of alteration which are shown in the TIMA analysis section. The contact between the two rocks is sheared and the rock sample that indicates this transitional boundary is a brecciated mixed zone between HW and quartz reef. The metabasalts (HW) are highly metamorphosed and their mineral assemblages comprise amphiboles, carbonates, quartz veins and serpentine. In thin section, the quartz veins that crosscut the metabasalts are associated with minor disseminated sulphide mineralisation, have a granoblastic texture, and occur as a network of veins. The sulphides are fine to medium-grained anhedral pyrrhotite crystals and are concentrated in areas showing alteration. The pyrrhotite is also associated with minor chalcopyrite that occurs as inclusions and around the margins of the pyrrhotite.

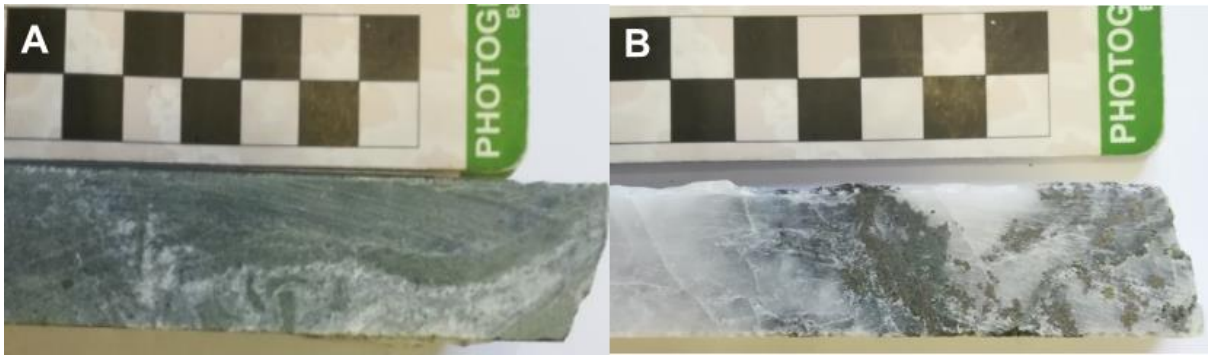


Figure 15: Photograph of hand samples that represent the Girlie - Pienaar Reefs hanging wall (A) and quartz reef (B). Metabaslats and recrystallised quartz make up the handing wall and coarse-grained quartz with pyrrhotite mineralisation make up the quartz reef (Borehole GP022: Hanging wall (A) at 62.60 – 62.80 m and Reef (B) at 73.65 – 73.82 m).

The quartz grains that make up the Quartz Reef are coarse-grained and highly fractured (Figure 16A). These fractures are mineralised and filled with alteration material and carbonates. In some areas, the quartz grains have a granoblastic texture with grain sizes ranging from medium to fine-grained when they interact with the carbonate veins. The carbonate veins also contain inclusions of serpentine. Sulphide mineralisation in the Quartz Reef occurs in the same way as the hanging wall. However, the pyrrhotite crystals are larger, more concentrated and develop within the carbonate veins and quartz fractures (Figure 16A). Other minor ore minerals in the quartz reef are fine-grained anhedral disseminated crystals of chalcopyrite and pyrite, (Figure 16B).

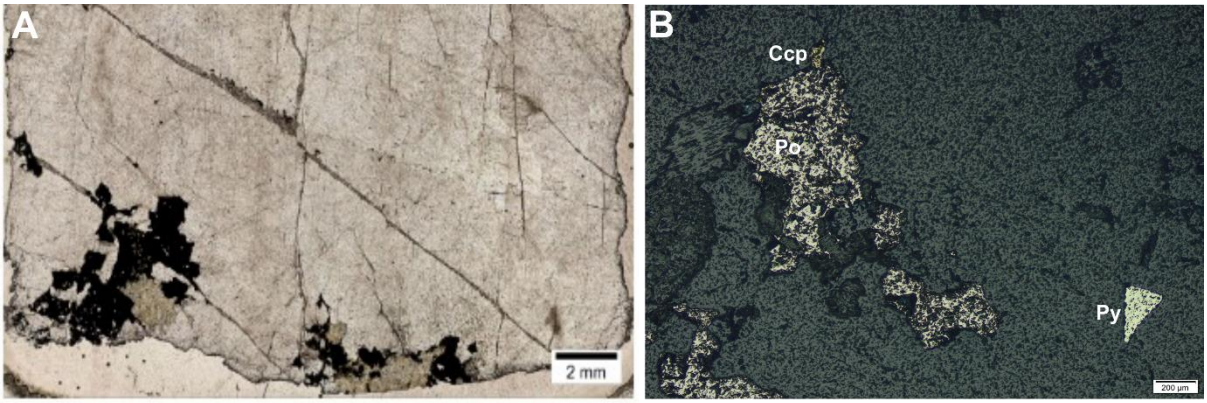


Figure 16: Photomicrographs of samples from the Girlie - Pienaar Reef (A) Full scan image of the Girlie – Pienaar's quartz reef that comprises highly fractured coarse-grained quartz. The fractures are filled with pyrrhotite, alteration material and carbonates. (B) Image showing the different sulphides that occur within the quartz reef. These include Po – Pyrrhotite, Py – Pyrite and Ccp – chalcopyrite (Borehole GP022 - Reef at 73.65 – 73.82 m).

The borehole samples from the Zandrivier Reefs represent the reef and footwall (FW) from three different borehole core logs (Z01, Z02 and Z11). The lithology of the reef from the Z01 and Z02 core show the same characteristics and the host rock is a fine-grained metasedimentary rock that is crosscut by multiple quartz and carbonate veins. The quartz veins displace the carbonates that they intersect. The hand samples also contain medium-grained feldspar fragments and foliated mafic veins. In thin section, the metabasalts indicate intense recrystallisation and their mineral assemblage comprises carbonates, tourmaline, quartz, muscovite, and serpentine. The quartz exhibits a polygonal granoblastic texture, and the fine-grained carbonate groundmass contains thin stringers of serpentine and quartz. The metabasalts from the Z01 and Z02 core logs contain subhedral columnar elongated – needle-like tourmaline but the tourmaline is more abundant in Z02. The tourmaline from the Z02 reef occurs as brown fine groundmass and fracture infill material with a mineral fabric. These tourmalines also exhibit a decussate texture with randomly oriented platy and tabular elongated crystals interlocking. This texture is clearly shown around the edges of the groundmass material in association with granoblastic quartz.

The Z01 and Z02 samples are mineralised with abundant sulphides and contain fine to medium-grained euhedral arsenopyrite in the form of (1) Disseminated crystals, (2) Layered aggregates and (3) Massive fractured anhedral crystals (Figure 17). The arsenopyrite is hosted by quartz and serpentine veins, along with tourmaline that exhibits a mineral fabric.

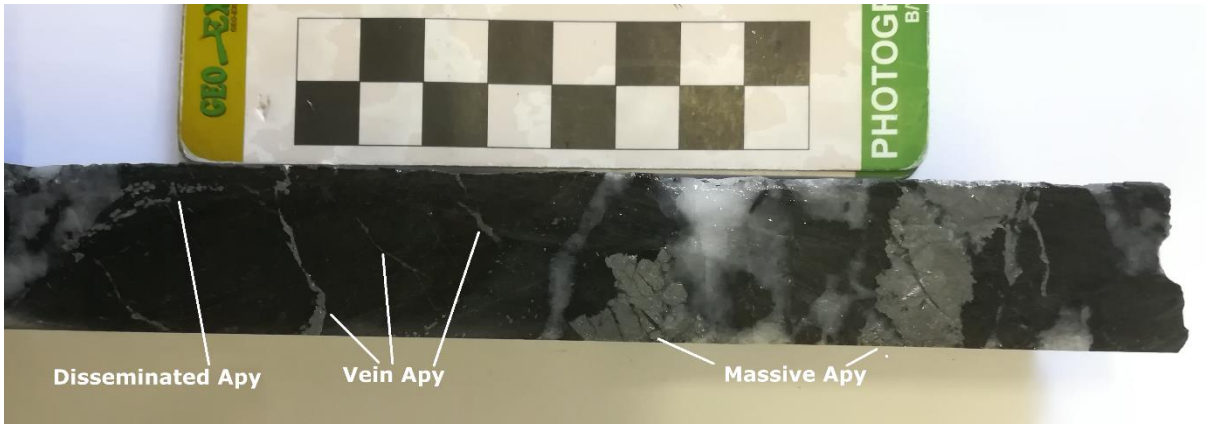


Figure 17: Photograph that shows a hand sample from the Zandrivier Reef (Borehole Z02 at 123.07 – 123.24 m). The hand sample also demonstrates the different styles of Apy - arsenopyrite mineralisation which includes massive, layered, and disseminated grains.

Anhedral arsenopyrite is also hosted in a vein undergoing serpentinization with carbonate developing and enclosing it (Figure 18A). Arsenopyrite is the dominant mineral in the Zandrivier Reef and other sulphides include disseminated anhedral crystals of pyrite, chalcopyrite, pyrrhotite and iron oxides. The chalcopyrite mainly occurs as inclusions within the other sulphides and as fracture fill material in the arsenopyrite. The iron oxides comprise hematite, magnetite and ilmenite which occurs: (1) Along the arsenopyrite grain boundaries; or as (2) Inclusions in sulphides; and (3) Interstitial material between and within quartz and carbonates. Ilmenite and arsenopyrite have a clear spatial association (Figure 18B). These ore minerals, however, are sometimes in equilibrium and occur as poly - sulphides instead. The serpentine also occurs along sulphide boundaries or as infill material in the fractures within the country rocks and creates what appears to be a mylonitic texture. The amount of pyrrhotite mineralisation increases with depth in the Z01 core log and the arsenopyrite also contains micro inclusions of gold which are illustrated in Figure 18 (C and D).

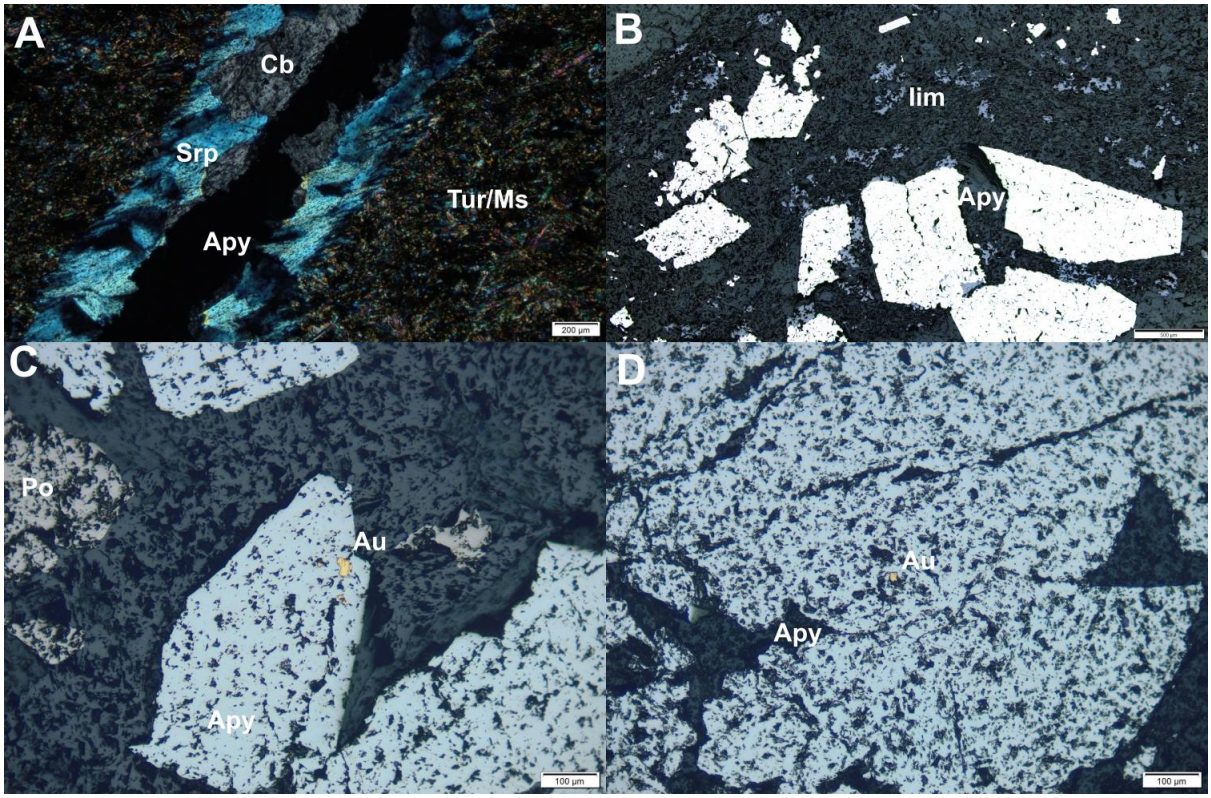


Figure 18: Photomicrographs of samples from the Zandrivier Reef (A) Occurrence of Apy - arsenopyrite mineralisation hosted in a vein that is undergoing serpentinization, Srp - serpentine (Borehole Z02 at 123.07 – 123.24 m). The arsenopyrite mainly occurs on top of carbonates that enclose it. (B) Euhedral – subhedral fractured arsenopyrites that are spatially associated with Ilm - ilmenite (Borehole Z01 at 132.88 – 133.09 m). C and D illustrate massive arsenopyrite crystals that are fractured and deformed with micro inclusions of Au – gold (Borehole Z01 at 184.78 – 185.10 m).

The metasedimentary rocks from the Z11 borehole core log reef also contain the same mineral assemblage as the Z01 and Z02 samples. However, Z11's style of mineralisation is net textured and disseminated with anhedral-euhedral sulphide grains which are concentrated at the contact between serpentine and amphibole veins. The hand sample of Z11 is shown in Figure 19A, and the sulphides differ in occurrence, style, and type when compared to the Z01 hand sample - Figure 17. The ore minerals for Z11 indicate a poly – sulphide assemblage that comprises pyrite, chalcopyrite, and pyrrhotite with inclusions of iron oxides, Figure 19 (B and C). The paragenetic sequence illustrated by the sulphides is chalcopyrite – pyrrhotite + hematite/magnetite. The pyrite and pyrrhotite crystals are also highly fractured and surround fractured quartz.

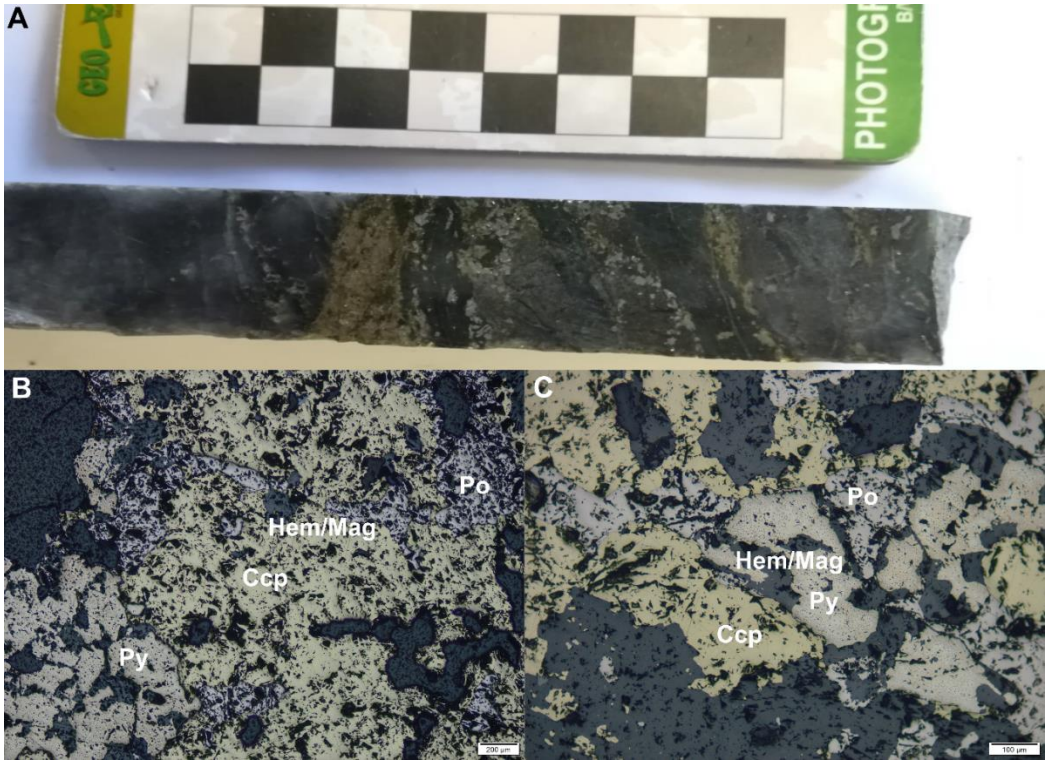


Figure 19: (A) Photograph that represents the Z11 hand sample. The sulphides morphologies are shown under thin section in B and C. These images indicate a poly – sulphide mineral assemblage from the Z11 borehole core log. The sulphides comprise of Py – pyrite, Po – pyrrhotite and Ccp – chalcopyrite with inclusions of Hem – hematite or Mag – magnetite (Borehole Z11 at 235.41 – 235.81 m).

The footwall (FW) rock samples from borehole Z02 comprise fine-grained metabasalts which are crosscut by a network of quartz veins. The metabasalts also underwent intense recrystallisation and alteration. This is supported by granoblastic quartz and tabular – elongated serpentine that forms a mylonitic and decussate texture. The FW is mineralised, and the sulphides preferentially align along the mylonitic foliation. The dominant sulphide is pyrrhotite with minor chalcopyrite and pyrite that contains inclusions of iron oxides. The sulphides occur in different morphologies such as (1) Disseminated anhedral and euhedral grains, (2) Thin mineral stringers or veins that develop parallel to the mylonitic foliation and (3) Interstitial mineral aggregate.

4.2 Structural Features

Different structural features were found in the samples from the Pienaar and Zandrivier reefs and are illustrated below. Specific sections within the samples were further analysed for primary phase and element mapping. It should be noted that the boreholes were not orientated and therefore the orientations for the structural features illustrated in this section are not precise and based on the picture's orientation. The North direction is illustrated on the lower right-hand side for each image.

Sample P11 contains multiple veins that have three different orientations (Figure 20). Quartz vein 1 (QV1) is highlighted in yellow in the image and comprises thin quartz veins with a Northeast to Southwest trend and a micro fault with a North to South trend. QV1 is crosscut by a thicker North to South trending quartz vein (QV2), which is highlighted with red in Figure 20. QV1 is associated with an iron-rich serpentinine – berthierine and calcite, whereas QV2 is associated with disseminated sphalerite, chalcopyrite, and galena. The QV3 has a North to South trend, highlighted with green (Figure 20) and comprises serpentine undergoing hydrothermal alteration. In addition, both the QV3 and micro faulting seen in QV1 have the same orientation.



Figure 20: Full scan image of multiple veins with different orientations. The veins comprise quartz, berthierine and calcite. Some of the veins are mineralised and contain sphalerite, chalcopyrite, and galena. These ore minerals are highlighted with purple in the image and hosted in a quartz vein, which is highlighted in red (Borehole P11 at 130.87 – 131.07 m).

A full scan image of Sample Z01 – 2B illustrates the properties of two different deformational regimes and sulphide occurrences (Figure 21). On the left-hand side of the image, the sample represents a more ductile regime with disseminated euhedral arsenopyrite and anhedral pyrrhotite that is elongated in a specific direction. The right–hand side of the image indicates the brittle regime which comprises (1) Net textured, fractured and massive euhedral – subhedral arsenopyrites and (2) Poly – sulphides that contain pyrrhotite, chalcopyrite and arsenopyrite with associated iron oxides. The ductile and brittle regimes are dominantly mineralised with pyrrhotite and arsenopyrite, respectively. A closer look into the different ore minerals within these regimes is shown in the Appendix, (Figures 42 and 43). The boundary between the two regimes illustrates a sharp contact between the minerals. The host rock for the Z01 – 2B sample contains an iron-rich serpentine – berthierine with two distinct morphologies depending on the regime in which it is found. The berthierine occurs around the arsenopyrite boundaries within the brittle regime and elongates in the direction of pyrrhotite within the ductile regime.

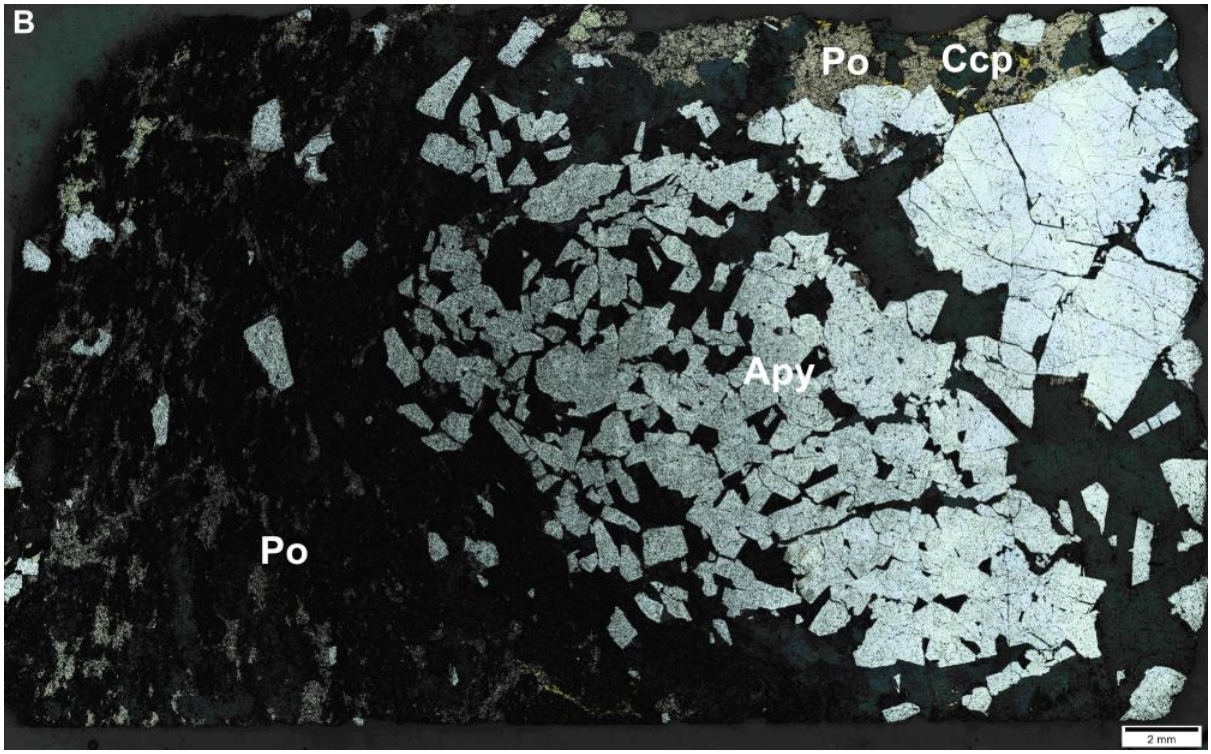


Figure 21: Full scan image showing two different deformations regimes with different sulphide occurrences. The left-hand side represents the ductile regime and contains anhedral pyrrhotite mineralisation. The right-hand side represents the brittle regime and contains net textured, fractured, and massive arsenopyrite mineralisation. The brittle regime also contains pyrrhotite and chalcopyrite poly - sulphides (Borehole Z01 at 184.78 – 185.10 m).

Sample P11 contains boudinaged quartz veins where the quartz pinches out in different sections (Figure 22). The boudin structures in this sample extend in the same direction and have the same orientation. Some of the quartz veins also exhibit a curving morphology.



Figure 22: Image showing different structural features associated with quartz veins (1) Boudin structures and (2) Curving quartz veins (Borehole P11 at 130.84 – 131.07 m).

Sample Z01 – 1B has the same structural features as sample Z01 – 2B but illustrates them in different morphology (Figure 23). The brittle regime is the only deformational phase represented in Figure 23. The arsenopyrite occurs in two different stages; the earlier stage is represented by anhedral, fractured, and massive arsenopyrite crystals and the later stage contains disseminated – euhedral arsenopyrites which is thought to have been deposited by a hydrothermal fluid that intersected the country-rock. This structural feature is highlighted by blue in the image and has a NE – SW trend. The country rock and its associated sulphide mineralisation stages are later cross-cut by quartz veins (highlighted in yellow). The quartz veins contain sulphide inclusions and both structural features (quartz veins and fractures in the arsenopyrites) trend in the NW – SE direction.

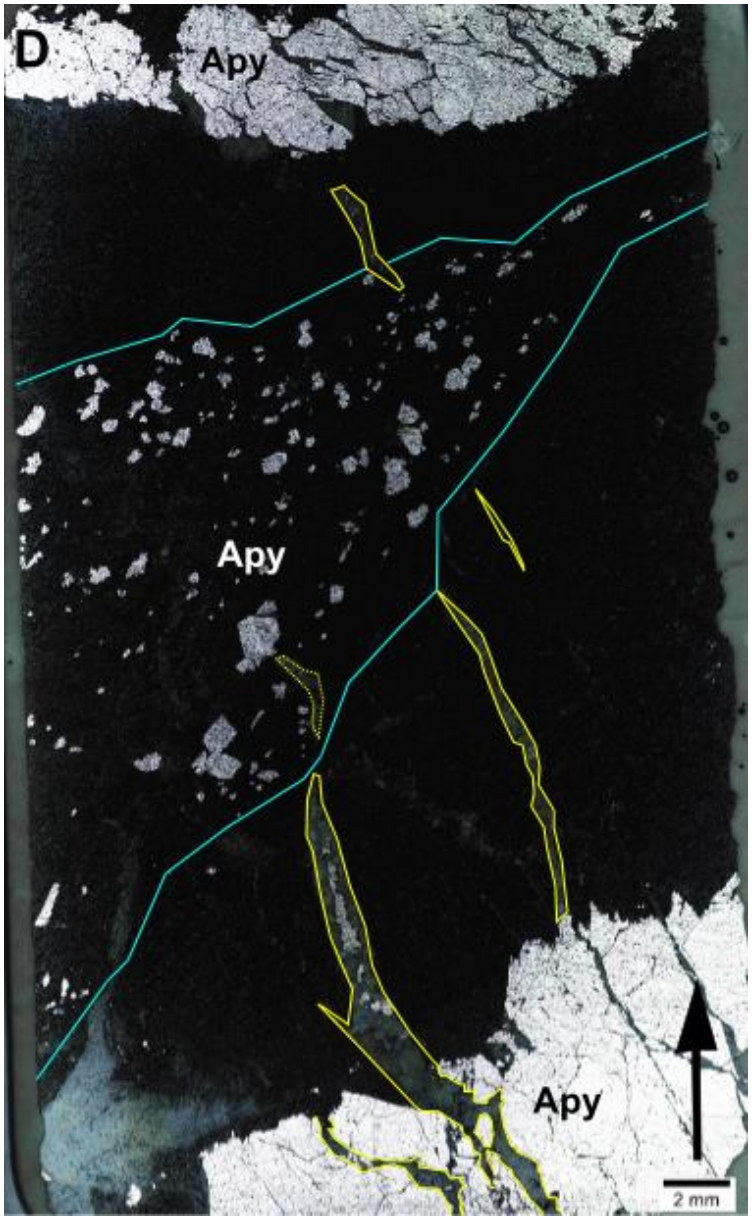


Figure 23: Full scan image that represents the brittle regime with different sulphide mineralisation occurrences. The dominant sulphide is arsenopyrite and occurs as (1) massive, fractured, and anhedral crystals and (2) disseminated - euhedral arsenopyrites which were deposited by a hydrothermal fluid that intersected the country rock (highlighted in blue). The arsenopyrite is later crosscut by quartz veins (highlighted in yellow) which contain small inclusions of arsenopyrite (Borehole Z01 at 132.88 – 133.09 m).

4.3 TIMA - Primary Phase Maps

The primary phase maps are used to provide further information about the samples from the different reef's mineral assemblages and textural occurrences at a greater magnification. The samples chosen from each reef contained high amounts of sulphide mineralisation with a distinctive morphology in thin section. In addition, these samples indicated high gold grade results which were provided by the Eersteling Gold Mine.

P11 – 1A

Primary phase maps indicate that P11 – 1A's mineralisation contains sphalerite, chalcopyrite and pyrite (Figure 24). These ore minerals occur within the large quartz vein (QV2) shown in Figure 20 above. However, the TIMA analysis indicated that the ore minerals only occur in areas rich in calcite (Figures 24 and 25). Further element mapping imaginary identified sphalerite based on its chemical composition and identified the development of micro galena grains along the chalcopyrite and sphalerite grain boundaries. The chalcopyrite and pyrite grains are in equilibrium and micro chalcopyrite occurs as inclusions within the sphalerite. In addition, pyrrhotite also occurs as inclusions in pyrite. The mineral assemblage also contains an iron-rich serpentine - berthierine, which is confined to areas of aluminosilicate alteration. This area of alteration is shown in Figure 25 and it is a representation of the host rocks composition with albite, anorthite and orthoclase developing. The orthoclase is also the only feldspar that is developing within areas enriched with quartz.

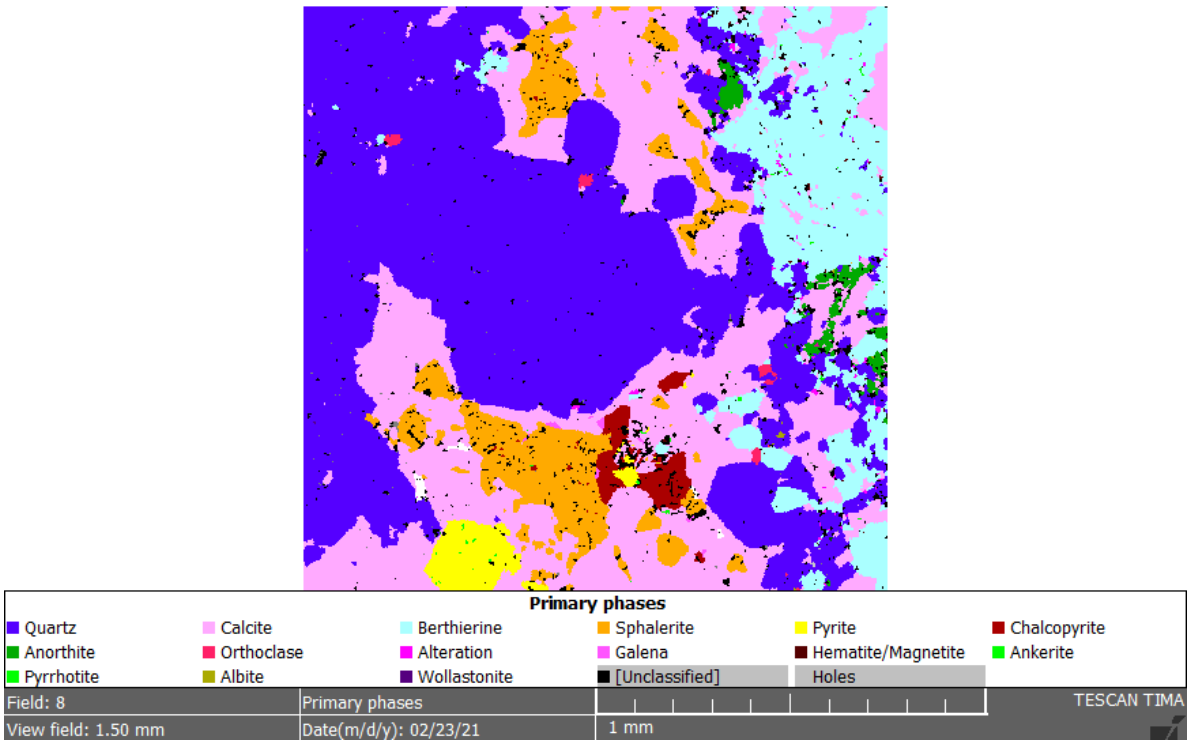


Figure 24: Primary Phase Map of P11 – 1A illustrating a mineral assemblage that comprises chalcopyrite, sphalerite, and pyrite with minor pyrrhotite and galena. The ore minerals only occur within the calcite (Borehole P11 at 130.87 – 131.07 m).

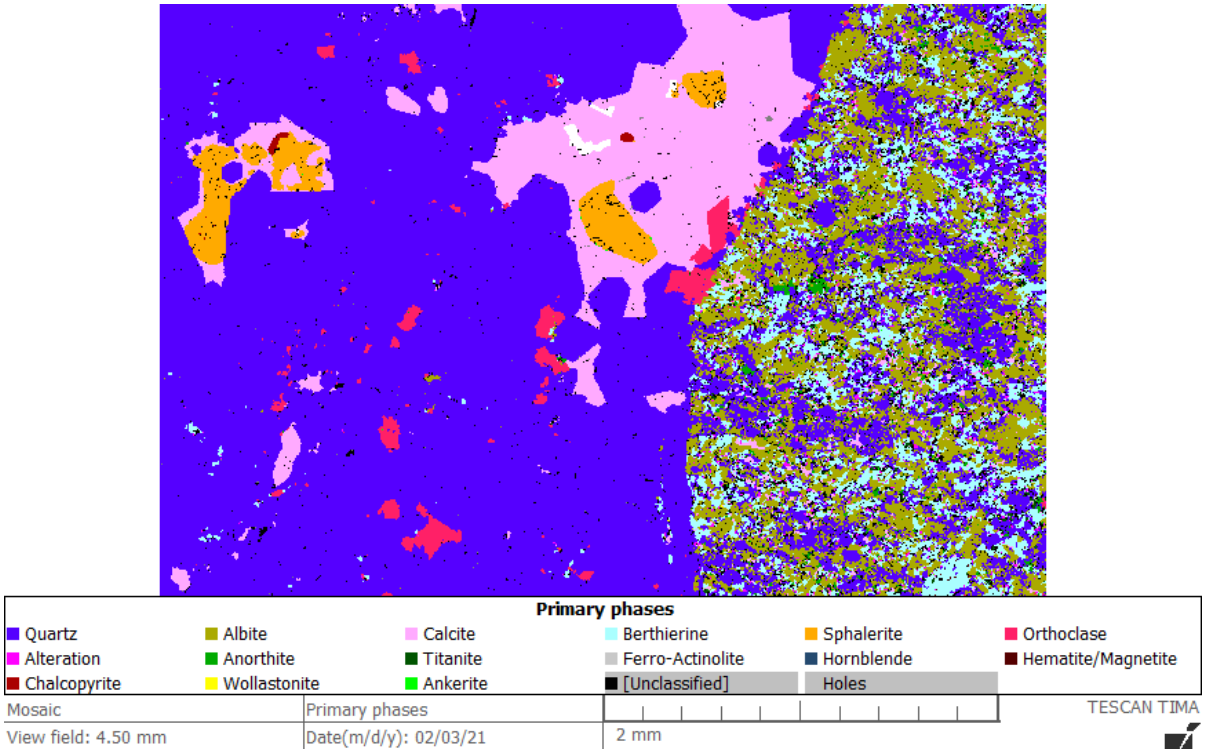


Figure 25: Primary Phase Map of P11 – 1A representing the host rocks composition which is undergoing aluminosilicate alteration. These areas of alteration are also associated with the development of albite, orthoclase and anorthite (Borehole P11 at 130.87 – 131.07 m).

GP02 – 2B

Ore minerals found in the Girlie – Pienaar's Quartz Reef, including their style of mineralisation are shown in Figure 26. According to the primary phase map, pyrrhotite is the dominant sulphide with minor pyrite and insignificant hematite/ magnetite, rutile and titanite. The sulphides are also seen under petrographic analysis; (Figure 16). The mineralisation is only concentrated in fractures that crosscut the quartz host rock and comprise aluminosilicate alteration and calcite veining. These areas of alteration are also associated with the development of ankerite, berthierine and actinolite.

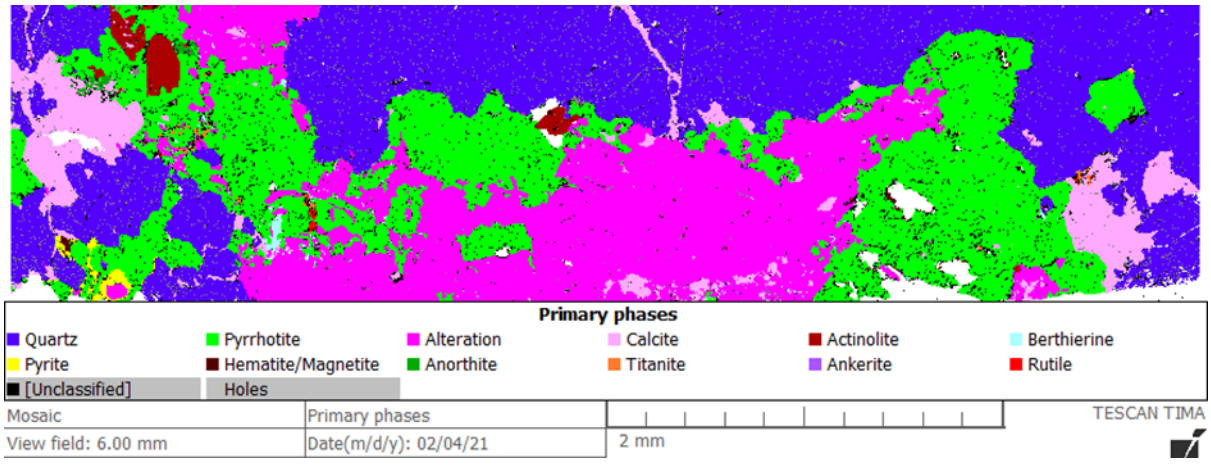


Figure 26: Primary Phase Map of GP02 – 2B indicating that the Girlie – Pienaar Quartz Reef comprises pyrrhotite with minor pyrite, hematite/ magnetite, rutile and titanite. The minerals are also concentrated in areas that have alteration forming (Borehole GP02 at 62.60 – 62.80 m).

Z01 – 1A

In the hand samples, thin sections and primary phase maps from the Zandrivier Reef arsenopyrite is the dominant sulphide mineral. However, the primary phase map (Figure 27), indicates additional minerals that are associated with the host rock. These include muscovite, albite, actinolite, schorl and ankerite. In addition, the muscovite contains ilmenite inclusions and the carbonate associated with Z01 – 1A is mainly ankerite. Other ore minerals that were detected by the TIMA analysis include pyrite, pyrrhotite and hematite/magnetite but their grain sizes make them insignificant. The muscovite in this sample appears to have been deformed in a ductile manner which can be related to the mylonitic texture seen in hand sample.

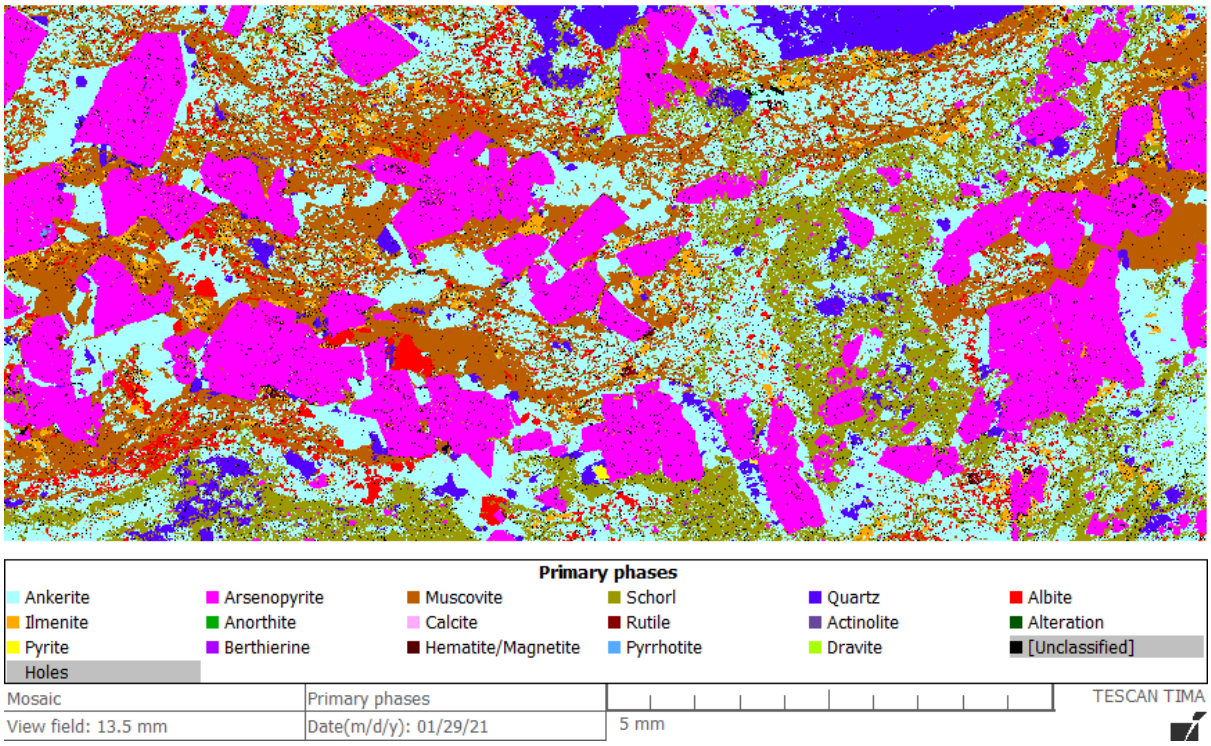


Figure 27: Primary Phase map of Z01 – 1A that contains euhedral – subhedral arsenopyrite grains that occur as layers with associated ilmenite. The map also indicates the host rocks composition which comprises muscovite, albite, actinolite, schorl, and ankerite (Borehole Z01 at 132.88 – 133.09 m).

Z01 – 2B

The arsenopyrite occurs as massive, anhedral, and fractured grains (Figure 28). This primary phase map indicates equilibrium between pyrrhotite, chalcopyrite and pyrite. The pyrrhotite contains inclusions of chalcopyrite and hematite/ magnetite while the chalcopyrite contains inclusions of pyrite which are not visible in thin section. The hematite/magnetite also contain berthierine inclusions. The pyrrhotite and hematite/magnetite also occur as fracture infill material within the arsenopyrite and the contact between the arsenopyrite and pyrrhotite is sharp.

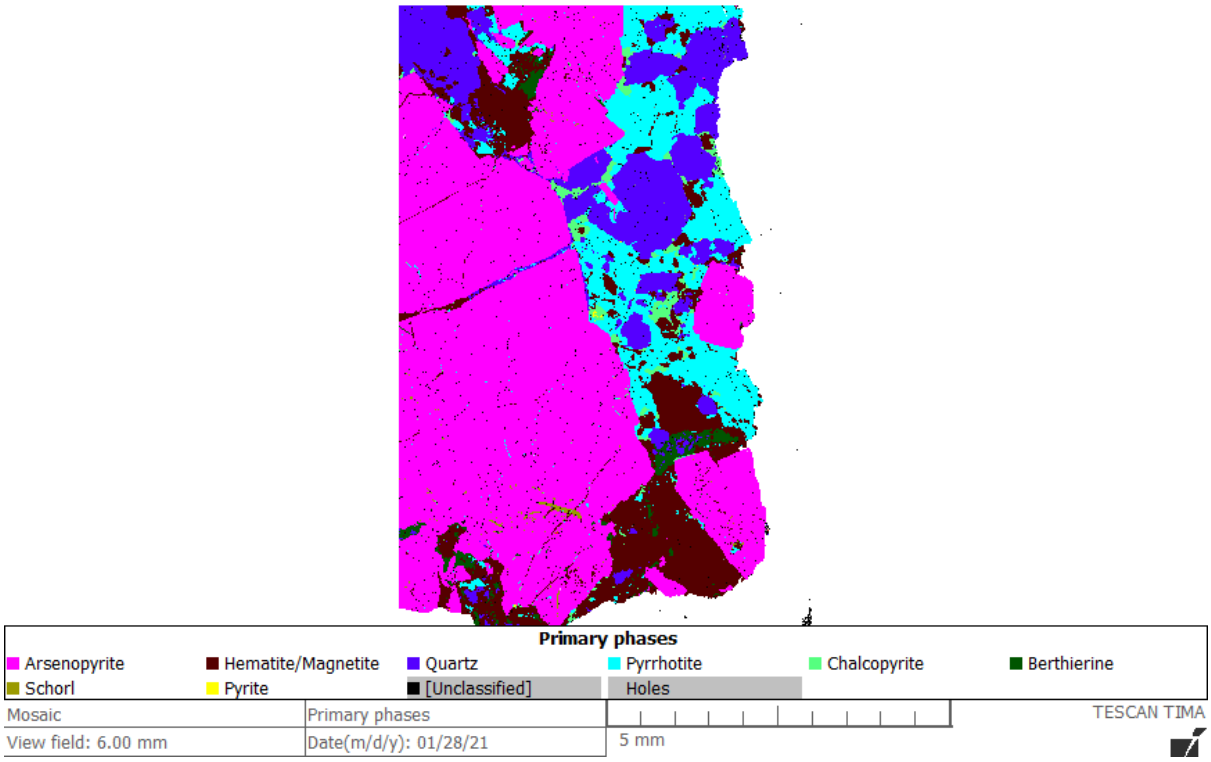


Figure 28: Primary Phase Map for Z01 – 2B which contains massive, anhedral, and fractured arsenopyrite that has a sharp contact with pyrrhotite. The pyrrhotite also contains inclusions of chalcopyrite, pyrite, and hematite/magnetite. The pyrite only occurs as chalcopyrite inclusions and the hematite/magnetite grains are associated with berthierine inclusions (Borehole Z01 at 184.78 – 185.10 m).

Z01 – 2C

The Z01 – 1A and Z01 - 2C samples were extracted from the same borehole core, where the Zandrivier Reef is located. However, the Z01 - 2C (184.78 – 185.10 m) is found at a lower depth in comparison to Z01 – 1A (132.88 – 133.09 m). The primary phase map of sample Z01 – 2C is shown in Figure 30. In comparison with Z01 – 1A (Figure 27), the arsenopyrite morphology in Z01 – 2C has changed into massive mineralisation with a few euhedral crystals. The hematite, berthierine and pyrrhotite concentration has also increased in Z01 – 2C. In this sample, the arsenopyrite and pyrrhotite are in equilibrium. The iron-rich serpentine – berthierine is also concentrated in areas of hematite/ magnetite mineralisation. This spatial relation is also shown in Figures 29 and 30. The pyrrhotite in these primary phase maps occurs along arsenopyrite margins (Figure 29) and contains inclusions of chalcopyrite and minor ilmenite and rutile (Figure 30).

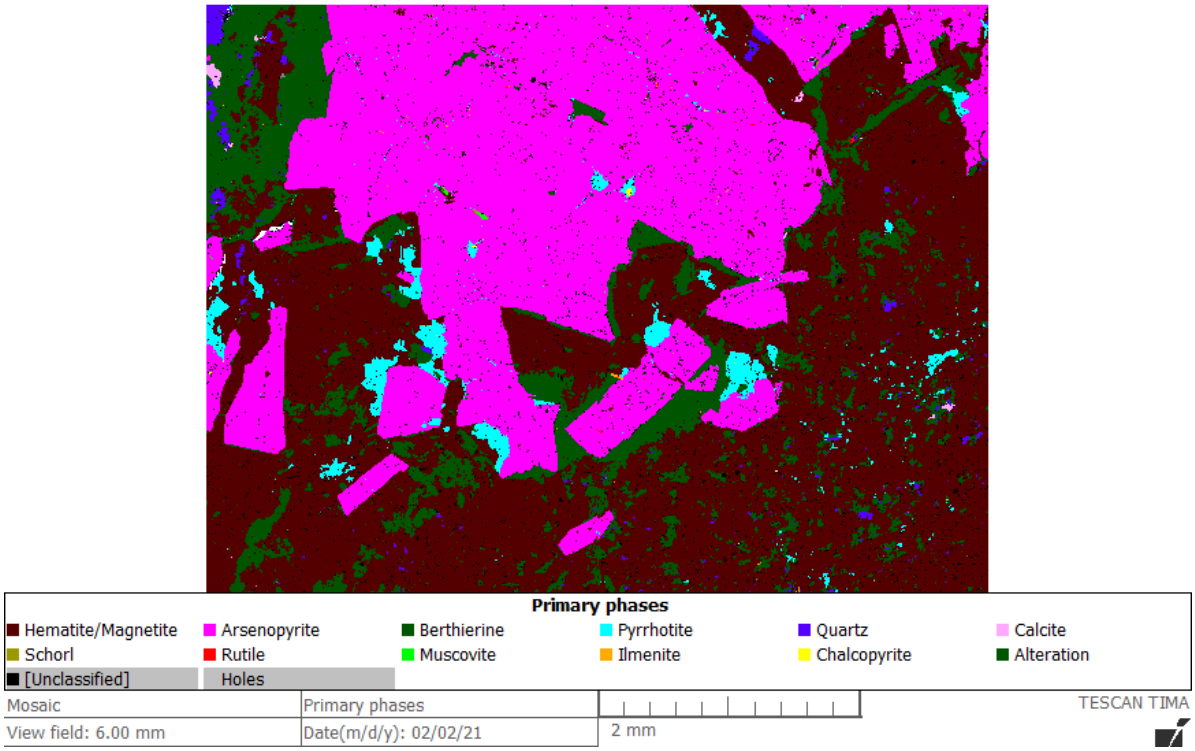


Figure 29: Primary Phase Map of Z01 – 2C representing massive arsenopyrite that is in equilibrium with pyrrhotite and a groundmass of hematite/magnetite that contains berthierine inclusions. The berthierine also surrounds the arsenopyrite and occurs as inclusions within the arsenopyrite (Borehole Z01 at 184.78 – 185.10 m).

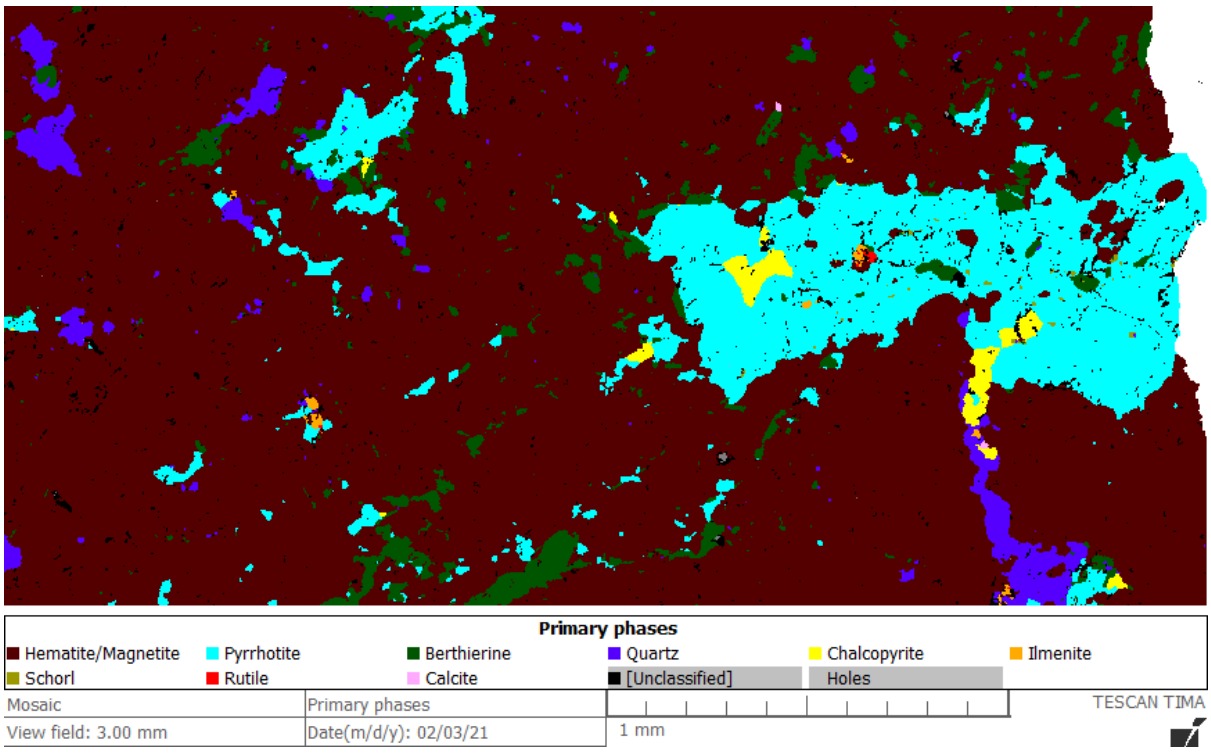


Figure 30: Primary Phase Map of Z01 – 2C showing massive and disseminated pyrrhotite that contains inclusions of chalcopyrite, ilmenite, berthierine, and rutile. The dominant ore mineral in the image is hematite/magnetite and contains inclusions of berthierine, which also occurs along the pyrrhotite grain boundaries (Borehole Z01 at 184.78 – 185.10 m).

Z02 – 1C

Massive arsenopyrite contains micro inclusions of rutile, hematite/magnetite and schorl (Figure 31). The arsenopyrite is fractured and crosscut by carbonate (calcite and ankerite) and quartz veins. These veins are associated with sphalerite and pyrite mineralisation. In comparison to the Pienaar Reef's primary phase maps (Figure 24), sphalerite was only associated with calcite. However, in the Zandrivier Reef, ankerite is present.

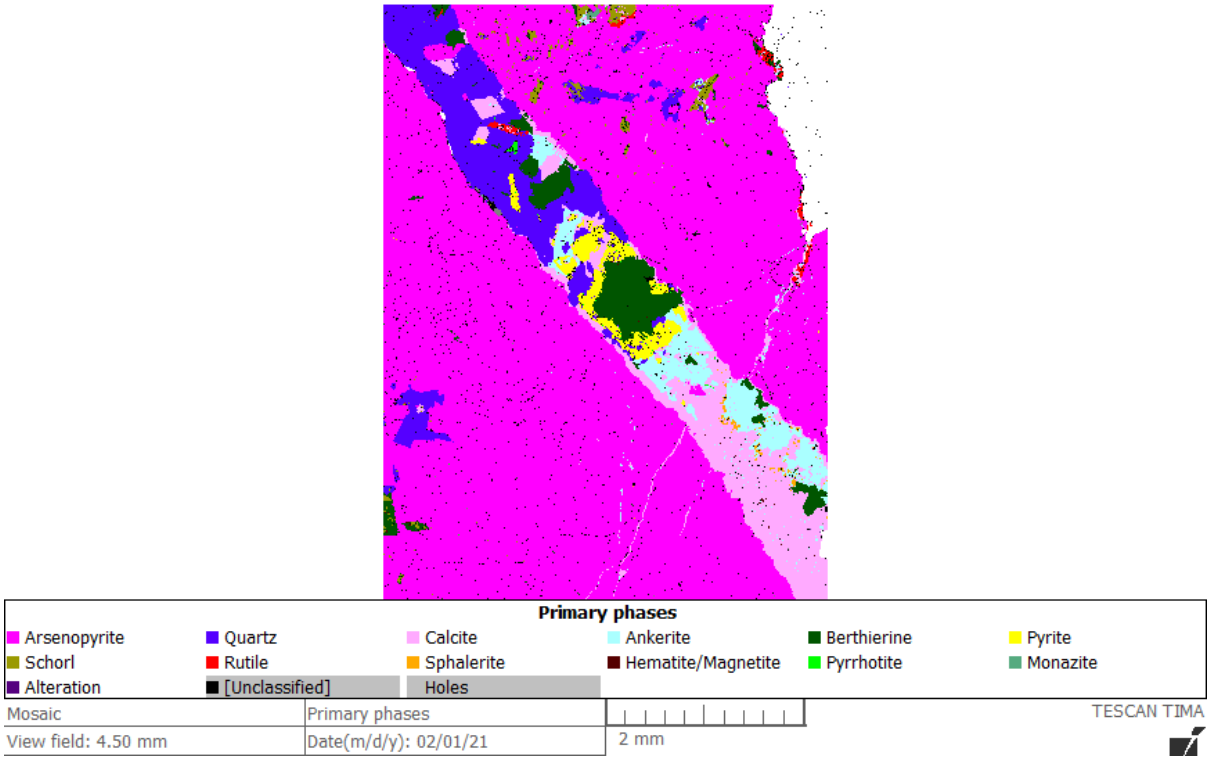


Figure 31: Primary Phase Map of Z02 – 1C with massive arsenopyrite being crosscut by a carbonate (calcite and ankerite) and quartz vein. The vein contains pyrite mineralisation and minor inclusions of rutile, sphalerite and pyrrhotite (Borehole Z02 123.07 – 123.24 m).

4.4 TIMA – Elemental Maps

The elemental maps are used to try and locate gold grains and possibly any variation in trace element contents within the sulphides from the different reefs. These maps are also used to confirm gold grain inclusions found in thin section. The samples chosen either had (1) Gold grain inclusions hosted in sulphides which could be seen using an optical microscope or (2) No gold grains observed in thin section even though gold fire assay data reported by the SGS laboratory in Randfontein indicated high gold grades in that specific sample.

Z01 – 1A

The elemental maps of the Zandrivier Reef host rocks exhibit traces of aluminium and calcium (Figure 32, A and B) which reflect the presence of muscovite, schorl and ankerite minerals identified in the primary phase maps (Figure 27).

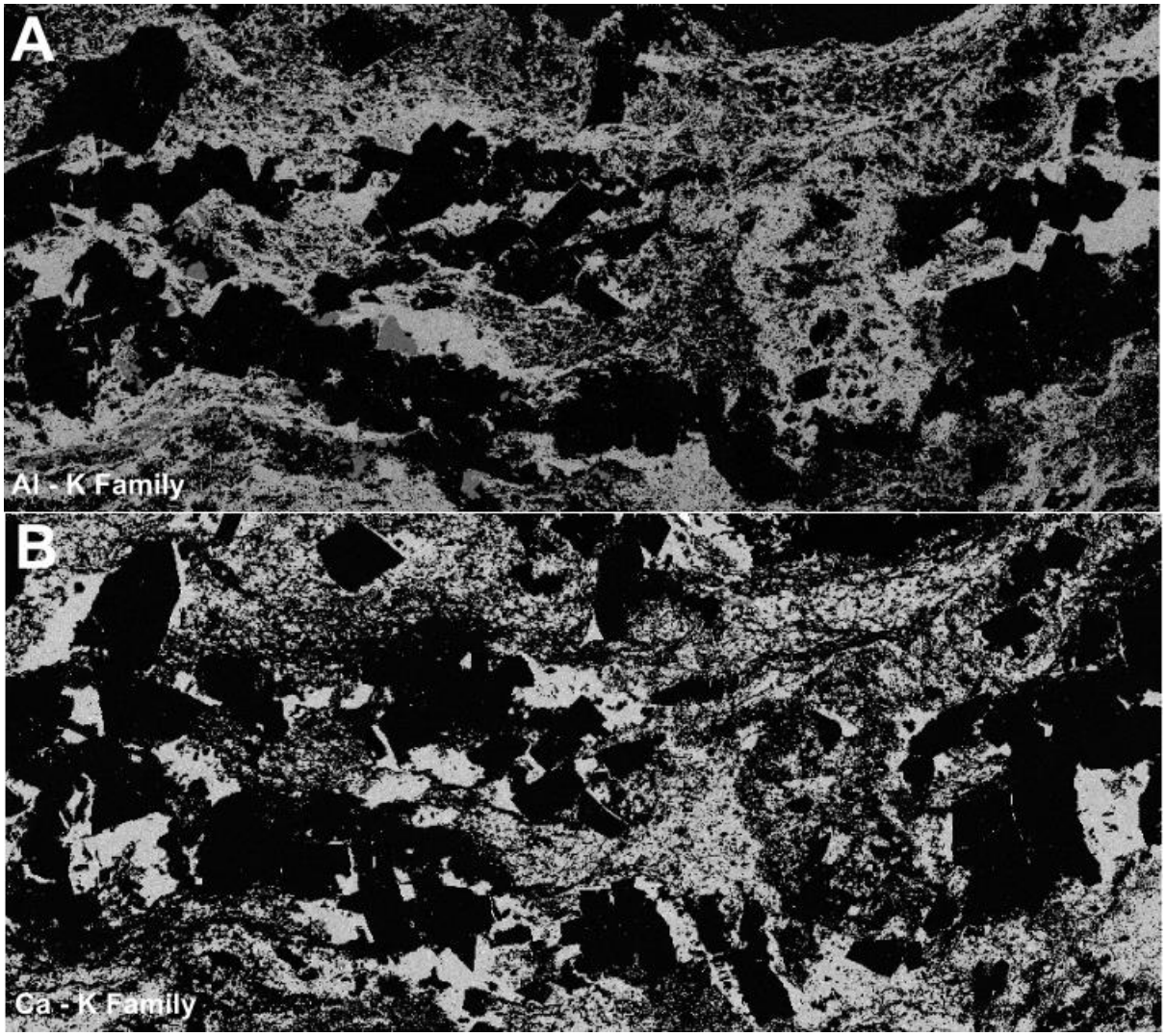


Figure 32: Element Maps showing a field view of 13.5 mm for Z01 – 1A. In A and B, the host rocks composition contains traces of aluminium and calcium which can be associated with muscovite, schorl, and ankerite (Borehole Z01 at 132.88 – 133.09 m).

The element maps also indicate a correlation between arsenic and bismuth. However, the bismuth is not associated with any gold mineralisation. Instead, the gold is found as micro inclusions within the arsenopyrite (Figure 33C). The arsenopyrite is also in equilibrium with pyrite which occurs along the arsenopyrites grain boundaries. In comparison to arsenopyrite, the pyrite contains several gold inclusions (Figure 33 - C1 and C2). The gold grade results retrieved from the Eersteling Gold Mines geochemical assay for the Z01 borehole core log is 4.95 ppm Au at a depth of 132.60 – 133.09 m. This is the same location the Z01 – 1A sample was taken.

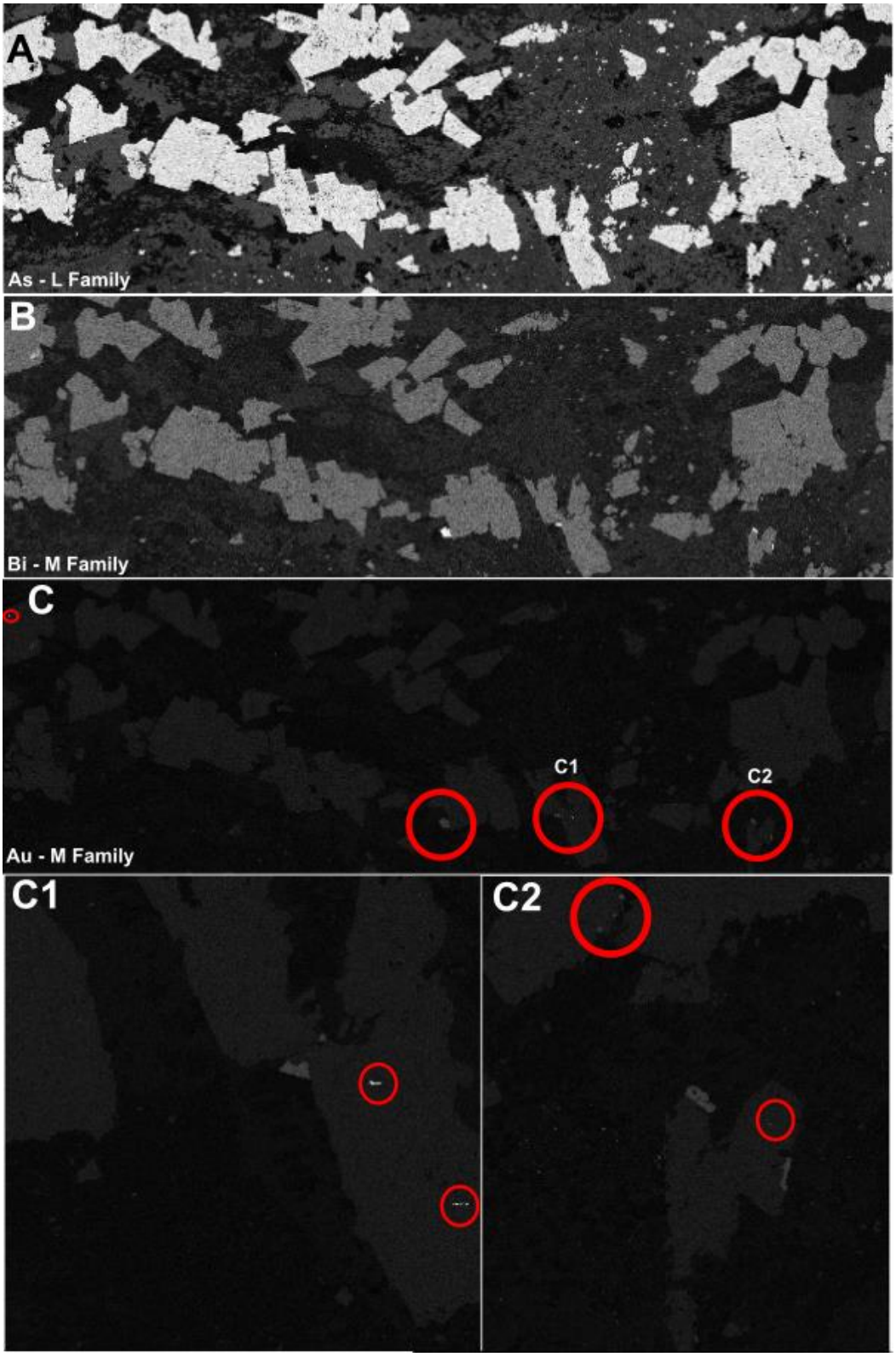


Figure 33: Element Maps (A – C) for Z01 – 1A showing a field view of 13.5 mm. Element Maps indicate arsenopyrite having high traces of arsenic (bright grey) and B associates these areas with bismuth. However, the pyrite and pyrrhotite have a higher bismuth composition in comparison to the arsenopyrite. C focuses on the occurrence of gold with traces of gold being identified as micro inclusions in arsenopyrite and some covering the whole pyrite grains surface area. The different morphologies for gold are shown in C1 and C2. (Borehole Z01 at 132.88 – 133.09 m).

Z01 – 2B

The trace element maps indicate a poly – sulphide mineral assemblage that comprises arsenopyrite, hematite/magnetite, pyrrhotite, chalcopyrite and pyrite (Figure 34 - A, B and C). The gold occurs as isolated inclusions in arsenopyrite (Figure 34D). However, the elemental maps also suggest the presence of gold inclusions in the chalcopyrite, pyrrhotite and pyrite.

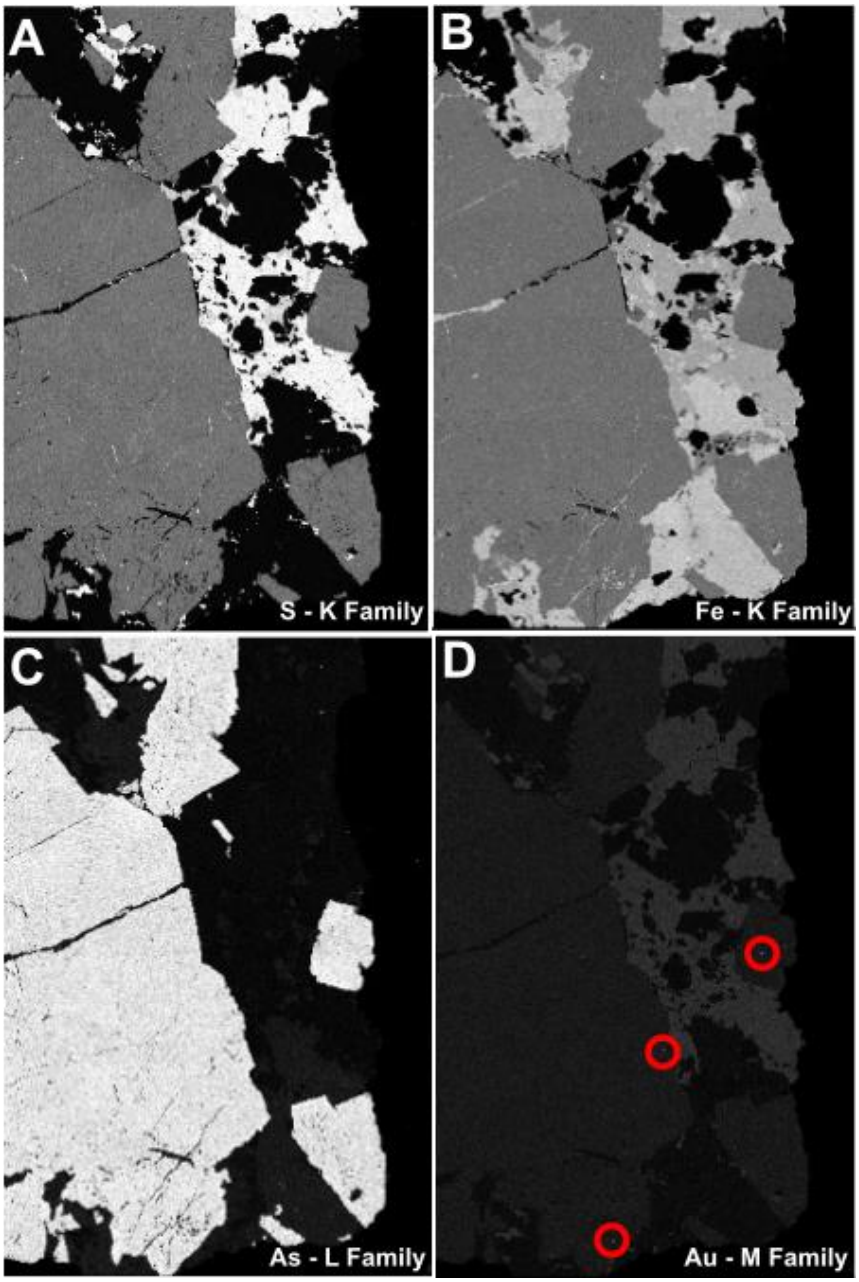


Figure 34: Element Maps for the Z01 – 2B Primary Phase Map showing a field view of 6 mm. In A the poly sulphide mineral assemblage contains predominantly pyrrhotite with inclusions of chalcopyrite and pyrite. The image indicates that the sulphides have a high sulphur composition (bright white – grey). The sulphides also have a high iron composition which is shown in B, however, the amount of the traces of iron detected depends on the mineral. The hematite/magnetite has the highest trace of iron and pyrrhotite and arsenopyrite have the lowest, respectively. In C the arsenopyrite is the only mineral with traces of arsenic. The traces of gold detected in the mineral assemblage is shown in D. The gold occurs as micro inclusions within arsenopyrite (red circles) and as inclusions that cover the whole surface area for the other sulphides – pyrrhotite (Borehole Z01 at 184.78 – 185.10 m).

Z01 – 2C

The elemental maps indicate traces of gold occurring as micro inclusions in arsenopyrite and within the pyrrhotite grains (Figure 36E). Figure E1 shows the elemental map at a greater magnification and covers a field of view of 1.5mm. The gold inclusion shown in Figure 36 - E1 is also detected under an optical microscope (Figure 19C). The gold grade determined by the SGS laboratories gold fire assay is 7.27 ppm Au for this sample.

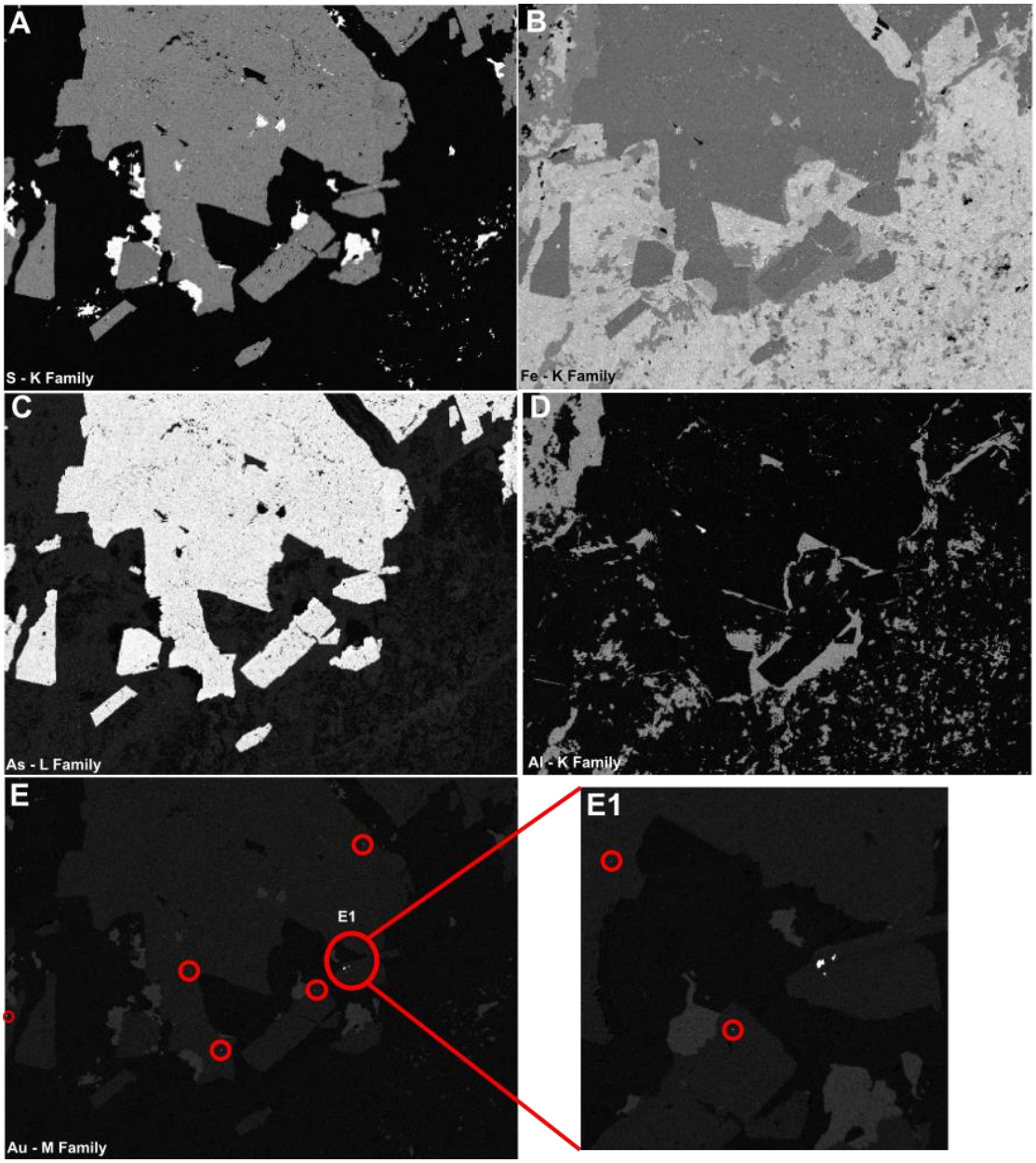


Figure 35: Element Maps for the Z01 – 2C Primary Phase Map showing a field view of 6 mm. In A the pyrrhotite and arsenopyrite represent a poly – sulphide and pyrrhotite has a higher trace of sulphur (bright white). However, the arsenopyrite has a higher trace of arsenic which is shown in C. The element map in B indicates a very high background of iron composition which is associated with hematite, magnetite, berthierine and pyrrhotite. The arsenopyrite on the other hand does not contain significant iron that could be detected by the TIMA analysis. In D the iron serpentine – berthierine indicates an aluminium composition. The gold traces detected are shown in E and E1. The gold occurs as micro inclusion within the arsenopyrite and inclusions that cover the pyrrhotite surface area (red circles). In E1 there is a larger gold inclusion detected (bright white) which can be seen under the microscope. This gold inclusion has a bigger grain size in comparison to the other gold inclusions detected (Borehole Z01 at 184.78 – 185.10 m).

Z02 – 1C

Traces of gold are associated with areas of high sulphur and bismuth concentrations (Figure 36A and 36C). The gold cannot be seen under an optical microscope but rather occurs as micro inclusions. In comparison to the Z01 samples, the arsenopyrite from the Z02 borehole core does not contain any visible gold inclusions. A gold fire assay performed by the SGS laboratory for the Z02 borehole core log at a depth of 123.06 – 123.51m yielded a gold grade of 4.65 ppm Au. With the gold grade increasing by approximately 35% at a lower depth of 133.36 – 133.87 m, reaching 7.15 ppm Au.

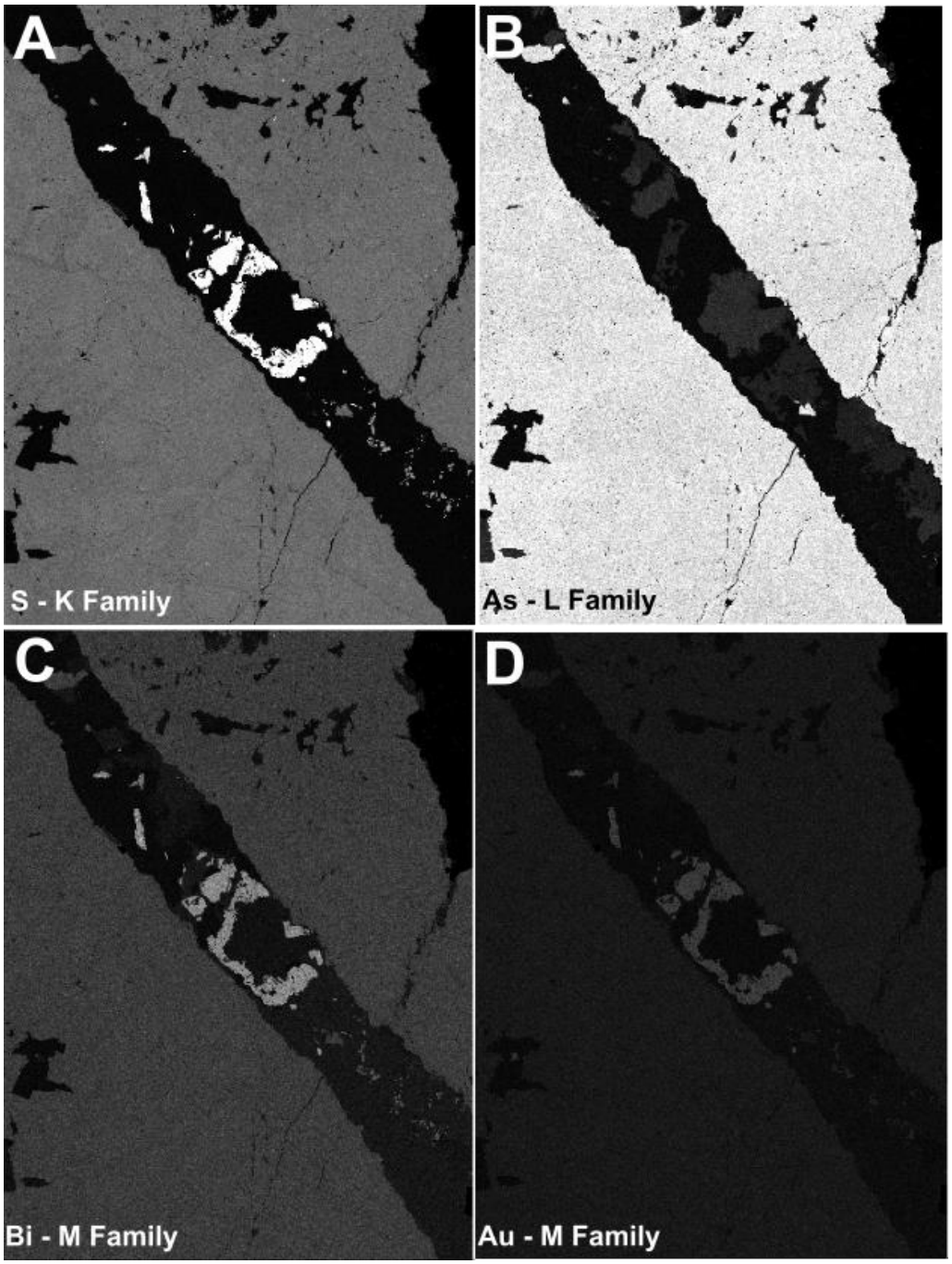


Figure 36: Element Maps for the Z02 – 1C Primary Phase Map showing a field view of 4.50 mm. In A the areas that indicate high traces of sulphur which are associated with pyrite and pyrrhotite mineralisation. These sulphides occur only in the quartz, calcite and ankerite vein that crosscuts the massive arsenopyrite. In B traces of arsenic are shown in arsenopyrite. In C traces of bismuth are shown in arsenopyrite, pyrite and pyrrhotite. The gold traces in D only occur as inclusions that cover the pyrite and pyrrhotite surface areas. The areas of gold traces can be associated with traces of bismuth (Borehole Z02 123.07 – 123.24 m).

P11 – 1A

The elemental maps for this sample indicate high traces of sulphur, zinc, lead, and iron (Figure 37), which is associated with sulphides. However, the lead elemental map is misleading because there are no lead-bearing minerals observed in this sample. The Pb and Au elemental maps represent an overprint in trace element which could be caused by analytical issues (Figure 37E and 37F). The gold inclusions found in the sulphides (sphalerite, chalcopyrite, and pyrite) could not be seen using a microscope but rather occur as invisible gold grains covering the whole sulphide crystals surface area (Figure 37F).

The thin section that was cut from the P06c borehole core log was not in good conditions to be placed for further TIMA analysis. However, the gold grade retrieved by the SGS laboratory gold fire assay was 4.03 ppm Au at a depth of 91.70 – 92.03m. The P06c sample represented the Pienaar Reef, and the host rock comprised of quartz and carbonates. Given that the ore minerals only occurred in areas associated with quartz and carbonates in P11 – 1A, it can only be assumed that the ore minerals found in P06c are the same as those found in P11 – 1A.

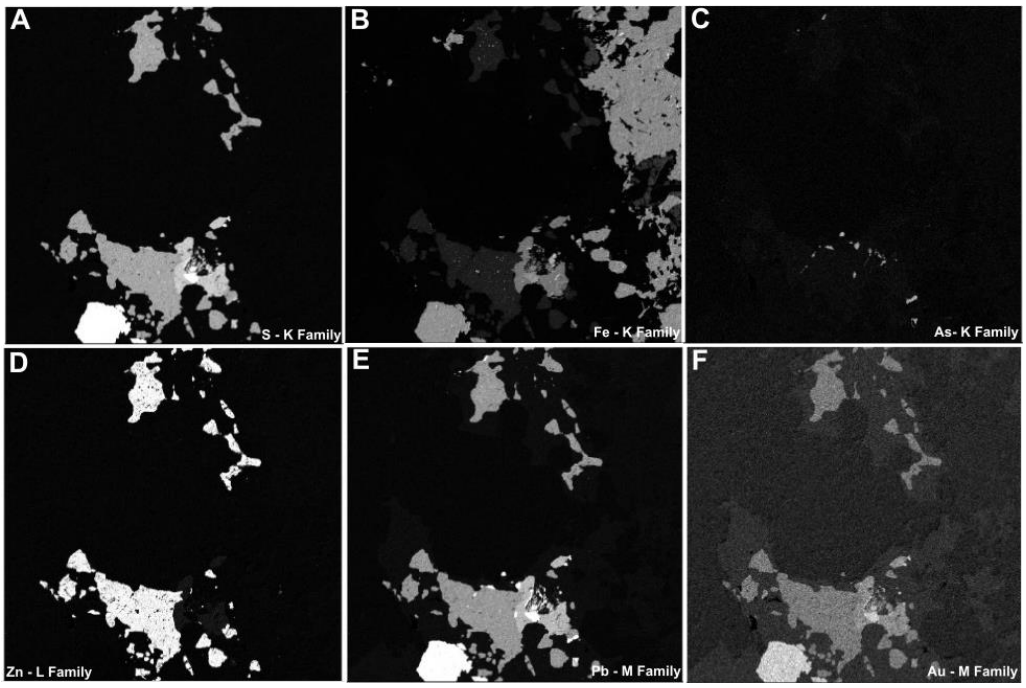


Figure 37: Element Maps for the P11 – 1A Primary Phase Map showing a field view of 1.50 mm. In A the pyrite has the highest sulphide composition (bright white), and the composition decreases from chalcopyrite to sphalerite, respectively. In B the sphalerite has less to no iron, but the other sulphides including an iron serpentine – berthierine reflect a bright grey colour. The element map shown in C indicates an insignificant arsenic composition associated with the sulphides. In D the image shows areas with a high zinc composition, and these are associated with sphalerite. The element maps E and F represent lead and gold composition, respectively. The gold in F is invisible and covers the whole surface area of the sulphides. The highest gold-bearing sulphide is pyrite (bright white) and is followed by chalcopyrite and sphalerite – grey (Borehole P11 at 130.87 – 131.07 m).

GP02 – 2B

The element map of a sample from the Girlie – Pienaar Quartz Reef indicates that the sulphide mineralisation is associated with an alteration assemblage of iron, magnesium, and aluminium (Figures 38 A – D). Under the microscope, there are no gold gains or inclusions observed. However, the element maps indicate a uniform level of gold hosted in the pyrite and pyrrhotite (Figures 38E). These areas of gold enrichment are correlated with bismuth (Figure 38F), although this may be an analytical artifact. The Eersteling Gold Mines gold assay indicated a gold grade of only 0.23 ppm Au.

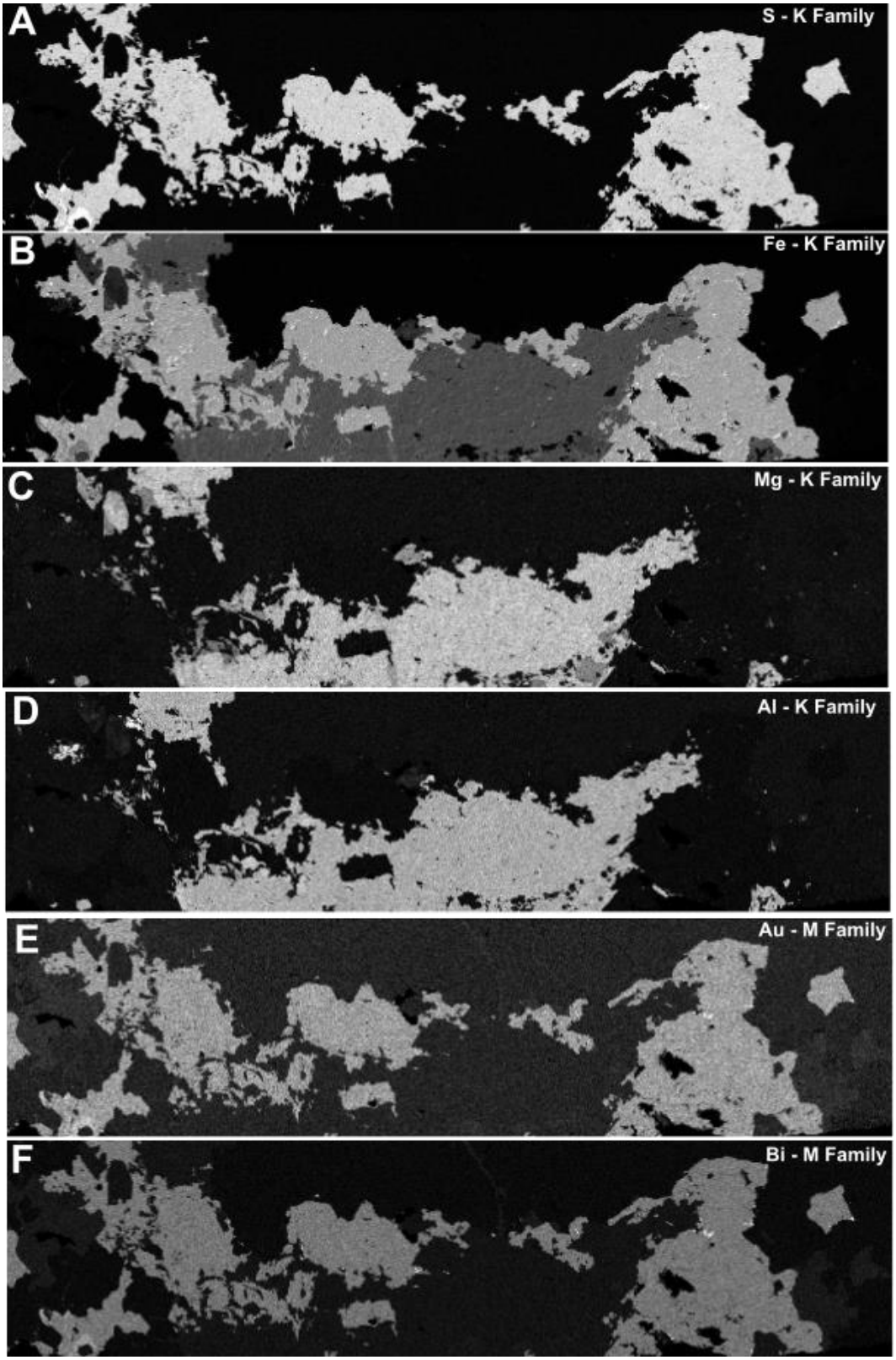


Figure 38: Element Maps showing a field view of 6 mm for the Girlie – Pienaar Quartz Reef, sample GP02 – 2B. In A the sulphur composition for pyrite is higher (bright white) and pyrrhotite is relatively low (grey). These sulphides contain iron (B) and the samples areas of alteration are associated with aluminium and magnesium (C and D). The occurrence of gold is indicated in E and is situated all over the pyrrhotite and pyrite grains surface area (grey). In F gold mineralisation is associated with bismuth (Borehole GP02 at 62.60 – 62.80 m).

5. DISCUSSION

5.1 Lithology and Mineralogy

The Maltz Reef exhibits multiple phases of deformation that are associated with quartz veining and late-stage amphibole veins with a mylonitic texture. The quartz veins represent hydrothermal fluids and quartz precipitating when temperatures decrease (Kerrich and Fyfe, 1981). The quartz veins are not associated with any ore-bearing minerals. However, the amphibole veins contain traces of sulphide minerals which are concentrated in areas experiencing seritization and serpentinization. The wall rock and fluid interaction resulted in pyrite crystallisation. The types of alterations associated with this reef are controlled by a hydrothermal system. Serpentinization indicates the introduction of water into a mineral's crystal structure and seritization is caused by fluid infiltration into a permeable rock. The association of sulphides and serpentine mineralisation indicates a late-stage mineralising event, in which sulphides were transported and deposited into the county rock by hydrothermal fluids or precipitation occurred later when fluid was trapped as interstitial material and started to cool down.

The Pienaar Reef is different from the other reefs because there is carbonate is present and is associated with late-stage quartz veining. The contact between the country rocks, quartz and carbonates illustrates a cross-cutting relationship. The carbonates contain deformational lamellae. These structures are considered to have formed at extremely low temperatures due to a plastic deformation mechanism and the intercrystalline kink structures are expressions of strain (Strekeisen, 2021). Therefore, there might have been another deformation stage related to the strain that only affected the carbonates after the development of quartz veins or the carbonates were introduced into the system after they have undergone deformation. The second scenario is more likely because the distribution of the deformational lamellae is only found in the carbonates.

The carbonates and quartz may have crystallised under different conditions and environments because they require different conditions for precipitation to occur in a hydrothermal system. For quartz precipitation, the hydrothermal system must experience cooling first but for carbonate precipitation cooling solutions must exhibit boiling first (Kerrich and Fyfe, 1981). In addition, hydrothermal fluids are required to ascend and cool down for quartz veins to develop. Kerrich and Fyfe (1981), suggests that carbonates can only form during hydrothermal fluid rising and cooling when (1) CO_2 experiences boiling during an intrusion or (2) Carbonate veins undergo heating due to convection in a hydrothermal system. When CO_2 is boiled, the carbonates solubility increases as the temperature drops, and precipitation is encouraged given that the systems confining pressure is less than the vapour pressure (Kerrich and Fyfe, 1981). This process can only happen at terrestrial depths << 2km. The borehole samples also contain breccias which could be the result of ascending hydrothermal fluids or intrusions related to the surrounding granitoids. However, these observations do not fully support the possibility of CO_2 boiling being the leading mechanism behind carbonates precipitation.

High volumes of serpentine are also present in the quartz and carbonate veins. This mineral can be sourced from ultramafic rock (peridotites) or unmetamorphosed sedimentary rock that is found at low temperature and pressure conditions during wall rock and fluid interaction (Lipko et al., 2020). Peridotites contain iron, magnesium and silica which can be constituents for carbonate mineralisation because a reaction can take place between the Fe, Mg and CO_2 to form carbonate minerals (Kerrich and Fyfe, 1981). This would explain the close spatial relationship observed between areas of alteration, carbonate minerals and serpentine in the Pienaar Reef. The sulphide minerals are found in carbonate inclusions within the quartz veins and may represent a single-phase mineralisation with a sphalerite – chalcopyrite – galena - pyrite paragenetic sequence. These sulphides were most likely

precipitated after stages of deformation by hydrothermal fluids because they lack deformation features, and the pyrite grains retain their euhedral shape.

The Girlie – Pienaar Reef is primarily hosted in a quartz reef and there is a spatial relationship between areas of alteration, quartz fracturing and sulphide mineralisation. The country rocks exhibit multiple stages of deformation. These include (1) The hanging wall is cross-cut by quartz and carbonate veins that were associated with metamorphism and development of the quartz reef, (2) The quartz reef has experienced fracturing, (3) Crystallisation of carbonates within fractures associated with alteration when hydrothermal fluids infiltrated the system, (4) Precipitation of pyrrhotite with minor pyrite inclusions, and (5) Late-stage deformational event that destroyed the sulphides crystal shape. Determining the ages of the deformational events is not part of the scope of this research report. However, Powell et al., (1991) suggested that greenstone belt terranes like the PGB should be carbonated or intensely hydrated before metamorphism occurs.

In contrast to the other reefs, the dominant sulphide in the Zandrivier Reefs is arsenopyrite and it exhibits an increase in quartz veining and tourmaline, serpentine, and poly - sulphide mineralisation. The Zandrivier Reefs mineralisation suggests it experienced more hydrothermal fluid interaction in which there is a transition from upper greenschist to lower amphibole facies. Sulphide mineralisation in the Zandrivier Reef can be associated with multiple stages of hydrothermal fluids due to the presence of arsenopyrite with varying morphologies. The following is a paragenetic sequence for mineralisation that can be derived from the samples: (1) Massive, anhedral, and fractured arsenopyrite, (2) Disseminated and layered euhedral pyrite and (3) Poly - sulphide containing arsenic poor pyrrhotite, sphalerite, chalcopyrite, and pyrite. There is also a sample with sub-microscopic native gold inclusions within arsenopyrite. This is common in gold deposits where gold occurs as inclusions in arsenopyrite or arsenic-rich pyrites (Cook and Chryssoulis, 1990). According to Pokrovski et al., (2019), metallic-native visible gold normally forms in high temperature orogenic or porphyry deposits such as the PGB. As a result, conditions may have been favourable for the deposition of gold into arsenopyrite as inclusions at an earlier stage. The amount of native gold detected under thin section is however insignificant for this to be true.

5.2 Structural Features

Sample P11 illustrates multiple veins with different mineral assemblages that suggests different hydrothermal fluid compositions. Vearncombe (1993) suggests that multiple phases of veining can be associated with fracturing caused by hydrothermal fluids that closed fissures near lithostatic pressures as fluid pressure and temperature conditions decreased. Hydrothermal veining in the Pienaar Reef can be divided into three distinct periods. Even though there is some overlap between certain features and alteration compositions, the varying orientations of the veins suggest different stages of formation.

The first phase of veining, QV1, comprises serpentine enclosing carbonates with minor quartz. The quartz veins observed in QV2 are classified as modified veins because the quartz crystals are recrystallised and failed in preserving their original crystal texture (Vearncombe, 1993). The morphology of the quartz veins and their carbonate constituents suggests that the quartz vein acted as a transportation mechanism for the ore minerals it contains. The last and final phase QV3 - is associated with serpentine and micro faulting. The orientation of the micro faults from QV3 is similar to the fracturing in QV1. The boudin structures shown by the quartz veins in Figure 22 illustrate that the Pienaar Reef also experienced some degree of differential stress during shearing. According to Goscombe et al., (2004), these boudin structures are classified as shear band boudins because their asymmetric nature represents extensional strain processes that develop during formation.

Sample Z01 – 2B illustrates two different deformations regimes with different sulphide mineralisation compositions and morphologies (Figure 21). The mineral assembly indicates a brittle-ductile transition environment where the upward ductile strength is equivalent to the downward brittle strength. According to Craig (2001), the different sulphide textures and morphologies can help determine the conditions responsible for mineralisation to occur. The pyrrhotite is situated within the ductile regime and therefore it can be assumed that it was subjected to some form of thermal deformation process in which heat exerted on it caused it to react in a plastic manner because thermal conditions may have been unstable for it to maintain its crystal structure. Yund and Kullerud (1966), conducted a thermal stability experiment in a Cu – Fe system and their results indicated that pyrrhotite can only be stable between 334 - 700°C. Klein and Hurlbut (1985), support this by demonstrating that iron-rich pyrrhotite is stable at temperatures above 254°C. Therefore, ductile regime conditions had to exceed 254°C for pyrrhotite to deform.

The brittle-ductile transition zone of minerals is not confined to a specific temperature; it is rather dependent on the minerals ability to withstand a certain amount of energy while remaining stable without fracturing. Therefore, the conditions that caused pyrrhotite to deform may have been insignificant in causing the arsenopyrite to deform in the same way, resulting in different morphologies. This can be true because arsenopyrite is stable at various hydrothermal environments either at high (250 - 500°C) or low (<250 - 300°C) temperatures (Pokrovski et al., 2002). Both pyrrhotite and arsenopyrite could have crystalised simultaneously and been subjected to thermal deformation, causing pyrrhotite to react in a plastic manner and the arsenopyrite to fracture. The heat source could have been a late-stage hydrothermal fluid that deposited the anhedral poly - sulphides that exhibit no deformational structures. This paragenetic sequence is supported by Figure 21, which shows arsenopyrite as euhedral disseminated grains that were precipitated by a hydrothermal system.

The development of serpentine within Z01 – 2B (Figure 21) supports the idea that the Zandrivier Reef underwent deformation after sulphide mineralisation. Serpentine in this sample is associated with elongated – ductile pyrrhotite and euhedral arsenopyrite, Appendix (Figure 42 and 43).

5.3 TIMA – Primary Phase Maps

The mineral assemblage of the Pienaar Reefs comprises sphalerite, galena, chalcopyrite, and pyrite which occur in areas rich in carbonates. Carbonates are commonly found in gold-bearing vein deposits hosted by Archaean Greenstone Belts, and the carbonate mineral that precipitates is dependent on the host rock and hydrothermal fluid composition (Kerrich and Fyfe, 1981). Based on the calcite and ankerite carbonates detected by the primary phase maps the host rocks are suggested to be felsic and mafic, respectively. For carbonation and quartz veining to occur large amounts of CO_2, H_2O and SiO_2 are required (Kerrich and Fyfe, 1981). The primary phase maps for the Pienaar Reef indicates traces of orthoclase, anorthite, albite and berthierine. This may imply wall rock-fluid interaction where the hydrothermal system contained a significant amount of SiO_2 that allowed the precipitation of feldspar.

The primary phase maps illustrate a sphalerite – chalcopyrite – galena paragenetic sequence for the Pienaar Reef, in which these sulphides are in equilibrium (Figure 24). According to Anderson (1973), this mineral assemblage is more likely to form in an increased reduced sulphur environment where galena and sphalerite crystalise with chalcopyrite in the system. A reducing nature of hydrothermal fluids for this mineral assemblage is also supported by Pašava et al., (2014). The hydrothermal nature of the deposit is also illustrated by chalcopyrite inclusions within sphalerite (Figure 24). According to Scott (1983), this texture is common for hydrothermal Cu – Zn sulphide ores.

The dominant sulphide in the Girlie – Pienaar Reef is pyrrhotite with minor pyrite. The pyrite is exhibits oxidation with hematite forming on top of it. The primary phase map illustrates that the mineral

assemblages are mainly associated with areas of hydrothermal alteration. The samples primary phase map does not provide the specific composition of the alteration minerals; however, it can be associated with berthierine. This is shown in the Appendix (Figure 41). There are also traces of titanite and rutile found as inclusions within pyrrhotite. These are ilmenite replacement minerals found in metamorphosed rocks and represent different pressure conditions irrespective of temperature (Angiboust and Harlov, 2017). The rutile and titanite are associated with high and low pressures, respectively. The replacement process is controlled by fluid reactions implying that the Girlie – Pienaar Reef underwent hydrothermal metamorphism. The reaction also requires the presence of calcium-bearing and sulphur-bearing minerals – especially pyrite and pyrrhotite to be successful (Angiboust and Harlov, 2017). The Ca and S are more likely sourced from the hydrothermal fluids that resulted in the formation of calcite, pyrite and pyrrhotite.

The Zandrivier Reef exhibits similarities in ore petrology and mineral assemblages with the Pienaar and Girlie – Pienaar Reef. Various authors consider the Zandrivier Reefs host rocks to be metasedimentary instead of metabasalt. The sulphides associated with the Zandrivier Reef are arsenopyrite and poly - sulphides which are in equilibrium. The poly - sulphides paragenetic sequence is pyrrhotite – chalcopyrite – pyrite. The pyrrhotite also contains traces of ilmenite and rutile like the minerals found in the Girlie – Pienaar Reef.

The arsenopyrite mineralisation occurs in different morphologies and sizes which could have resulted from multiple phases of hydrothermal fluids. The arsenopyrite grains are massive, euhedral and have minor fractures. This suggests that the arsenopyrite experienced less metamorphism or deformation during late-stage poly - sulphide mineralisation. The development of pyrrhotite along the arsenopyrites grain boundaries and as inclusions is shown in Figure 29, meaning pyrrhotite crystalised after arsenopyrite. The co-existence of arsenopyrite and pyrrhotite is related to ore-forming fluids of low oxygen and sulphur fugacity (Meng et al., 2020). In addition, this is associated with a reduced sulphur forming system. The high amounts of arsenopyrite in the reef also indicate an increase in arsenic fugacity within the hydrothermal system (Meng et al., 2020).

5.4 TIMA – Elemental Maps

Within the chalcopyrite and pyrite of the Pienaar Reef, there are traces of arsenic even though petrographic and primary phase analysis does not indicate any arsenic-bearing minerals. There are also traces of lead within these sulphides. Cave et al., (2020), suggests that chalcopyrite can only contain traces of lead either as a micro inclusion of galena or as a lattice bound constituent. In which galena would crystalise as inclusions in areas of high Cu.

Traces of invisible gold are detected within the pyrite, sphalerite, and chalcopyrite. A primary phase and elemental map of the same sample from the Pienaar Reef is shown in the Appendix (Figures 44 and 45) where high bismuth concentrations are closely associated with gold mineralisation. The concentration of the bismuth decreases from Cu towards the Pb/Zn sulphides. This is shown in Figure 36C where pyrite contains higher traces of bismuth. Therefore, bismuth is more likely to preferentially partition into iron-bearing sulphides. The correlation between Au and Bi suggests that gold enrichment is related to hydrothermal fluids or melts rich in Bi (Wei et al., 2021). For Bi to be transported in a hydrothermal system, it requires a mixture of a hydroxide and chloride complex with low to medium salinity and high temperatures (>400°C) (Cave et al., 2020). These conditions are suitable for gold to be soluble and transported by a hydrothermal fluid in the sub-greenschist to upper amphibolite facies (Anhaeusser, 1976; Mikucki, 1998).

In chloride complexes, gold can be transported as $AuCl_2$– or as Au (HS) –2 in a complex with neutral pH values and high H_2S contents (Mikucki, 1998). Therefore, gold will partition into the sulphides if the

hydrothermal system has high S_2 and H_2S fugacity. Lipko et al., (2020) compiled a chemical experiment on gold partitioning in different sulphides under these conditions, and the author's results show a decrease in gold compatibility from galena to pyrite and later sphalerite. However, the elemental maps (Figure 37) indicate the opposite degree of compatibility and the result suggest different conditions may have allowed gold to partition into the sulphides. Previous work by (Cook and Chryssoulis, 1990; Fleet and Mumin, 1997) indicate strong correlations between arsenic and pyrite so that invisible gold can partition into the pyrite. The elemental maps in Figure 37C and 37F indicate the opposite because the pyrite is arsenic poor but also contains the highest concentration of invisible gold. According to Pokrovski et al., (2019), this can be explained by a simple reaction of substitution called chemisorption step in which Au replaces S or Fe on the pyrites crystal surface. The enrichment of gold in these sulphides may however indicate an analytical artifact because the amount of gold in these sulphides is far too uniform.

The gold in the sample from the Girlier Reef occurs as invisible gold and is only detected within pyrrhotite and minor pyrite. The correlation between gold and pyrrhotite is rare because gold mainly partitions into arsenopyrite or pyrite. It can be assumed that gold can partition into pyrrhotite because (1) Pyrrhotite is the only sulphide mineral in the system that can accommodate gold or (2) Pyrrhotite belongs to the same crystal system as arsenopyrite, making it possible for gold to partition into its crystal structure. In samples from the Pienaar Reef, areas containing invisible gold also contain elevated concentrations of bismuth which are similar to the samples from the Girlie – Pienaar Reef.

In the Zandrivier Reef, gold occurs as native and invisible gold. In the arsenopyrite and pyrrhotite poly - sulphide (Figure 35E) traces of gold are mainly detected in pyrrhotite. The pyrrhotite is a late-stage mineral in comparison to arsenopyrite. This implies that the late-stage hydrothermal fluids contained higher amounts of gold bisulphide complexes in comparison to the first arsenic-rich ore-forming fluids. When gold precipitated from arsenic-rich fluids with low oxygen fugacity, native gold developed, this is seen in Figure 35 - E1 (Meng et al., 2020).

Early-stage arsenopyrite grains are euhedral and contain high amounts of arsenic and bismuth (Figure 33, A and B). However, the gold content in both minerals is insignificant. The gold occurs as disseminated inclusions in the arsenopyrite, and invisible gold is concentrated in the pyrites forming along arsenopyrite grain boundaries. The gold grade results from the geochemical essay and shows that the Pienaar and Zandrivier Reefs have the highest gold grades at an average of 4 to 7 ppm Au. These gold concentrations correspond to the reef's poly - sulphide mineral assemblages and multiple stages of hydrothermal fluids activity which could have caused enrichment in gold during each hydrothermal pulse. The Girlie – Pienaar Reef contains minor sulphides which explains its low gold grade concentrations of 0.23 ppm Au. Even though the Pienaar and Zandrivier Reefs contain high gold grades the gold mainly occurs as invisible gold and a lower gold recovery can be expected.

6. CONCLUSIONS AND RECOMMENDATIONS

All the different reefs experienced multiple phases of deformation and mineralisation. The dominant deformational event is associated with hydrothermal fluids that deposited cross-cutting quartz veins and carbonate mineralisation. As a result, the hydrothermal fluids interacted with the county rocks and created areas of serpentinization and seritization. These areas are represented by the precipitation of berthierine, anorthite, albite and orthoclase. The different sulphides found within these reefs are rich in siderophile and chalcophile elements. These include pyrite, chalcopyrite, galena, sphalerite, pyrrhotite, and arsenopyrite. The Pienaar Reef has a high concentration of carbonate minerals with galena and sphalerite mineralisation. Elsewhere the Zandrivier Reef contains high amounts of hematite and arsenopyrite. These sulphides occur in massive, net textured and

disseminated forms and indicate phases of remobilisation. This includes (1) One sample containing a sulphide occurring in different morphologies, and (2) Traces of replacement minerals like rutile and titanite. For further analysis, a study on the geochemistry of these sulphides can be conducted to determine whether the sulphides have the same composition which could suggest the same source for mineralisation.

The sulphides discovered in these gold reefs also indicate a reduced sulphur environment would be suitable for precipitation. The elemental maps of the Pienaar and Girlie – Pienaar Reefs indicate enrichment of invisible gold within pyrite, pyrrhotite and chalcopyrite. This may be an analytical artifact because the traces of gold are far too uniform to be real. This also implies that gold is structurally bonded to the sulphides and would result in low gold recovery. In contrast, the Zandrivier Reefs gold mainly occurs as inclusions on the margins of these sulphides which would make it easily liberated. The traces of gold from the reefs are associated with high traces of bismuth and sulphur. This suggests that gold prefers to partition into minerals with higher sulphur compositions rather than arsenic. This is supported by the Pienaar and Zandrivier Reefs having the highest gold grades at an average of 4 to 7 ppm Au. There are also traces of native gold within the Zandrivier Reefs arsenopyrite. However, the amount of gold found is insignificant to assume that is how the gold occurs for the whole reef. Therefore, more research should be undertaken to determine the enrichment of gold within these sulphides.

REFERENCES

Anderson, G.M., 1973. The hydrothermal transport and deposition of galena and sphalerite near 100 degrees C. *Economic Geology*, **68**(4) 480-492.

Angiboust, S. and Harlov, D., 2017. Ilmenite breakdown and rutile-titanite stability in metagranitoids: Natural observations and experimental results. *American Mineralogist*, **102**(8) 1696-1708.

Anhaeusser, C.R., 1992. Structures in granitoid gneisses and associated migmatites close to the granulite boundary of the Limpopo Belt, South Africa. *Precambrian Research*, **55**(1-4)81-92.

Anthony, M. and Flanders, I., 1992. The exploration for, and possible genesis of, some Archaean granite/gneiss-hosted gold deposits in the Pietersburg granite-greenstone terrane.

Barton Jr, J.M., Klemd, R., Beattie, M. and Byron, C.L., 1990. Albitization and the gold-bearing Roodepoort pluton, Pietersburg granite-greenstone terrane, South Africa. *South African Journal of Geology* **93**(5/6)776-784.

Beattie, M., 1991. *Alteration and gold mineralisation in the Roodepoort Goldfield, Pietersburg granite-greenstone terrane* (PhD thesis, University of Johannesburg).

Beattie, M. and Barton, J., 1992. Alteration and occurrence of gold mineralisation in the Roodepoort Goldfield, Pietersburg granite-greenstone terrane. *South African Journal of Geology*, **95**(3)131-140.

Byron, C.L. and Barton, J.M., 1990. The setting of mineralisation in a portion of the Eersteling goldfield, Pietersburg granite-greenstone terrane, South Africa. *South African Journal of Geology* **93**(3)463-472.

Cave, B., Lilly, R. and Barovich, K., 2020. Textural and geochemical analysis of chalcopyrite, galena and sphalerite across the Mount Isa Cu to Pb-Zn transition: Implications for a zoned Cu-Pb-Zn system. *Ore Geology Reviews*, **124** 103647.

Cook, N.J. and Chryssoulis, S.L., 1990. Concentrations of invisible gold in the common sulfides. *The Canadian Mineralogist*, **28**(1) 1-16.

Craig, J.R., 2001. Ore-mineral textures and the tales they tell. *The Canadian Mineralogist*, **39**(4) 937-956.

de Wit, M.J., 1991. Archaean greenstone belt tectonism and basin development: some insights from the Barberton and Pietersburg greenstone belts, Kaapvaal Craton, South Africa. *Journal of African Earth Sciences (and the Middle East)* **13**(1)45-63.

de Wit, M.J., Jones, M.G. and Buchanan, D.L., 1992. The geology and tectonic evolution of the Pietersburg greenstone belt, South Africa. *Precambrian Research* **55**(1-4)123-153.

de Wit, M.J., Armstrong, R.A., Kamo, S.L. and Erlank, A.J., 1993. Gold-bearing sediments in the Pietersburg greenstone belt; age equivalents of the Witwatersrand Supergroup sediments, South Africa. *Economic geology* **88**(5) 1242-1252.

Eersterling Gold Mining – Technical Statement, 2007 [Online] https://www.caledoniamining.com/wp-content/uploads/2019/02/Eersteling_Absa_Venmyn_050207_Final.pdf (Accessed – April 2021)

Fleet, M.E. and Mumin, A.H., 1997. Gold-bearing arsenian pyrite and marcasite and arsenopyrite from Carlin Trend gold deposits and laboratory synthesis. *American Mineralogist*, **82**(1-2) 182-193.

Franey, N.J., 1987. *A geological model of shear zone gold deposits in the Pietersburg greenstone belt, South Africa* (PhD thesis, Rhodes University).

Foster, R.P. and Piper, D.P., 1993. Archaean lode gold deposits in Africa: Crustal setting, metallogenesis and cratonization. *Ore Geology Reviews* **8**(3-4)303-347.

Good, N. and de Wit, M.J., 1997. The Thabazimbi-Murchison lineament of the Kaapvaal craton, South Africa: 2700 Ma of episodic deformation. *Journal of the Geological Society*, **154**(1) 93-97.

Goscombe, B.D., Passchier, C.W. and Hand, M., 2004. Boudinage classification: end-member boudin types and modified boudin structures. *Journal of Structural Geology*, **26**(4) 739-763.

Henderson, D.R., Long, L.E. and Barton Jr, J.M., 2000. Isotopic ages and chemical and isotopic composition of the Archaean Turfloop Batholith, Pietersburg granite-greenstone terrane, Kaapvaal Craton, South Africa. *South African Journal of Geology*, **103**(1) 38-46.

Hrstka, T., Gottlieb, P., Skala, R., Breiter, K. and Motl, D., 2018. Automated mineralogy and petrology applications of TESCAN Integrated Mineral Analyzer (TIMA). *Journal of Geosciences* **63**(1) 47-63.

Jones, M.G., 1990. *The geology of the Mt. Màre area, Pietersburg greenstone belt, South Africa* (PhD thesis, Imperial College London (University of London)).

Kalbskopf, S.P. and Barton, J.M., 2003. The Zandrivier Deposit, Pietersburg Green Belt, South Africa: An Auriferous Tourmalinite. *South African Journal of Geology* **106**(4)361-374.

Kerrich, R. and Fyfe, W.S., 1981. The gold—carbonate association: source of CO2, and CO_2 fixation reactions in Archaean lode deposits. *Chemical Geology*, **33**(1-4) 265-294.

Kramers, J.D., Henzen, M. and Steidle, L., 2014. Greenstone belts at the Northernmost edge of the Kaapvaal Craton: timing of tectonic events and a possible crustal fluid source. *Precambrian Research* **253** 96-113.

Klein, C. and Hurlbut, Jr.C.S., *Manual of Mineralogy,* Wiley, 20th ed, 1985, 278-9.

Kröner, A., Jaeckel, P. and Brandl, G., 2000. Single zircon ages for felsic to intermediate rocks from the Pietersburg and Giyani greenstone belts and bordering granitoid orthogneisses, Northern Kaapvaal Craton, South Africa. *Journal of African Earth Sciences* **30**(4)773-793.

Laurent, O., Paquette, J.L., Martin, H., Doucelance, R. and Moyen, J.F., 2013. LA-ICP-MS dating of zircons from Meso-and Neoarchean granitoids of the Pietersburg block (South Africa): crustal evolution at the Northern margin of the Kaapvaal craton. *Precambrian Research*, **230** 209-226.

Lipko, S., Tauson, V. and Bychinskii, V., 2020. Gold partitioning in a model multiphase mineral-hydrothermal fluid system: Distribution coefficients, speciation and segregation. *Minerals*, **10**(10) 890.

McCourt, S., 1995. The crustal architecture of the Kaapvaal crustal block South Africa, between 3.5 and 2.0 Ga. *Mineralium Deposita* **30**(2)89-97.

Meng, L., Huang, F., Gao, W., Wang, D., Zhu, J., Xing, C., Tan, W. and Tang, X., 2020. Multi-stage hydrothermal processes at the Laozuoshan gold deposit in NE China: Insights from textures and compositions of sulfide assemblages. *Ore Geology Reviews*, **117** 103275.

Mikucki, E.J., 1998. Hydrothermal transport and depositional processes in Archean lode-gold systems: A review. *Ore geology reviews*, **13**(1-5) 307-321.

Pašava, J., Tornos, F. and Chrastný, V., 2014. Zinc and sulfur isotope variation in sphalerite from carbonate-hosted zinc deposits, Cantabria, Spain. Mineralium Deposita, **49**(7) 797-807.

Pokrovski, G.S., Kara, S. and Roux, J., 2002. Stability and solubility of arsenopyrite, FeAsS, in crustal fluids. *Geochimica et cosmochimica acta*, **66**(13) 2361-2378.

Pokrovski, G.S., Kokh, M.A., Proux, O., Hazemann, J.L., Bazarkina, E.F., Testemale, D., Escoda, C., Boiron, M.C., Blanchard, M., Aigouy, T. and Gouy, S., 2019. The nature and partitioning of invisible gold in the pyrite-fluid system. *Ore Geology Reviews*, **109** 545-563.

Powell, R., Will, T.M. and Phillips, G.N., 1991. Metamorphism in Archaean greenstone belts: calculated fluid compositions and implications for gold mineralisation. *Journal of Metamorphic Geology*, **9**(2) 141-150.

Rajesh, H.M., Liu, S.J. and Wan, Y., 2020. Mesoarchean TTG magmatism from the Northeastern margin of the Kaapvaal Craton, Southern Africa: Arguments for an exotic terrane (remnant of Pilbara Craton?). *Precambrian Research*, **337** 105 - 552.

Robb, L.J., Brandl, G., Anhaeusser, C.R. and Poujol, M., 2006. Archaean granitoid intrusions. *The Geology of South Africa*, 57-94.

Roering, C., van Reenen, D.D., De Wit, M.J., Smit, C.A., De Beer, J.H. and Van Schalkwyk, J.F., 1992. Structural geological and metamorphic significance of the Kaapvaal Craton-Limpopo Belt contact. *Precambrian Research*, **55**(1-4) 69-80.

Ruygrok, M., 1992. *The tectono-metamorphic evolution of a portion of the Rhenosterkoppies Greenstone Belt, in relation to the Limpopo Orogeny, South Africa* (PhD thesis, University of Johannesburg).

Saager, R. and Muff, R., 1986. The gold occurrences of the Eersteling Goldfield, Pietersburg greenstone belt. In *Mineral Deposits of Southern Africa* 205-211.

Scott, S.D., 1983. Chemical behaviour of sphalerite and arsenopyrite in hydrothermal and metamorphic environments. *Mineralogical Magazine*, **47**(345) 427-435.

Sieber, T., 1991. *Styles of hydrothermal alteration in Archaean rocks of the Northern Kaapvaal Craton, South Africa, with implications for gold mineralisation* (PhD thesis, University of Johannesburg).

Smit, C.A., Roering, C. and van Reenen, D.D., 1992. The structural framework of the southern margin of the Limpopo Belt, South Africa. *Precambrian Research*, **55**(1-4) 51-67.

Strekeisen, A., 2021. Deformation Lamellae. Available at: http://www.alexstrekeisen.it/english/meta/lamellae.php (Accessed: 10 May 2021).

Stettler, E.H. and du Plessis, J.G., 1988. The structure of the Pietersburg greenstone belt, South Africa, as derived from geophysics. *South African Journal of Geology* **91**(2)292-303.

Stettler, E.H., de Beer, J.H., and Kleywegt, R.J., 1990. The structure of the Palmietfontein and Entabeni granite plutons as derived from geophysical studies. *South African Journal of Geology*, **93**(4) 676-682.

Suryanarayana, C., 2017. Microstructure: An Introduction. *Springer Science + Business Media* 105-123.

van Reenen, D.D., Roering, C., Ashwal, L.D. and De Wit, M.J., 1992. Regional geological setting of the Limpopo Belt. *Precambrian Research*, **55**(1-4) 1-5.

van Schalkwyk, J.F., de Wit, M.J., Roering, C. and van Reenen, D.D., 1993. Tectono-metamorphic evolution of the simatic basement of the Pietersburg greenstone belt relative to the Limpopo Orogeny: evidence from serpentinite. *Precambrian research* **61**(1-2)67-88.

Vearncombe, J.R., 1993. Quartz vein morphology and implications for formation depth and classification of Archaean gold-vein deposits. Ore Geology Reviews, **8**(5)407-424.

Vezinet, A., Moyen, J.F., Stevens, G., Nicoli, G., Laurent, O., Couzinié, S. and Frei, D., 2018. A record of 0.5 Ga of evolution of the continental crust along the Northern edge of the Kaapvaal Craton, South Africa: Consequences for the understanding of Archean geodynamic processes. *Precambrian Research* **305** 310-326.

Wei, B., Wang, C.Y., Wang, Z., Cheng, H., Xia, X. and Tan, W., 2021. Mantle-derived gold scavenged by bismuth-(tellurium)-rich melts: evidence from the Mesozoic Wulong gold deposit in the North China Craton. *Ore Geology Reviews*, 104047.

Willemse, J., 1938. The gold occurrences south-west of Pietersburg. Printed in the Union of South Africa by the Government Printer.

Yund, R.A. and Kullerud, G., 1966. Thermal stability of assemblages in the Cu—Fe—S system. *Journal of Petrology*, **7**(3) 454-488.

Zeh, A. and Gerdes, A., 2012. U–Pb and Hf isotope record of detrital zircons from gold-bearing sediments of the Pietersburg Greenstone Belt (South Africa)—Is there a common provenance with the Witwatersrand Basin? *Precambrian Research* **204** 46-56.

Zhou, W., Apkarian, R., Wang, Z.L. and Joy, D., 2006. Fundamentals of scanning electron microscopy (SEM). In *scanning microscopy for nanotechnology* 1-40. Springer, New York, NY.

APPENDIX

Borehole Samples Localities

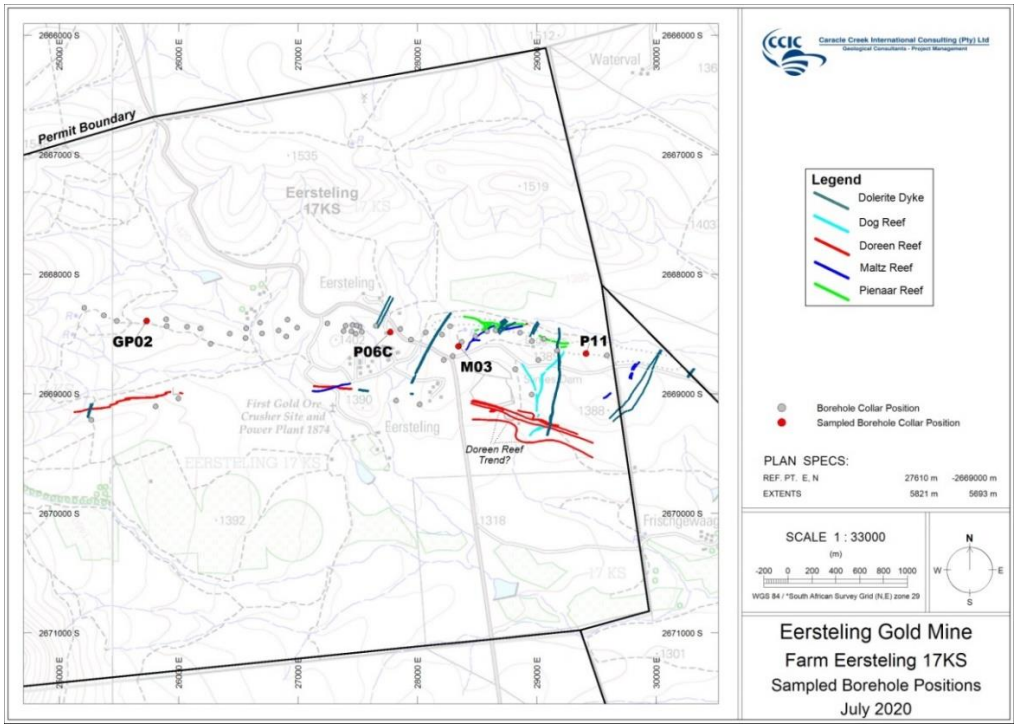


Figure 39: Map showing the localities of the boreholes: GP022; P06c; M03; and P11 from the Eerterling 17KS farm. The map also indicates the different reefs orientations and permit boundary surrounding the project area (Eersterling Gold Mine, 2020).

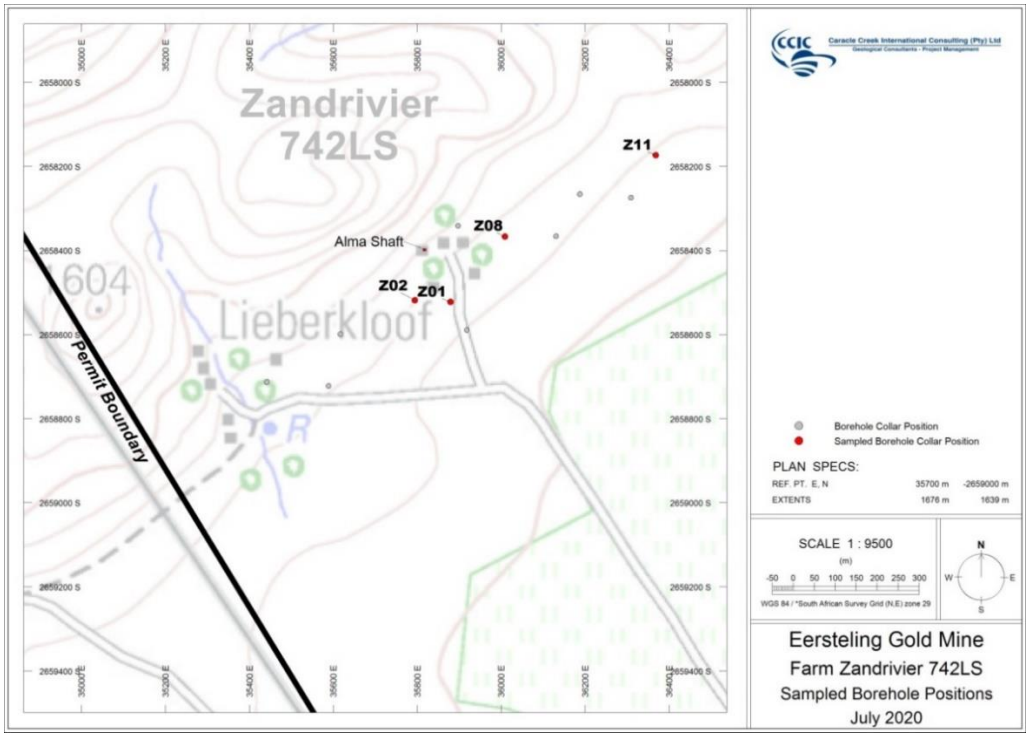


Figure 40: Map showing the localities of the boreholes: Z01; Z02; and Z11 from the Zandrivier 742LS farm (Eersterling Gold Mine, 2020).

Petrographic Analysis

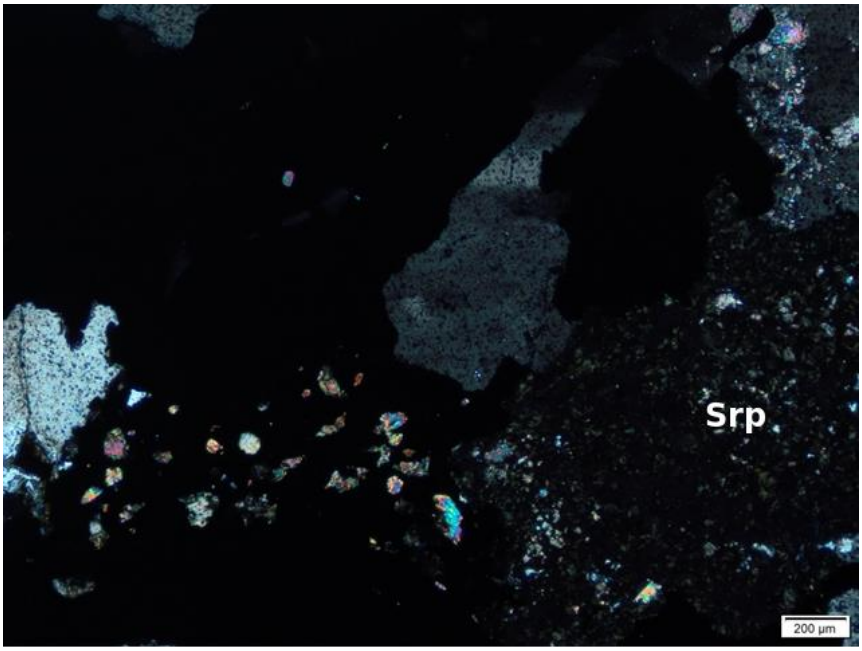


Figure 41: Photomicrograph of a sample from the Girlie – Pienaar Reef. Occurrence of berithierine (Srp) in massive quartz veins fractures (Borehole GP022: Reef at 73.65 – 73.82 m).

Structural Features

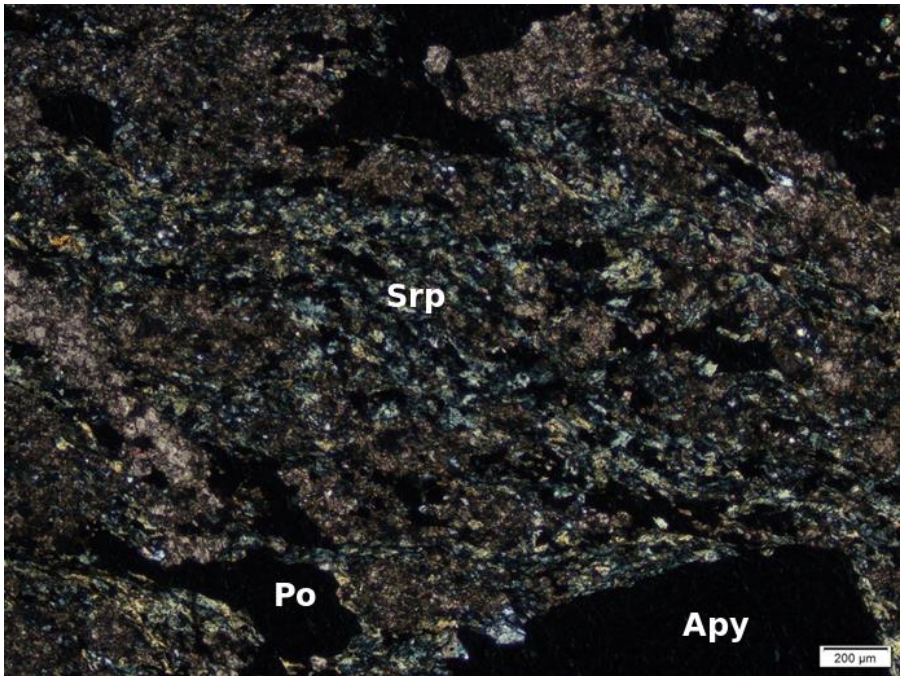


Figure 42: Photomicrograph of a sample from the Zandrivier Reef illustrating a more ductile regime with anhedral elongated pyrrhotite (Po) and serpentine (Srp). The arsenopyrite (Apy) has a different morphology even though both ore minerals are sourced from the same sample (Borehole Z01 at 184.78 – 185.10 m).

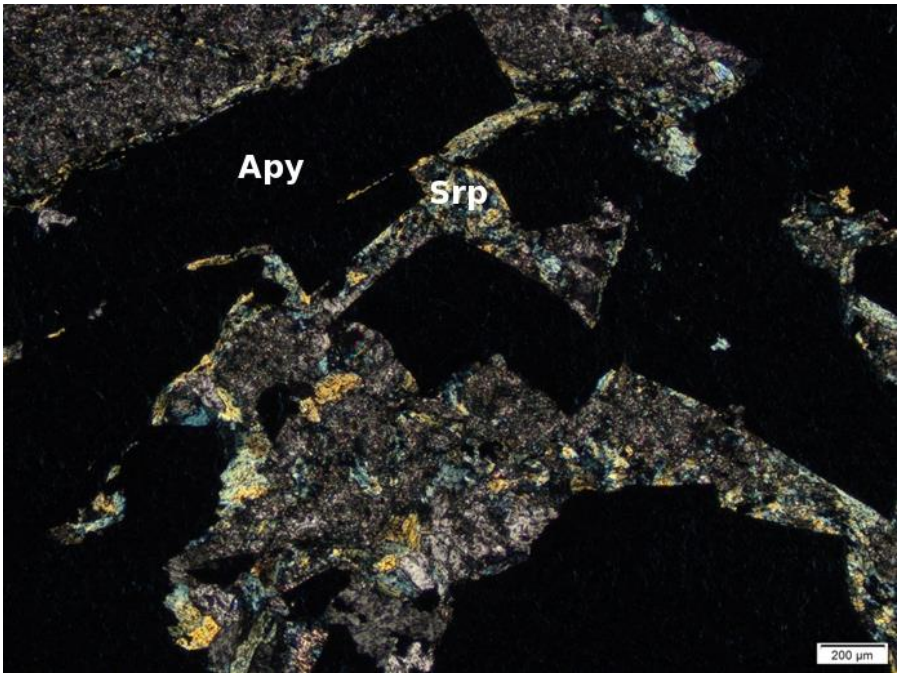


Figure 43: Photomicrograph of a sample from the Zandrivier Reef illustrating a more brittle regime with anhedral elongated pyrrhotite (Po) and serpentine (Srp). The arsenopyrite (Apy) still has its euhedral crystal shape and occurs as net textured, fractured, and massive grains. The serpentine in the brittle regime is concentrated along the sulphide's edges and encloses.

TIME – Primary Phase and Elemental Maps

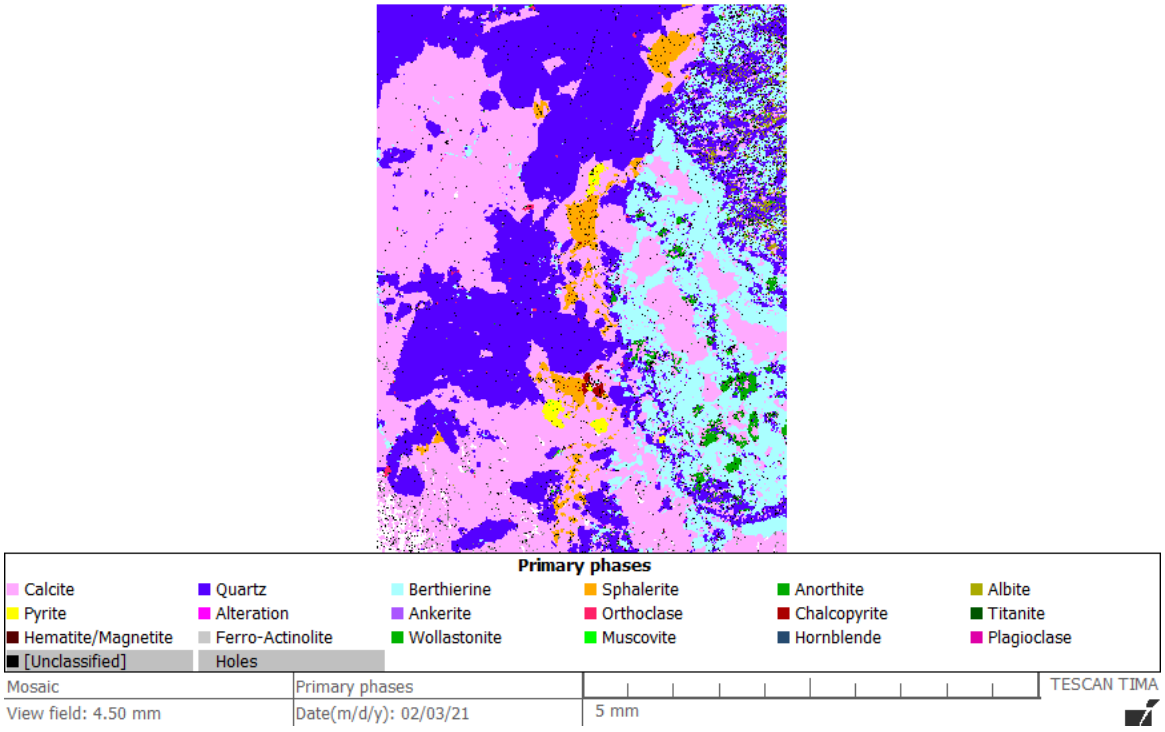


Figure 44: Primary Phase Map of P11 – 1A illustrating a mineral assemblage that comprises chalcopyrite, sphalerite, and pyrite. The ore minerals only occur within the calcite and the host rock is rich in anorthite and berthierine - a serpentine alteration mineral (Borehole P11 at 130.87 – 131.07 m).

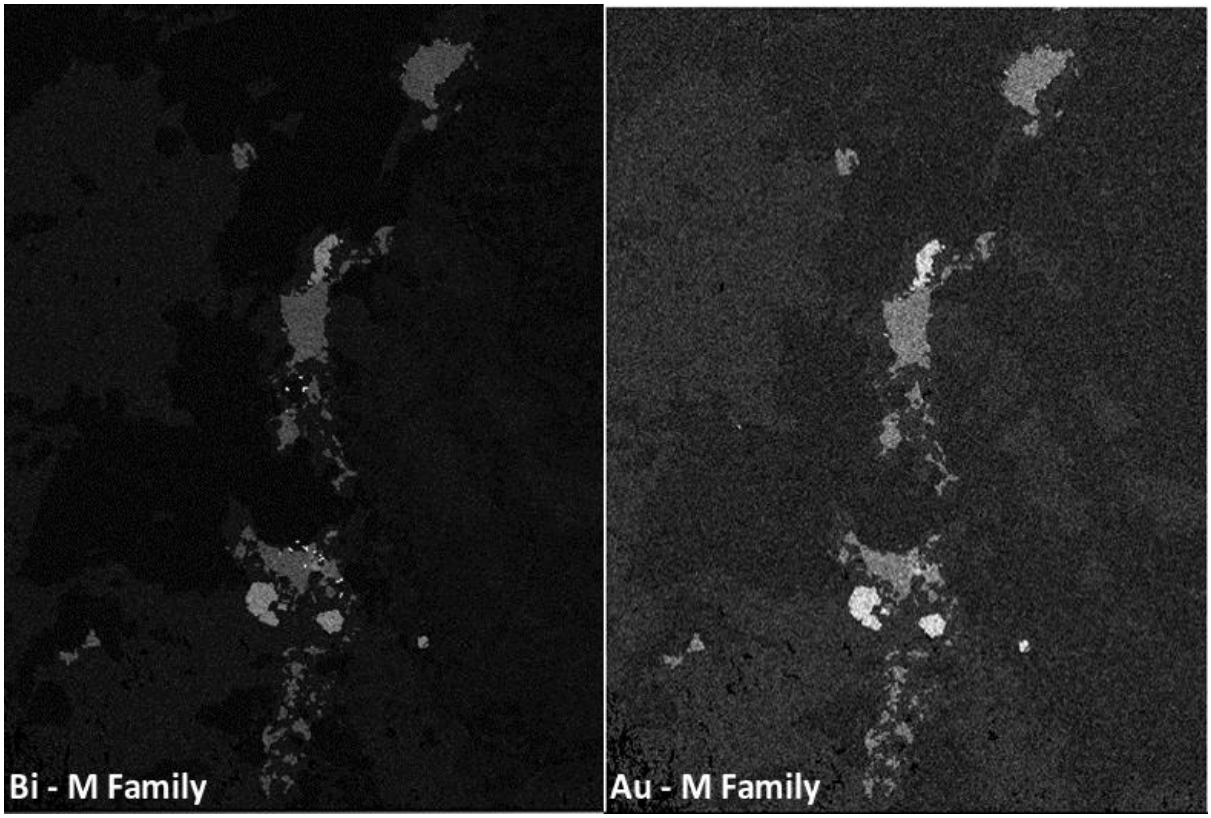


Figure 45: Element Maps for the P11– 1A Primary Phase Map showing a field view of 2mm. The elemental maps illustrate a correlation between bismuth and gold. In addition, areas that reflect high bismuth concentrations are closely associated with gold mineralisation. Both elements are structurally hosted in pyrite (Borehole P11 at 130.87 – 131.07 m).

Borehole Core Logging

This is a geological interpretation method that is used to portray the stratigraphic column of the different borehole logs from the different gold reefs. The data used to construct the different borehole logs was provided by the Eersteling Gold Mine and included the lithology, specifications – dimensions, lithological contacts, mineralisation, contact angles and alterations. The successions were then correlated were applicable and used to check if there are any geological or petrological similarities between the reefs, considering the depth of the succession. The localities where the samples analysed for this project were taken are also shown below.

Pienaar Reef

P06C

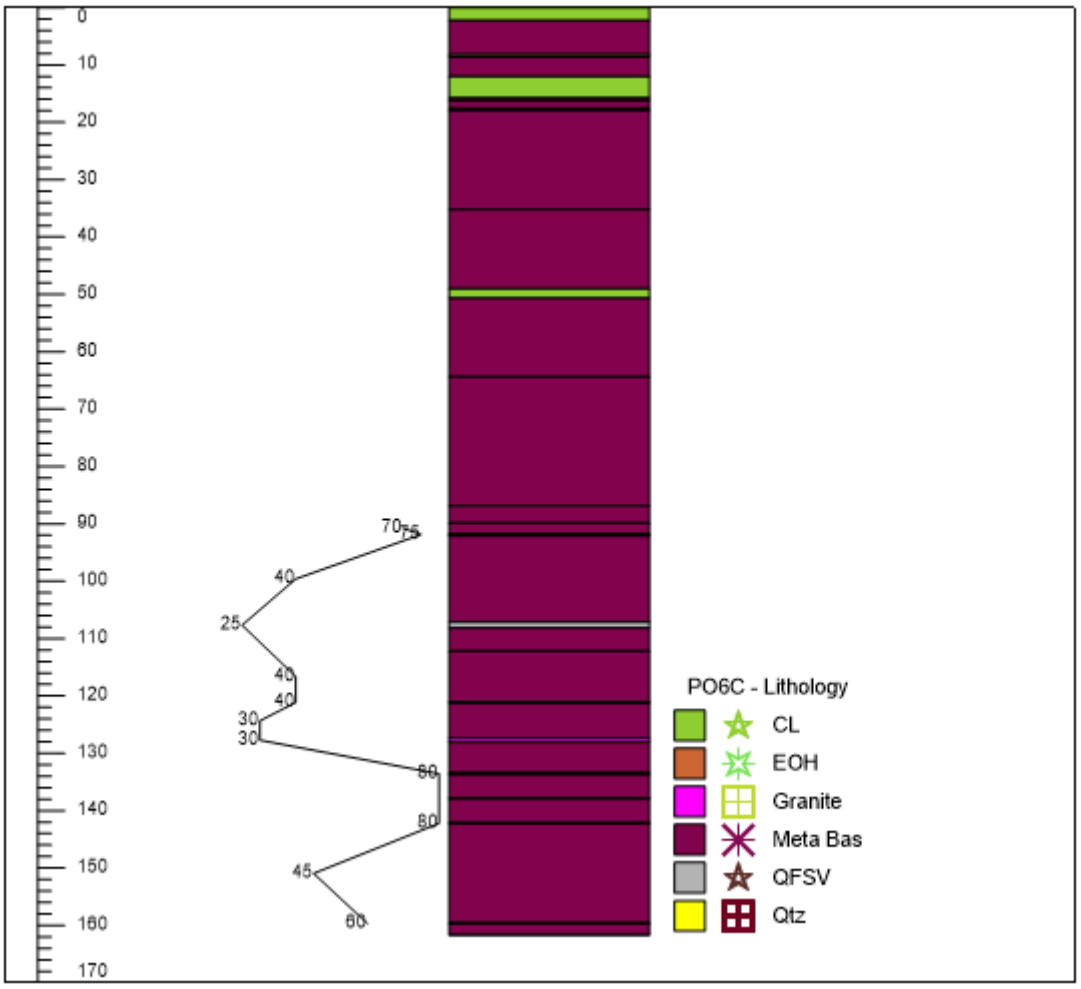


Figure 46: Stratigraphic view of the Pienaar Reefs borehole core log (P06c) which indicated the different lithologies that make up the reef. The dominant rock type is metabasalt which is crosscut by thin layers of chlorite, quartz, and granite as you move down the stratigraphic column. Sample P06c was extracted from a depth of 91.70 – 92.0 m and the quartz and metabasalt along this depth exhibited a gradational contact at 70 – 75°. In comparison to the host rock, the quartz is coarser and has no foliation.

P11

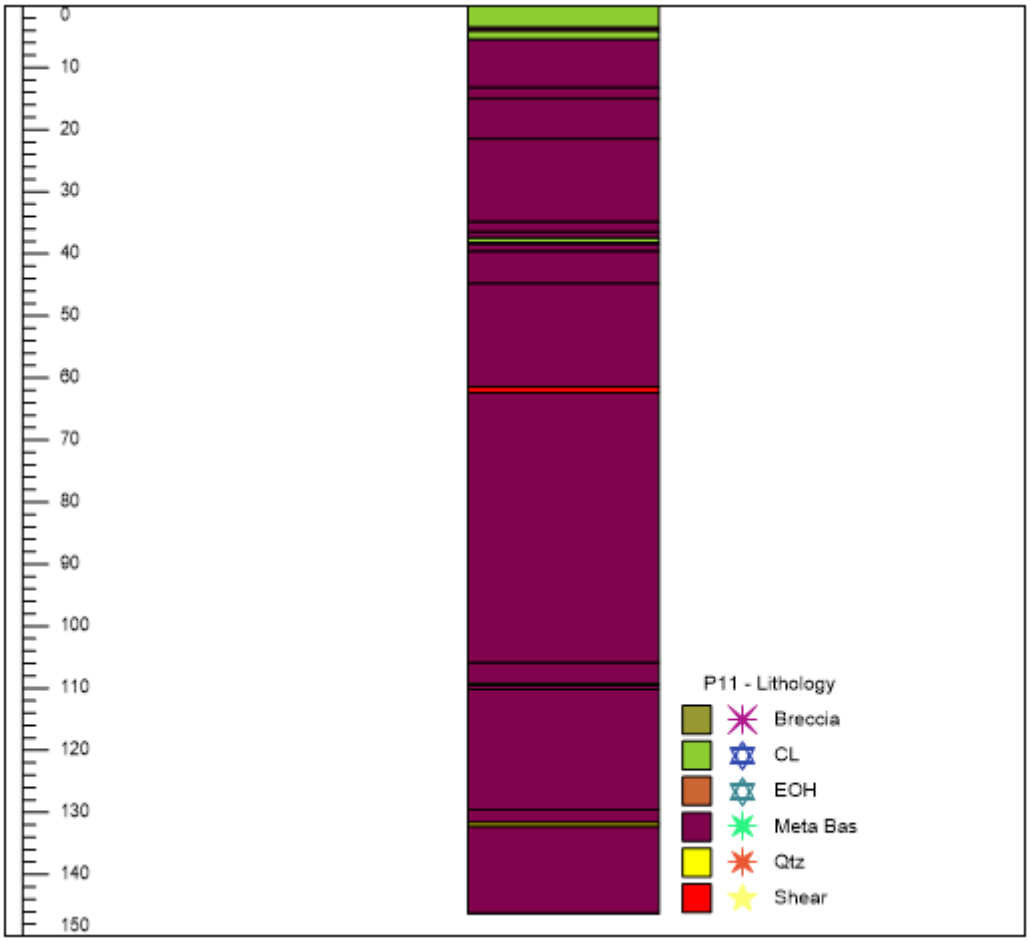


Figure 47: Stratigraphic view of the Pienaar Reefs borehole core log (P11) that comprises of different lithologies. The dominant rock type is metabasalt which is crosscut by thin layers of chlorite, quartz and breccias as you move down the stratigraphic column. The reef also experienced some shearing at 61 – 62m which is associated with disseminated sulphides. Sample P11 was extracted from a depth of 129 – 133 m and exhibited a shear contact with the neighbouring lithology.

Girlie – Pienaar Reef

GP022

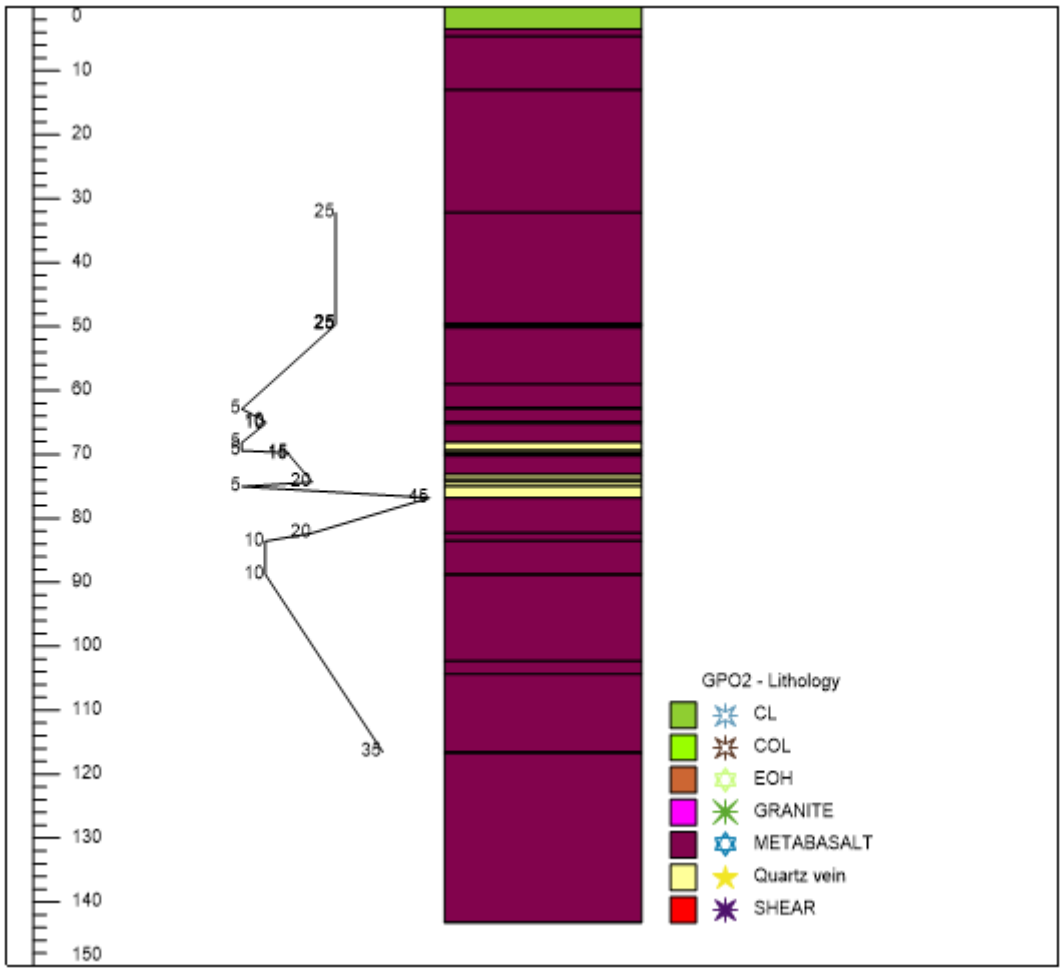


Figure 48: Stratigraphic view of the Girlie - Pienaar Reefs borehole core log (GP0) that comprises different lithologies. The dominant rock type is metabasalt that covered by chlorite overburden and crosscut by quartz veins at a depth range of 60 – 76 m. The quartz veins represent the reef where most sulphide mineralisation occurs. The average contact angle between the different lithologies is between 5 and 20° and exhibits a sharp and sheared contact.

Zandrivier Reef

Z01

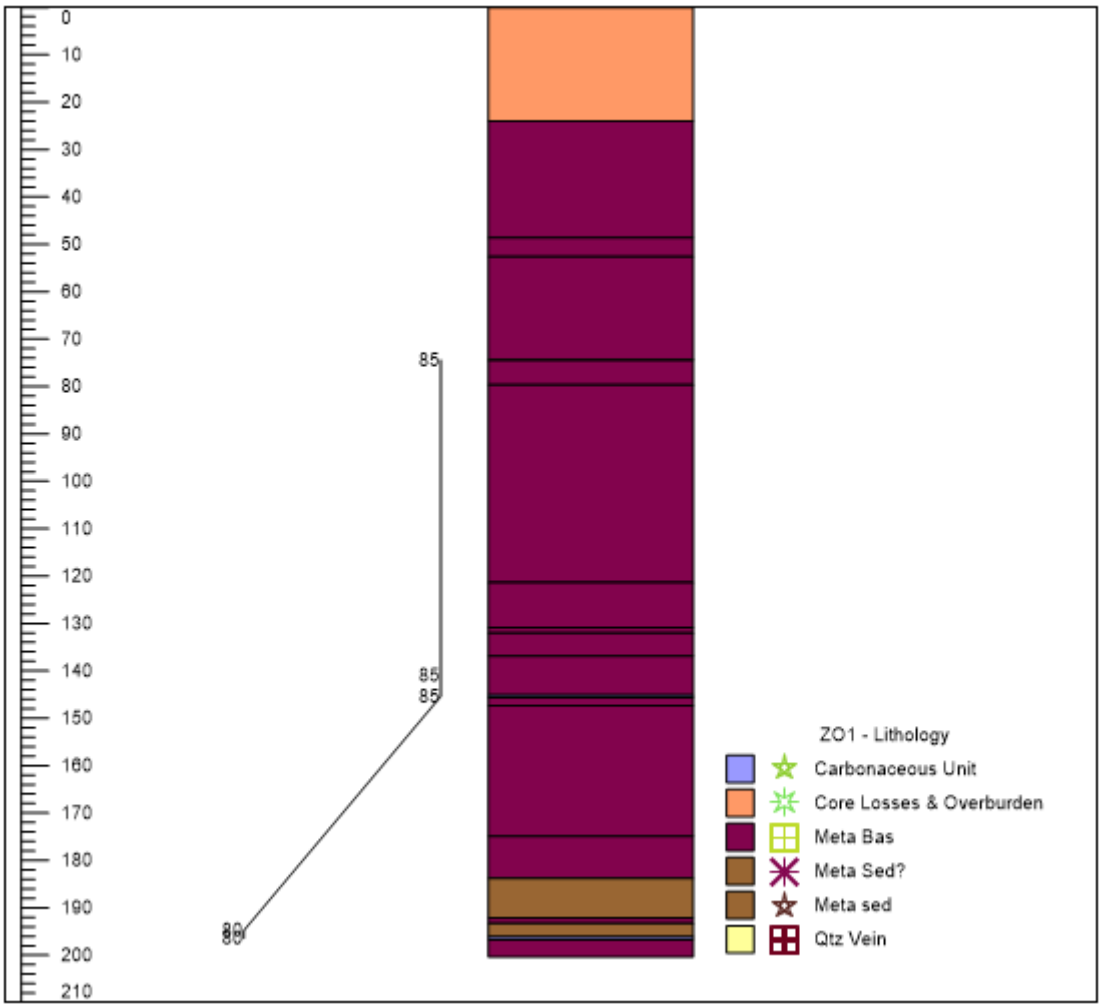


Figure 49: Stratigraphic view of the Zandrivier Reefs borehole core log (Z01) that comprises metabasalts and interbedded carbonates within the metasediments - as you go down stratigraphy. The overburden is mainly broken rock that cannot be identified. The average contact angle between the metabasalts and carbonaceous units is 85° and this region is associated with massive arsenopyrite mineralisation with sulphides preserving their cubic crystal shape.

Z02

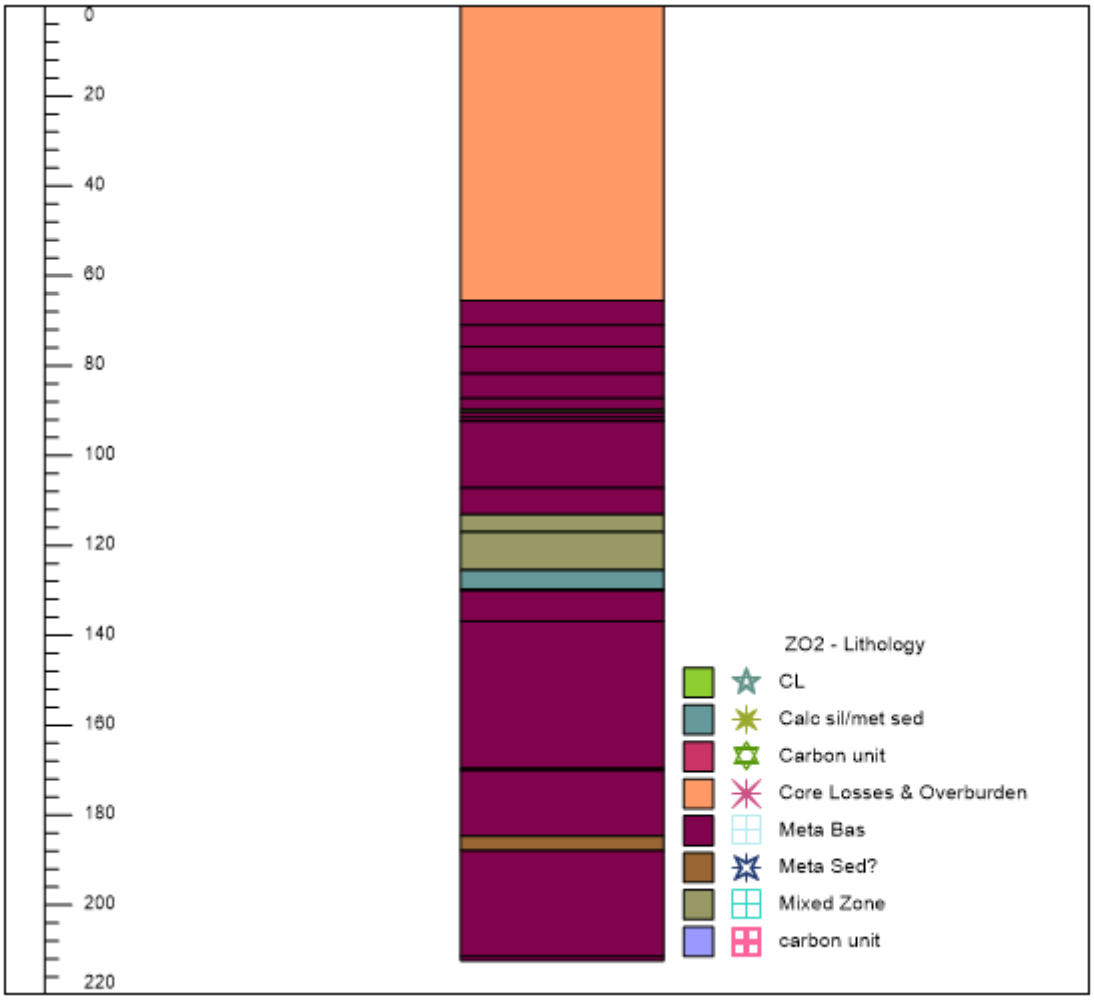


Figure 50: Stratigraphic view of the Zandrivier Reefs borehole core log (Z02) that comprises metabasalts, mixed zone (transition zone), carbonates and metasediments - as you go down stratigraphy. The overburden is mainly broken rock that cannot be identified.

Z11

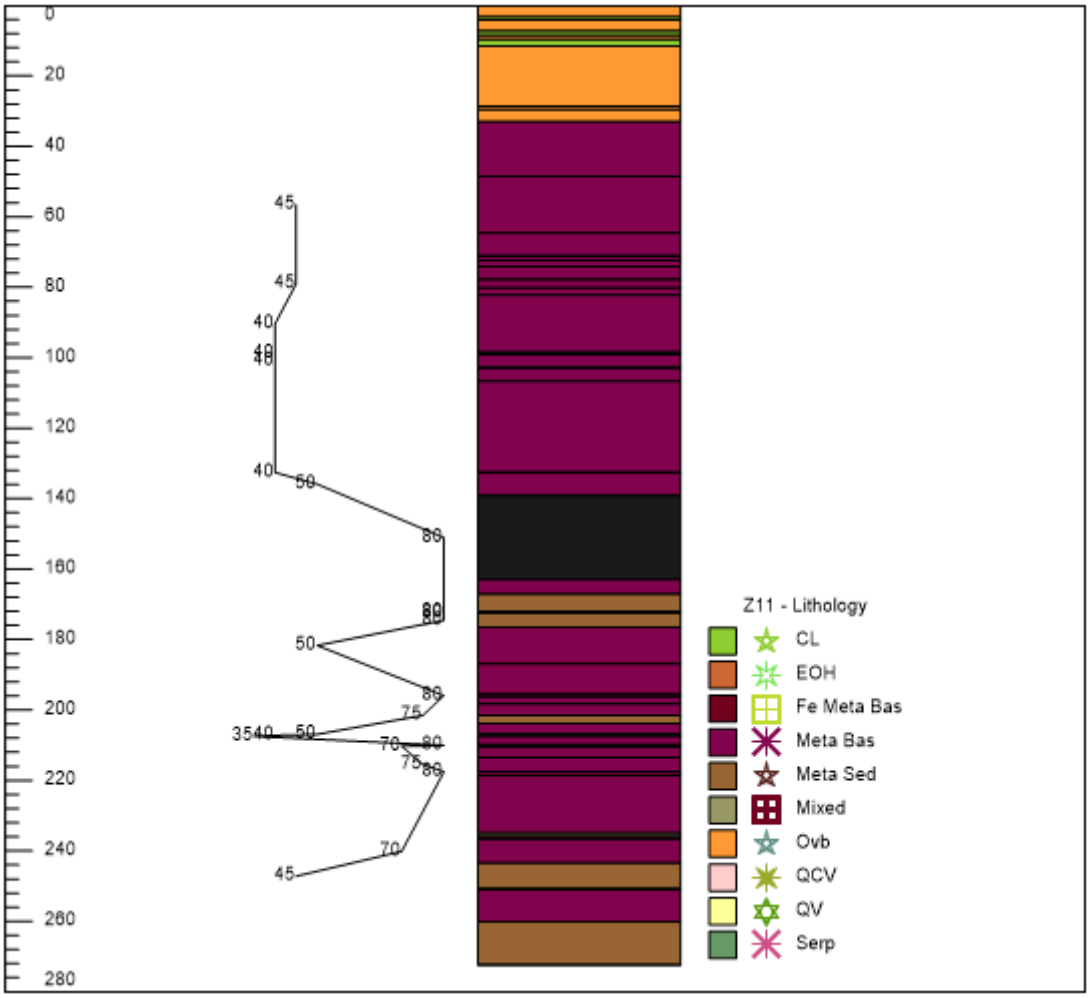


Figure 51: Stratigraphic view of the Zandrivier Reefs borehole core log (Z11) that comprises metabasalts, mixed zone (transition zone), carbonates and metasediments - as you go down stratigraphy. The stratigraphy is crosscut by a dyke (at 140 - 160m) which exhibits a sharp contact with the surrounding rocks. The contact angle between the lithologies is gentle at depths of 60 – 140m (40 - 50°) and transitions into a steeper angle at 150 – 220m (70 - 80°).